EFFECT OF THERMAL AGING ON ELECTROMIGRATION FAILURE OF A FLIP-CHIP SnAgCu SOLDER JOINT

Md. Tusher Ahmed

Department of Mechanical Engineering
Bangladesh University of Engineering and Technology
Dhaka, Bangladesh

July 2019

EFFECT OF THERMAL AGING ON ELECTROMIGRATION FAILURE OF A FLIP-CHIP SnAgCu SOLDER JOINT

by

Md. Tusher Ahmed

A thesis submitted in partial fulfillment of the requirements for the degree of
MASTER OF SCIENCE IN MECHANICAL ENGINEERING

Department of Mechanical Engineering
Bangladesh University of Engineering and Technology
Dhaka, Bangladesh
July 2019

The thesis titled "**EFFECT OF THERMAL AGING ON ELECTROMIGRATION FAILURE OF A FLIP-CHIP SnAgCu SOLDER JOINT**" submitted by **Md. Tusher Ahmed**, Roll No.: **0417102035**, Session: **April, 2017**, has been accepted as satisfactory in partial fulfillment of the requirement for the degree of MASTER OF SCIENCE IN MECHANICAL ENGINEERING on July 09, 2019.

BOARD OF EXAMINERS

Dr. Mohammad Abdul Motalab Associate Professor Department of Mechanical Engineering, BUET, Dhaka- 1000	Chairman (Supervisor)
Dr. Md. Ashraful Islam Professor and Head Department of Mechanical Engineering, BUET, Dhaka- 1000	Member (Ex- officio)
Dr. Md. Afsar Ali Professor Department of Mechanical Engineering, BUET, Dhaka- 1000	Member
Dr. Kazi Md. Shorowordi Professor Department of Materials and Metallurgical Engineering, BUET, Dhaka- 1000	Member (External)

CANDIDATE'S DECLARATION

It is hereby declared that this thesis or any part of it has not been submitted elsewhere for the award of any degree or diploma.

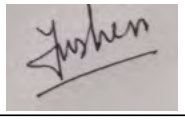

Md. Tusher Ahmed
Author

Dedicated to My Parents and Sister

Table of Contents

List of Figures viii

List of Tables xiii

Acknowledgement xiv

Abstract xv

CHAPTER 1 1

Introduction……...1

1.1 Moore's Law 1

1.2 Package Type Definitions 3

1.2.1 Ball grid array package (BGA) 3

1.2.2 Flip chip packages (FC) 3

1.2.3 Chip scale package (CSP) 4

1.3 Why Lead Free Solders 5

1.4 Different Failure Modes of Solder Joint 6

1.5 Electromigration 7

1.6 Mechanism of Electromigration 9

1.7 Intermetallic Compound (IMC) 12

1.7.1 Cu_6Sn_5 13

1.7.2 Cu_3Sn 14

1.8 Study of Random Vibration in SAC Solder Joint 14

1.8.1 Random vibration 15

1.8.2 Power spectrum density 16

1.8.3 The mode superposition method 16

1.8.4 MSM for random base excitations 17

1.9 Objectives of the Study 19

CHAPTER 2 20

Literature Review……20
CHAPTER 3 24
Finite Element Modeling...……..24
3.1 Electromigration Analysis 24
3.2 Material Models 27
3.2.1 Multilinear isotropic hardening 27
3.2.2 Yield criterion 28
3.2.3 Flow rule 28
3.2.4 Hardening rule 29
3.3 Mechanical Properties 29
3.3.1 Mechanical properties of SAC solder material 29
3.3.2 Mechanical properties of copper 32
3.3.3 Mechanical properties of intermetallic compounds 32
3.4 Basic equations for electromigration 33
3.4.1 Electromigration evolution method 34
3.5 Electromigration Properties 39
3.6 Simulation Methodology for Random Vibration Analysis 40
CHAPTER 4 43
Results and Discussions on Electromigration Analysis……..43
4.1 Current Density Distribution in the Solder Joint 43
4.2 Effects of Current Density 46
4.2.1 Effects of current density on diffusion flux 46
4.2.2 Effects of current density on plastic work per volume (PLWK) 47
4.3 Effects of Ambient Temperature 49
4.3.1 Effects of ambient temperature on diffusion flux 49
4.3.2 Effects of ambient temperature on PLWK 50
4.4 Effects of Thermal Aging 52

4.4.1 Effect of thermal aging on diffusion flux 52
4.4.2 Effects of thermal aging on PLWK 57
4.5 Effects of *Ag* percentage 61
4.5.1 Effects of *Ag* percentage on diffusion flux 61
4.5.2 Effects of *Ag* percent*ag*e on PLWK 66
4.6 Effects of Thermal Aging on Hydrostatic Pressure 70
4.7 Effects of Thermal Aging on Electromigration Life 72
4.8 Effect of IMC Formation on Thermally Long Aged Solder Joints 74
4.9 Numerical Validation 79
4.10 Grid Independence Test 81
CHAPTER 5 82
Electromigration Analysis with Random Vibration 82
5.1 Modal Shapes of SAC Solder Joint 82
5.2 Effect of Random Vibration on Electromigration 85
5.2.1 Effect of random vibration on diffusion flux 85
5.2.2 Effect of random vibration on PLWK 87
5.2.3 Effect of thermal aging on electromigration with random vibration ... 89
5.2.4 Effect of *Ag* percentage on electromigration with random vibration... 90
CHAPTER 6 93
Conclusions 93
6.1 Conclusions 93
6.2 Limitations of the Work 94
6.3 Recommendation for Future Works 95
References 96
Appendix 104

List of Figures

Figure 1.1 A plot of circuit density per chip of Si memory and logic devices against year [2]. 2
Figure 1.2 Typical (a) BGA, (b) Flip Chip and (c) CSP structures [7] 4
Figure 1.3 Schematic diagram of electromigration of diffusing atom (a) before and (b) at the activated state, where it possesses a very large scattering cross section [13] 10
Figure 1.4 Example of a Cu_6Sn_5 IMC needle in the bulk microstructure of a SAC alloy BGA solder joint [10]. 13
Figure 1.5 Example of a Cu_3Sn interfacial IMC of a SAC alloy BGA solder joint on OSP board [10] 14
Figure 1.6 A system subject to random input; SDOF model of vehicle suspension system as it traverses a road contour [11]. 15

Figure 3.1 Thermal-Electric Coupled Field Element Geometry [55] 24
Figure 3.2 Finite Element Model of Analysis Geometry Showing Current Conduction Path 27
Figure 3.3 Finite Element Model of Analysis Geometry Showing Structural Constraints 27
Figure 3.4 Yield surface for Multilinear Isotropic Hardening Model 28
Figure 3.5 Stress States for Isotropic Hardening Model 29
Figure 3.6 Mechanical properties of SAC 305 solder material at different isothermal aging conditions at 100°C and uniaxial tensile testing temperatures of (a) 100 ^{o}C and (b) 125°C [56] 30
Figure 3.7 Computational procedure for numerical simulation of the EM evolution: void growth period [59] 38
Figure 3.8 Schematic process flow of void evolution [59] 39
Figure 3.9 Applied acceleration PSD profile 41
Figure 3.10 Computational procedure for combined electromigration and random vibration simulation of the solder joint 42

Figure 4.1 Current density distribution of a flip-chip SAC305 solder joint for current stressing of 100 hr at input current of 0.01A at a temperature of 100°C (a) Contour Plot and (b) Vector Plot 44

Figure 4.2 Variation of maximum initial current density (*j*) and maximum current density (*j*) at the time of failure as a function of electrical current of a flip-chip SAC305 solder joint..... 45

Figure 4.3 Variation of diffusion flux with applied current density for unaged SAC 305 solder joint 46

Figure 4.4 Plastic Work per Volume distribution (PLWK) of a flip-chip SAC305 solder joint for current stressing of 100 hr at an input current density of (a) 2.76×10^{7} A/m^{2} (b) 8.28×10^{7} A/m^{2} at an experimentation temperature of 100°C for unaged condition 48

Figure 4.5 Maximum PLWK at different value of current density at unaged condition at experimentation temperature of 100°C for SAC305 solder material.. 49

Figure 4.6 Maximum diffusion flux at different value of current density at unaged condition for different values of ambient temperature for SAC305 solder material 50

Figure 4.7 Plastic Work per Volume distribution (PLWK) of a flip-chip SAC305 solder joint for current stressing of 100 hr at input current density of 8.28×10^{7} A/m^{2} at an experimentation temperature of (a) 100°C and (b) 125°C at unaged condition..... 52

Figure 4.8 Maximum PLWK at different value of current density at unaged condition for different values of ambient temperature for SAC305 solder material 52

Figure 4.9 Variation of diffusion flux with electrical current density at different thermal aging conditions of a flip-chip SAC305 solder joint for current stressing of 100 hr at an electromigration temperature of (a) 100°C and (b) 125°C..... 53

Figure 4.10 Diffusion Flux distribution at electrical current density of 8.28×10^{7} A/m^{2} of a flip-chip SAC305 solder joint for current stressing of 100 hr at electromigration temperature of 100°C at aging duration of (a) 0 day, (b) 1 day, (c) 5 days and (d) 20 days 56

Figure 4.11 Plastic Work per Volume distribution (PLWK) of a flip-chip SAC305 solder joint for current stressing of 100 hr at input current density of 8.28×10^7 A/m^2 at a temperature of 100°C for isothermal aging period of (a) 0 day, (b) 1 day, (c) 5 days and (d) 20 days..... 60
Figure 4.12 Maximum Plastic Work per Volume (PLWK) of a flip-chip SAC305 solder joint for current stressing of 100 hr at different values of input current at a temperature of 100°C for isothermal aging for different aging conditions..... 61
Figure 4.13 Diffusion Flux distribution at electrical current density of 8.28×10^7 A/m^2 of a flip-chip SAC solder joint for current stressing of 100 hr at electromigration temperature of 100°C at unaged condition for *Ag* percentage of (a) 1%, (b) 2% and (c) 3% 64
Figure 4.14 Variation of diffusion flux with electrical current density of a flip-chip SAC solder joint for current stressing of 100 hr at an electromigration temperature of 100°C at thermal aging duration of (a) 0 hour and (b) 480 hours 65
Figure 4.15 SEM images of the microstructure of SAC solders a) SAC105 and b) SAC205 [71]..... 65
Figure 4.16 Variation of diffusion flux with the variation of *Ag* percentages of SAC material at different isothermal aging conditions at 100°C 66
Figure 4.17 PLWK Distribution at electrical current of I=1.11×10^8A/m^2 A of a flip-chip SAC solder joint for current stressing of 100 hr at an electromigration temperature of 100°C for unaged condition for *Ag* percentage of (a) 1% , (b) 2% and (c) 3%. 68
Figure 4.18 Variation of PLWK with electrical current density at different *Ag* percentage of a flip-chip SAC solder joint for current stressing of 100 hr at an experimentation temperature of 100°C for an aging period of (a) 0 hour and (b) 480 hour at 100°C 69
Figure 4.19 Variation of PLWK with the variation of *Ag* percentages of SAC material at different isothermal aging conditions at 100°C 70
Figure 4.20 Maximum value of hydrostatic pressure of a flip-chip SAC305 solder joint for current stressing of 100 hr at an input current density of

2.76× 10^7 A/m^2 at an experimentation temperature of (a) 100°C and (b) 125°C for different aged sample 71
Figure 4.21 Estimated Electromigration Life of SAC305 solder joint under different currents at different aging conditions at aging temperature of 100°C 73
Figure 4.22 Estimated Electromigration Life of SAC solder joint under different currents at unaged condition at different *Ag* percentages 73
Figure 4.23 Finite element model of SAC solder joint with IMC 75
Figure 4.24 Plastic Work per Volume distribution (PLWK) of a flip-chip SAC305 solder joint for current stressing of 100 hr at input current density of 8.28 × 10^7 A/m^2 at a temperature of 100°C for isothermal aging period of (a) 0 day without IMC and (b) 180 days with 4 micron IMC layer ... 76
Figure 4.25 Maximum Plastic Work per Volume (PLWK) of a flip-chip SAC305 solder joint for current stressing of 100 hr at different values of input current at a temperature of 100°C for isothermal aging for different aging conditions (a) comparing unaged and aged conditions and (b) aged portions enlarged 77
Figure 4.26 Diffusion flux distribution of a flip-chip SAC305 solder joint for current stressing of 100 hr at input current density of 8.28× 10^7 A/m^2 at a temperature of 100°C for isothermal aging period of (a) 0 day and (b) 180 days with 4 micron IMC 79
Figure 4.27 Microstructure evolution in the No. 2 joint. Electrons flowed from the chip side to the substrate side. The nominal current density was 2 × 10^4 A/cm^2 and the environmental temperature was 100°C [55]..... 79
Figure 4.28 Simulation Model capturing failure of *SnPb* solder joint 80
Figure 4.29 Variation of PLWK with element number for a flip-chip SAC305 solder joint for current stressing of 100 hr at applied current of 2.76× 10^7 A/m^2 at a temperature of 100°C for unaged condition 81

Figure 5.1 Modal shapes for SAC305 solder joint under base constraint with natural frequencies of (a) 18.7543 Hz, (b) 24.0477 Hz, (c) 25.7506 Hz, (d) 36.3911 Hz and (e) 42.1848 Hz at unaged condition..... 85

Figure 5.2 Diffusion flux distribution of a flip-chip SAC305 solder joint for current stressing of 100 hr at applied current density of 1.11×10^{8} A/m^2 at a temperature of 100°C for unaged condition under (a) the effect of electromigration only and (b) combined random vibration and electromigration effect 86

Figure 5.3 PLWK distribution of a flip-chip SAC305 solder joint for current stressing of 100 hr at applied current density of 1.11×10^{8} A/m^2 at a temperature of 100°C for unaged condition under (a) electromigration effect only and (b) combined random vibration and electromigration effect 88

Figure 5.4 Variation of maximum diffusion flux at applied current density of 1.11×10^{8} A/m^{2}at a thermal aging temperature of 100°C and experimentation temperature of 100°C for thermal aging duration of 0 hour to 480 hours of SAC305 solder with and without applied random vibration 89

Figure 5.5 Variation of the maximum value of PLWK at current density of 1.11×10^{8} A/m^2 at a thermal aging temperature of 100°C and experimentation temperature of 100°C for different thermal aging durations with and without applied random vibration. 90

Figure 5.6 Variation of the maximum value of diffusion flux at density of 1.11×10^{8} A/m^2 at a thermal aging temperature of 100°C and experimentation temperature of 100°C for thermal aging duration of 0 hour and 480 hour for different *Ag* percentages under applied random vibration 91

Figure 5.7 Variation of the maximum value of PLWK at density of 1.11×10^{8} A/m^2 at a thermal aging temperature of 100°C and experimentation temperature of 100°C for thermal aging duration of 0 hour and 480 hour for different *Ag* percentages under applied random vibration 91

List of Tables

Table 1.1 Different Failure Modes of Interconnects [7-8] 6
Table 1.2 Quantity-Type Conversions, C [12] 17
Table 1.3 Random Vibration Quantity Type Conversions, β [12] 18

Table 3.1 Stress- Strain Behavior of SAC305 under isothermal aging at temperature of 100°C and uniaxial tensile testing done at temperature of 100°C 31
Table 3.2 Stress- Strain Behavior of SAC305 under isothermal aging at temperature of 100°C and uniaxial tensile testing done at temperature of 125°C 31
Table 3.3 Elastic Modulus of SAC305 under isothermal aging at 100°C and uniaxial tensile testing done at temperature of 100°C and 125°C 32
Table 3.4 Elastic Properties of Copper 32
Table 3.5 Elastic Properties of IMCs 32
Table 3.6 Basic Electromigration Properties 39

Table 4.1 Electromigration and Mechanical Parameter of *SnPb* Solder Joint [63] ... 80

Acknowledgement

I would like to express my deepest gratitude and indebtedness to my supervisor Dr. Mohammad Abdul Motalab, Associate Professor, Department of Mechanical Engineering, BUET for his kind supervision, constant guidance, encouragement, support and thoughtful discussion throughout the entire research. Without his guidance, it was impossible to complete the thesis work.

I am also grateful to the Department of Mechanical Engineering, BUET, for giving me the opportunity to use the “Postgraduate Computer Lab” for the research. I would also like to thank CASR of BUET for financing and approving this thesis (Resolution 19, CASR meeting no 313 held on 12-02-2019)

I wish to thank my parents, sister, relatives, colleagues, friends and well-wishers for their help and mental support during the research. I specially wish to thank Mr. Md. Omarsany Bappy, Lecturer, Department of Mechanical Engineering, BUET, for his support.

Finally, I wish to thank almighty Allah for everything in my entire life.

Author

Abstract

Lead free solder materials have replaced lead based solder materials nowadays for increased environmental concern. Further miniaturization of electronic solder joints in packages has caused electromigration to dominate among all the reliability issues found in electronic packages. This current investigation deals with the review of mechanical property degradations of SAC (*SnAgCu*) solder materials of different *Ag* percentages due to thermal aging and their effects on electromigration oriented failure of small scale flip chip solder bumps. Thermal aging causes degradation of strength as well as elastic modulus of the SAC solder material. This degradation in stress-strain behavior plays an utterly important role in electromigration oriented mass diffusion and subsequent failure in the solder joints. This research highlights the linkage between thermal aging oriented strength degradation and its effect on electromigration oriented void propagation rate and time to failure. Structural-electric-diffusion analyses with commercial finite element analysis software have been performed for different aging conditions (1 to 20 days of aging at 100 ^{o}C) at different electromigration temperatures. Percentage of *Ag* generally varies between 1-4% in solder joints of commercially available packages. Presence of *Ag* in a higher amount causes formation of Ag_3Sn in a large amount which increases mechanical strength of SAC materials. So the effect of *Ag* percentage on SAC solder materials has also been analyzed in the current study. It is also found in literature that with aging for significantly long time, different intermetallic compounds (IMC) form at the interface of *Cu*-SAC joint. So, the effect of IMC on the electromigration has also been observed in the current research. Finally, the effect of random vibration observed in many real world applications on electromigration oriented failure of flip-chip solder joint has also been investigated. Findings from the analysis indicate that mass diffusion due to electromigration and associated stress migration actually reduces with the increment of aging time and thus increases time to failure in case of a flip chip solder joint. Moreover, increment in *Ag* percentage increases diffusion flux as well as plastic work per volume (PLWK) in SAC material. Furthermore, it has been found that PLWK and diffusion flux significantly reduce with IMC formation. Finally, analysis revealed that inclusion of random vibration expedites electromigration failure significantly. Simulation results

have been found to be in good agreement with the electromigration experiment results that are available in literature.

CHAPTER 1

Introduction

Electronic packaging is a diversified region of engineering that requires continuous progression towards higher functionality, ultra-miniaturization and low cost. In the previous era, integrated circuit (IC) is considered to be the backbone of all electronic devices. However, nowadays electronics packaging goes beyond to connect these ICs with other components in order to create an entire functional system. There are four different functions of electronic packaging which are (1) heat dissipation, (2) power distribution, (3) signal distribution, and (4) protection [1].

This research focuses on the failure of first-level packaging, specifically the interconnect system which connects the IC to the package. All those miniaturization raises the queries regarding the interconnection reliability concerns that arise in meeting up the functions of electronic packaging. A major concern associated with tiny interconnection dimensions such as solder bumps or microbumps is the phenomenon of electromigration, which produces failures due to high electrical current densities. This has become a prime interconnection reliability concern since especially in case of miniaturized components.

This chapter discusses about the different aspects regarding development of the electronic packaging for future challenges as well as reliability concerns impeding in the way of the attainment of that goal.

1.1 Moore’s Law

Microelectronic industry is supposed to have two major technologies; first one is the chip technology and the second one is the packaging technology. The development that has been taken place since the beginning of chip technology has been guided by Moore’s law. It’s statement is that the density of 2-dimensional integrated circuits (2D IC) on Si chips will double in every 18–24 months. It

remained a truth since the past 30–40 years. A plot of circuit density of memory and logic devices on Si chips against year is shown in Figure 1.1 [2]. For memory devices, it is observed that from 1975 to 1990 the number increased from 1 k (thousand) per chip to 1 m (million) per chip. Figure 1.1 also shows that it took 20 years, from 1990 to 2010 to reach the number from 1 million to 1 billion. However, it has become nearly impossible to project the future since the invention of nanotechnology; the critical feature size is reduced down to 22 nm which has approached the physical limit of miniaturizations.

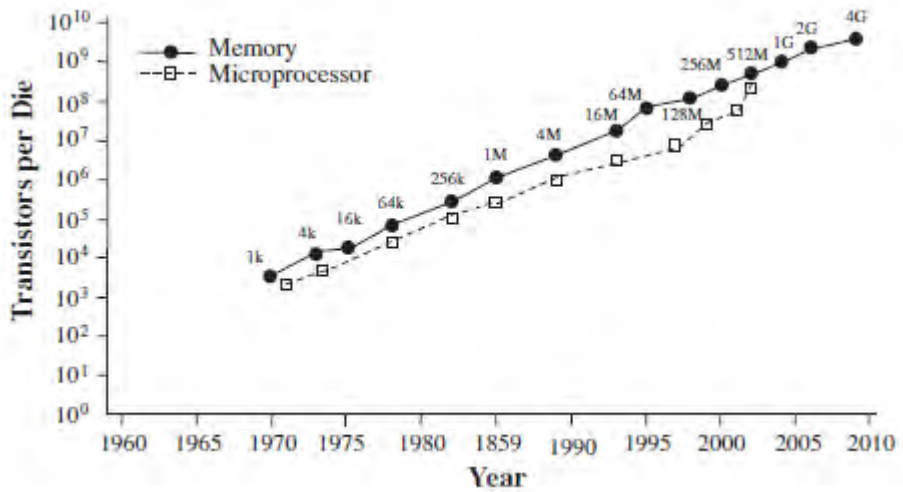

Figure 1.1 A plot of circuit density per chip of Si memory and logic devices against year [2].

For such reason, the microelectronic industry has to find out another direction to accumulate the increased amount of Si chips per packages. And the solution has come in the form of 3-dimensional integrated circuits (3D IC) [3–6]. In 3D IC, the chip technology and packaging technology are merged closer and closer together. Thus, it is of great interest that whether or not there is a Moore's law applicable for the packaging technology too.

1.2 Package Type Definitions

A chip is useless without an electronic package. It has multiple functions such as to deliver power to the chip, transfer information into and out of the chip to the Printed Circuit Board (PCB), draw heat from the chip and protect the chip from outside elements. There are a multiple type of Packages that could be found nowadays in electronic packaging industry. They are (1) BGA (Ball Grid Array, (2) CSP (Chip Scale Package) and (3) FC Package (Flip-Chip Package).

1.2.1 Ball grid array package (BGA)

The term BGA covers a wide range of package types. Here, BGA refers to a 35-mm or larger device with 760-µm solder balls. Different types of BGA packages are available in industries.

- MAPBGA - Molded Array Process Ball Grid Array
- PBGA - Plastic Ball Grid Array
- TEPBGA - Thermally Enhanced Plastic Ball Grid Array
- TBGA - Tape Ball Grid Array
- PoP - Package on Package
- MicroBGA

1.2.2 Flip chip packages (FC)

Flip chips are bare silicon devices that have solder bumps in the 75-µm range. It is a method to electrically connect the die to the package carrier. The bond wire is replaced with a conductive “bump” placed directly on the die surface. Under-fill epoxy is used to secure the attachment and absorb stress. The chip is then “flipped” face down onto the package carrier using a re-flow process. Bump sizes range from microns in diameter. It is also known as C4 (Controlled Collapsible Chip Connection).

1.2.2.1 Advantages of flip-chip

- Reduced signal inductance
- Shorter interconnect lengths
- Use power more efficiently
- Power directly at the core
- Higher interconnect density
- More routable area
- Smaller package size
- Chip scale packaging (CSP)
- I/O not controlling core size
- Area array placement
- Possible die shrink

1.2.3 Chip scale package (CSP)

The term CSP describes devices with 250-µm solder balls and an interposer layer between the die and solder balls. The overall package size of a CSP is typically no larger than 1.2 times the size of the silicon. In short, A Package is considered CSP when it is less than 20% larger than the Die.

Figure 1.2 shows different types of electronic packages which are used in the electronic industries.

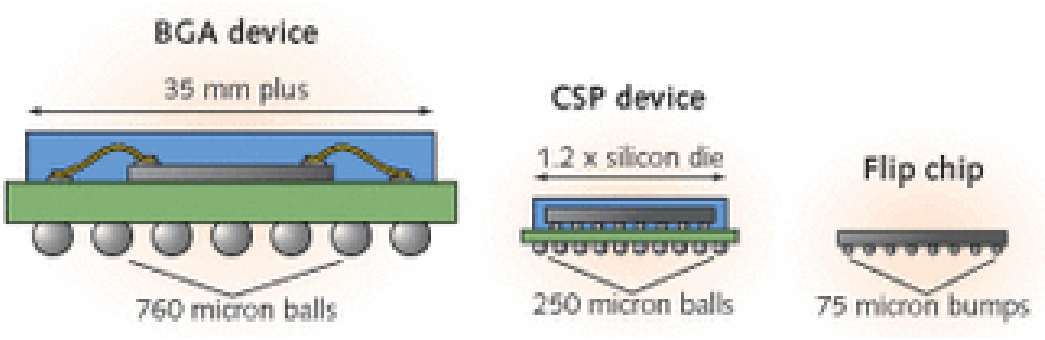

(a) (b) (c)

Figure 1.2 Typical (a) BGA, (b) Flip Chip and (c) CSP structures [7]

1.3 Why Lead Free Solders

Application of lead free soldering has been introduced because of the legislation being enacted around the globe regarding health safety concerns. In the EC, the WEEE (Waste from Electrical and Electronics Equipment) Directive had brought a sharp focus onto lead free soldering technology. Although this motive of this directive was mainly towards recycling, it also directed profuse attention aimed at banning the use of lead in certain categories of electrical and electronic equipment. This restriction on lead based electronic solder joints paved the way for research to find out lead free solder materials as an alternative to the former one.

The traditional solder material was comprised of a mixture of 63% tin and 37% lead known as *SnPb* solder material. Actually, the use of lead in electronic packaging industry is only 1% of the entire use of lead throughout the world. However, it's impact on the environment was severe due to the practice of dumping electronic wastages in landfills in UK. These practices raised a concern such that these leads may contaminate ground water supplies by leaching into it.

Lead free solder materials are interconnect materials that are used globally for manufacturing in electronic packaging industries. Lead free solder materials avoid the use of lead in solder materials for the wellbeing of environment. The most commonly used lead free solder material is *SnAgCu* solder material or more commonly known as SAC solder material. SAC solder material is composed of bulk amount of *Sn* with a small amount of *Ag* and *Cu*. These materials show improved mechanical and electrical property compared to previously used conventional *SnPb* solder along with the ecofriendly nature reducing environment pollution. SAC solder material is used as interconnect between *Cu* conductors of BGA solder joints as well as SAC pillar to form microbump in stacked packages. Moreover, Some SAC interconnects are also used for heat dissipation, known as thermal interconnects. Typically available SAC solder joints show variation of *Ag* percentage in their formation. *Ag* percentage is varied from 1% to 4% in commercially available SAC

solder alloys. For such variation in *Ag* content, significant mechanical property variation is observed in SAC solder material.

The move to lead free soldering is of great importance to many areas of industry. Electronic circuitry is included in a very wide range of products including computers, white goods, brown goods, telecommunications, and other electronics. As lead free soldering technology as well as mechanical, thermal and structural property are significantly different to that using traditional tin-lead solder, it is of great interest to industry as a whole. Different researches are continued in order to determine the behavior of electronic packages under thermal cycling, thermal shock, electromigration and other reliability investigation experiments.

1.4 Different Failure Modes of Solder Joint

Failure of a solder joint is found to be significantly depending on several parameters. Different types of failure modes found in literature are summarized in Table 1.1.

Table 1.1 Different Failure Modes of Interconnects [7-8]

Interconnect Type	Diameter of Solder Joint	Observed Failure Mode	Schematic Diagram
Ball Grid Array Joint	580-760 μm	Due to the mismatch of thermal expansion coefficient, interconnects get subjected mainly to shear stress which causes failure of these solder joints by crack formation and propagation.	

Flip Chip Solder Joint	75-150 μm	Due to higher current density passing through these interconnects, void formation takes place due to effect of stress induced voiding caused by electromigration, and due to formation of open circuit to those interconnects and subsequent increment in resistance.	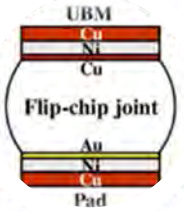
Microbump	20-40 μm	Significantly higher amount of current passes through these interconnects due to small physical size of these interconnects. This interconnects fail more rapidly due to the effect of electromigration.	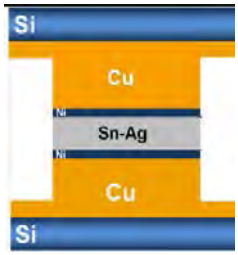

1.5 Electromigration

Electromigration is the process of mass transport in miniature components such as interconnects placed in integrated circuits where significantly higher current is passing through a tiny cross-section. This is the result of two counteracting forces; one is the electrostatic force and another one is the momentum exchange between the atoms and the electrons drifting opposite to the electric field. As stated earlier, electromigration is not visible below a threshold current density and temperature below which no atomic diffusion is possible based on the selected material for study. A pan-cake type void formation is observed due to mass depletion from cathode side to anode side which results open and short circuit at cathode and anode side respectively. If the atomic or vacancy flux is continuous in the interconnect, in other term, the anode can supply vacancies and the cathode can accept them continuously,

and no flux divergence is visible, then vacancy concentration is supposed to be in equilibrium everywhere, which means that electromigration-induced damage such as void and extrusion formation is absent here. So in absence of mass flux divergence, no electromigration damage will occur in any interconnect or rather fluxes of atoms and vacancies can pass through it uniformly [8]. For such reason, atomic or mass flux divergence is a mandatory condition for the electromigration failure in real devices. The most common mass flux divergence is the interfaces between dissimilar materials where the solder joint meets the *Cu* pad or under bump metallization. As a solder joint has two interfaces, one at the cathode and another at the anode, they are the common failure sites also known as “Current Crowding Zone”, especially the cathode interface where accumulation of vacancies occurs to form voids.

In short, electromigration phenomenon is consisted of both atomic and electron fluxes. Their distribution as well as balancing in interconnects is the prime concern in electromigration damage. Most importantly, if both distributions are uniform in a region, there will be electromigration, but no electromigration-induced damage due to the lack of flux divergence.

Electromigration is inherently an atomic diffusion process which requires to be thermally activated mandatorily. Another important factor is the design and processing of the interconnect structure. Non-uniform distribution or divergence in interconnects at microstructure irregularities such as grain boundary triple points and interphase interfaces can attribute largely to electromigration, and they can also be the most critical sites of failure initiation. Concerning the electron flux, the current density requires be high enough to be above a critical value for electromigration to occur. As transistors in devices are turned on by pulsed direct current, for transistor based devices such as computers we consider only electromigration under direct current. It is worth mentionable that in presence of AC current void formation and hillock formation is also altered after every cycle, thus nullifying the electromigration based damage. It is pretty obvious that a uniform current distribution is expected in straight lines whereas non-uniform current distribution is visible where a conducting current line turns, at interfaces where conductivity

changes, and also around the voids or precipitates present in a matrix. One of the most important factors attributive to electromigration in a flip chip solder joint is the unique line-to-bump geometry, where a drastic change of current density takes place from the line toward the bump, which in turn leads to a large current crowding at the junction between the line and the bump.

1.6 Mechanism of Electromigration

The electrical force acting on a diffusing atom (ion) proposed by Huntington and Grone is taken to be [9]

$$F_{em} = Z^{*}eE = (Z^{*}_{el} + Z^{*}_{wd})eE \quad (1)$$

where, e is the charge of an electron and E is the electric field ($E = \rho j$, where ρ is resistivity and j is current density) and Z^{*} is the effective charge number of electromigration. Z^{*}_{el} can be defined as the nominal valence of the diffusing ion in the metal which is responsible for the field effect and $Z^{*}_{el}eE$ is called the direct force. Z^{*}_{wd} is an assumed charge number which symbolizes the momentum exchange effect between electrons and the diffusing ion, and similarly $Z^{*}_{wd}eE$ is called the electron wind force which is generally found to be of the order of 10 for a good conductor. That's why the electron wind force is much greater than the direct force for electromigration in metals. Hence, in electromigration, the enhanced flux of atomic diffusion is in the direction governed by the electron flux.

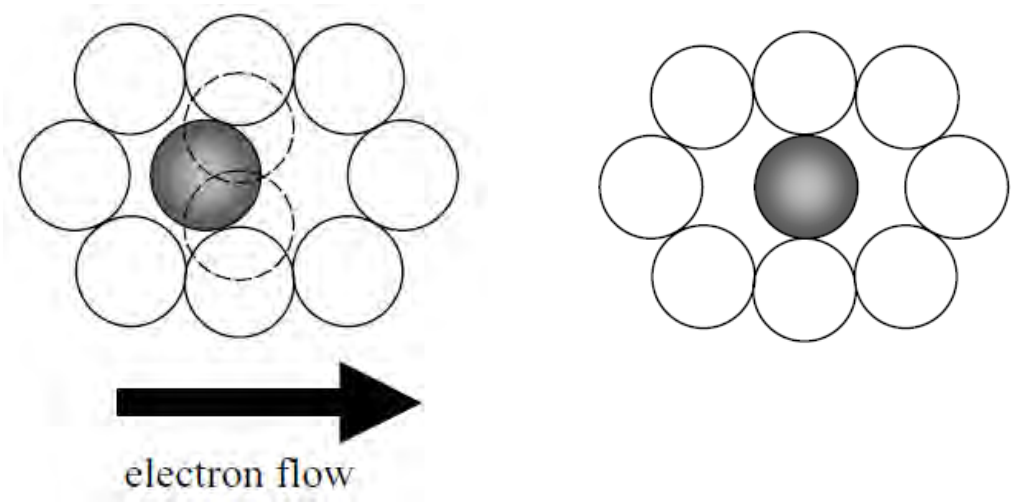

(a) (b)

Figure 1.3 Schematic diagram of electromigration of diffusing atom (a) before and (b) at the activated state, where it possesses a very large scattering cross section [13]

In order to illustrate the electron wind force conceptually, the configuration of a shaded *Al* atom and a neighboring vacancy in a face-centered cubic lattice structure before they exchange position along a <110> direction is showed in Figure 1.3(a). They have commonly four nearest neighbors including the two as shown in Figure 1.3 by the broken circles, one on top and another on the bottom of the close-packed atomic plane. When the shaded atom is diffusing halfway toward the vacancy as depicted in Figure 1.3(b), the atom is at it's activated state, sitting at a saddle point displacing the four nearest-neighbor atom. Since the saddle point is deprived of lattice periodicity, the atom at the saddle position is out of its equilibrium position and will make a much larger contribution to the resistance to electrical current than a normal lattice atom. It means that it will experience a greater electron scattering and as a result, a great electron wind force is produced which will push the atom to an equilibrium position known to be as the vacant site. The diffusion of the atom is gradually increased in the direction of the electron flow. It is worth to be mentioned that the diffusing atom is prone to experience the electron wind force, not just at the saddle point, but all the way from the beginning to the end in the entire jumping path of the diffusion.

In order to predict the electron wind force, the ballistic approach to the scattering process was developed by Huntington and Grone [14]. The model states about the transition probability of free electrons per unit time from one free electron state to another free electron state due to the scattering by the diffusing atom. The force which is the momentum transfer per unit time can be calculated by summing over the initial and final states of the electrons those have been scattered.

The system momentum is conserved during elastic scattering of electrons by a diffusing atom. The average change in electron momentum in the transport direction is equal *to* $2m_e\langle\upsilon\rangle$, where m_e is the electron mass and $\langle\upsilon\rangle$ is the mean

velocity of electrons in the direction of current flow. The force on the ion induced by the scattering is

$$\overrightarrow{F_{wd}} = \frac{2m_e<\upsilon>}{\tau_{col}} \tag{2}$$

where, τ_{col} is the mean time interval between two successive collisions. The net momentum lost per second per unit volume of electrons to the diffusing ions is then $2nm_e<\upsilon> / \tau_{col}$, and the force on a single diffusing ion is

$$\overrightarrow{F_{wd}} = \frac{2\mathrm{n}m_e < \upsilon >}{\tau_{col}N_d} \tag{3}$$

where, n is the electron density and N_d is the density of diffusing ions. The electron current density can be written as

$$j = -ne < v > \tag{4}$$

Substituting <υ> in Equation (4) into Equation (3), we obtain

$$\overrightarrow{F_{wd}} = -\frac{2m_e j}{e\tau_{col}N_d} = -[\frac{\rho_d}{N_d}][\frac{n}{\rho}]eE \tag{5}$$

where, $\rho = E/j$ is the total resistivity of a conductor, $\rho_d = m/ne^2\tau_{col}$ is the metal resistivity due to the diffusing atoms, and E is the applied electrical field.

Aside from the electron "wind" force, the electric field E will produce a direct force on the diffusing ion to be given by

$$\overrightarrow{F_d} = Z^*_{el}eE \tag{6}$$

where, Z^*_{el} can be regarded as the nominal valance of the metal ion when the dynamical scattering effect around the ion is ignored. Thus, the total force will be

$$\overrightarrow{F_{EM}} = [Z^*_{el} - Z[\frac{\rho_d}{N_d}][\frac{n}{\rho}]]eE \tag{7}$$

where, N is the atomic density of the conductor and $n = NZ$ is used. Equation (7) can be written as

$$\overrightarrow{F_{EM}} = Z^*eE \tag{8}$$

and,

$$Z^* = [Z^*_{el} - Z[\frac{\rho_d}{N_d}][\frac{n}{\rho}]] \tag{9}$$

Z^* is called the effective charge number of the ion in electromigration.

Electromigration model based on the ballistic scattering of electrons is considered as the first and simplest model of the phenomenon of electromigration.

Theoretical understanding is further developed by the contributions offered by many researchers. Despite of these theoretical developments, the model developed by Huntington and Grone, especially the drift velocity of electromigration, is well accepted as the theoretical basis in nearly each and every experimental studies of electromigration. For example, the drift velocity is taken as

$$v_d = MF = \frac{D}{kT} Z^* ej\rho \tag{10}$$

This indicates that the drift velocity is measured using short stripes and the diffusivity, D is known, it is possible to calculate Z^*.

The above model depicts the method of estimating the effective charge number with the use of specific resistivities of a diffusing atom and a normal lattice atom,

$$Z^*_{wd} = -Z \frac{\frac{\rho_d}{N_d}}{\frac{\rho}{N}} \frac{m_0}{m^*} \tag{11}$$

where, $\rho = m_0/ne^2\tau$ and $\rho_d = m^*/ne^2\tau_d$ are the resistivity of the equilibrium lattice atoms and the diffusing atoms, respectively. m_0 and m^* are the free electron mass and effective electron mass, respectively, and it is to be assumed that they are equal, and τ and τ_d are relaxation times. In an fcc lattice, there are 12 equivalent jump paths along the <110> directions. For a given current direction, the average specific resistivity of a diffusing atom must be corrected by a factor of one-half. By rewriting Equation (11), we have

$$Z^* = -Z[\frac{1}{2} \frac{\frac{\rho_d}{N_d}}{\frac{\rho}{N}} \frac{m_0}{m^*} - 1] \tag{12}$$

where, Z_{el} has been taken as Z, the nominal valence of the metal atom. This is known to be as the equation of Huntington and Grone for the effective charge number of electromigration. To calculate Z^*, It is necessary to know the specific resistivity of a diffusing atom, or its ratio to that of a lattice atom.

1.7 Intermetallic Compound (IMC)

Intermetallic Compounds (IMC) are stoichiometric combinations of two or more metal atoms where the atomic fractions of the metals remain fixed (for

example. Cu_3Sn). This can be differentiated with solid-solid solutions where the atomic fractions can sometimes vary as widely as 0 - 100%. Metals and alloys show characteristics of metallic bonding between the atoms whereas IMCs exhibit more or less covalent characteristics. That's the reason for IMCs tending to be much harder and have much higher elastic moduli than either of their respective metallic elements.

1.7.1 Cu_6Sn_5

The intermetallic Cu_6Sn_5 is important due to the fact that most of the tin-lead and lead-free solder joints formed directly from copper. This IMC causes an interfacial layer and can be visible mostly in the bulk microstructure of tin-lead solder joints where excessive time and temperature are present during the soldering process. In addition, the Cu_6Sn_5 intermetallic is a primary feature present in the microstructure of lead-free solder joints such as SAC 305 alloy (96.5*Sn*-3*Ag*-0.5*Cu*). Figure 1.4 is an example of a Cu_6Sn_5 IMC needle in the bulk microstructure of a SAC alloy BGA solder joint.

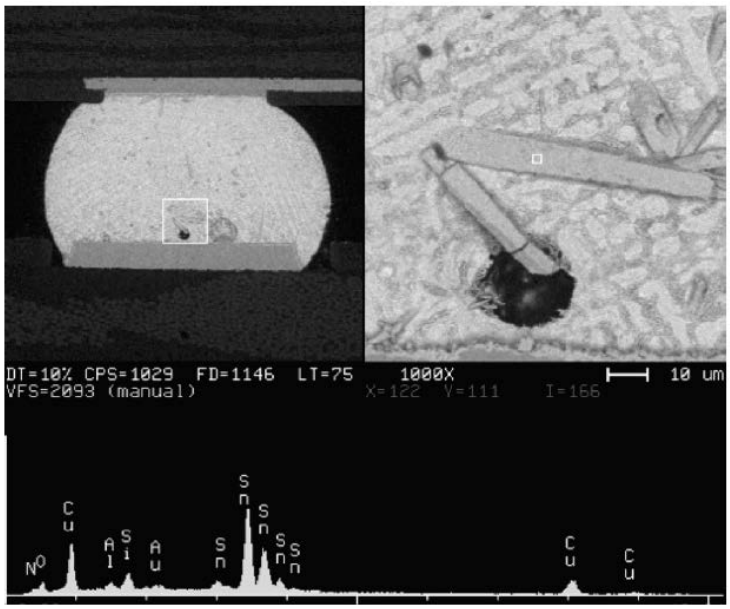

Figure 1.4 Example of a Cu_6Sn_5 IMC needle in the bulk microstructure of a SAC alloy BGA solder joint [10].

1.7.2 Cu_3Sn

The intermetallic Cu_3Sn is important due to the fact that it forms an interfacial layer between the copper and Cu_6Sn_5 IMC layer in tin-lead and lead-free solder joints and formed directly due to the presence of copper which is shown in Figure 1.5. The combination of the Cu_3Sn & Cu_6Sn_5 layers is assumed to be the key reason of the consequence of a very strong bond between the solder and the copper.

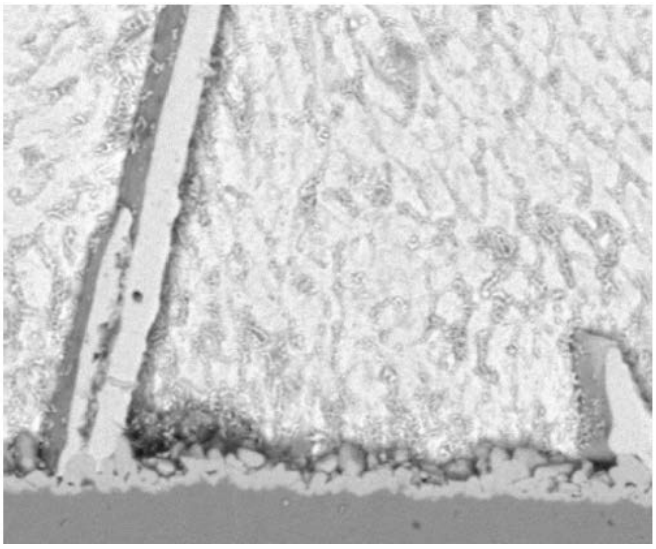

Figure 1.5 Example of a Cu_3Sn interfacial IMC of a SAC alloy BGA solder joint on OSP board [10]

1.8 Study of Random Vibration in SAC Solder Joint

Failure occurred in electronic components can be classified as shock/impact-induced, vibration-induced, diffusion-induced and thermal-induced failures. Since the thermal loading and electromigration appears to be the major cause of interconnect failures, most of the research work has focused on the failure mechanisms and fatigue life prediction models under thermal loading and electromigration reliability. However, very limited work has been performed towards the vibration loading. In the field-use conditions, and during their manufacturing process, shipping and service life, electronic components are exposed to different vibration environment. Especially for avionic and automotive electronic systems, which experience a great amount of vibration during their service life, the vibration-

induced failure is one of the most important reliability issues. Most electronic systems used in vibration environments are subjected to random vibration loading instead of ordinary harmonic excitations.

1.8.1 Random vibration

A time-dependent process is known to be as deterministic if and only if it's properties at a given time *t* can be estimated prior to the occurrence. A linear process will act as deterministic if its input is supposed to be deterministic. The processes of free and forced vibrations of single degree of freedom, multi degree of freedom, and continuous systems are all deterministic as their response can be predicted at any instant of time when subjected to a deterministic input. A nonlinear system may predict chaotically when subjected to deterministic input. Many physical systems do not have a deterministic input. An example is illustrated in Figure 1.6. The road contour encountered by the wheels of a vehicle is really made up of a series of bumps and depressions that is beyond prediction due to so many uncertainties. This is said to be random as it cannot be predicted at any time. Similar to this reason, many potential causes could be found for an input to act as random.

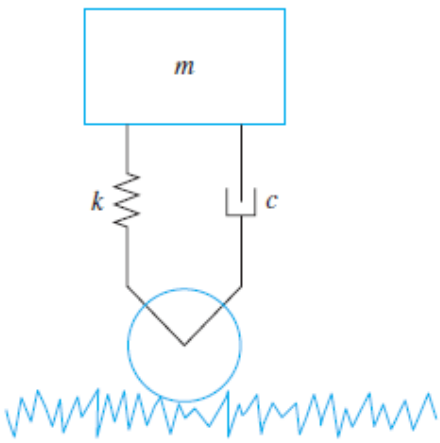

Figure 1.6 A system subject to random input; SDOF model of vehicle suspension system as it traverses a road contour [11].

1.8.2 Power spectrum density

PSD (Power Spectrum Density) is also known to be as acceleration spectral density (ASD) which is widely used in random vibration testing applications. It is intended primarily as a tool for the removal of the effect of bandwidth of a frequency spectrum. PSD is considered as a unit of measure which is described in terms of energy per "filter". It has been popularly used to identify and denote energy strength deviations. It can be used to obtain the total energy within a specific frequency range by taking the root sum squared of the PSD points within that specified range. Proper computation of PSD can be achieved by using FFT (Fast Fourier Transform) spectrum analysis and followed by the transformation of it considering actual analyzer filter bandwidth.

1.8.3 The mode superposition method

The mode superposition method has been utilized in random vibration analysis. With the mode superposition method, it is necessary to first extract eigenvectors, φ and calculate other derived eigenquantities, η such as eigenstresses and eigenstrains in the mode extraction phase of the analysis. Once the mode extraction phase is accomplished, the structure's response to any harmonic force excitation may be characterized by:

$$u_i = H_{ij}F_j \tag{13}$$

where, u_i stands for the "ith" degree of freedom displacement response, F_j is the "jth" degree of freedom force component, and:

$$H_{ij} = \frac{\eta_{ir}\varphi_{jr}}{(\omega_r^2-\Omega_r^2)+i(2\omega_r\Omega\xi_r)}) \tag{14}$$

where, the index r ranges over the numbers of mode. The coefficient i present in the denominator symbolizes an imaginary number which is often referred to as the complex frequency response function. ω_r is the “rth” eigen frequency, and Ω is the frequency. ϕ_{jr} represents the “rth” mass-normalized eigenvector. η_{ir} represents the "rth" mass-normalized eigenquantity. There is an implied summation over all repeated indices. To represent a base excitation:

$$u_i = H_{ij}Md\Omega^2N_j \tag{15}$$

where, M is the value of the large mass (as depicted by large mass method), N is a unit vector representing the direction of the applied load (the only non-zero components of which correspond to the large-mass unrestrained DOFs), Ω denotes the frequency of excitation, and d denotes the magnitude of the applied displacement (usually given as a function of frequency). The base excitation may be characterized by some time-derivative of displacement (velocity, acceleration, or g's) and the same holds for the response. Therefore:

$$u_i = H_{ij} N_j C_{KL} I \tag{16}$$

where, u and I represents a response and input excitation, respectively as any quantity appearing in Table 1.2, and C is the appropriate quantity-type conversion factor found by matching an input quantity from the leftmost column with an output quantity from the top row. Here the indices K and L in Equation [16] are fixed by the input and output quantity type shown in Table 1.2. For example, if input quantity is given in terms of velocity and output in acceleration, one would go to the third row and fourth column over - this would correspond to the coefficient C_{23}.

Table 1.2 Quantity-Type Conversions, C [12]

I/u	**Displacement**	**Velocity**	**Acceleration**	**g**
Displacement	$M\Omega^2$	$M\Omega^3$	$M\Omega^4$	$M\Omega^4/g$
Velocity	$M\Omega$	$M\Omega^2$	$M\Omega^3$	$M\Omega^3/g$
Acceleration	M	$M\Omega$	$M\Omega^2$	$M\Omega^2/g$
g	gM	$gM\Omega$	$gM\Omega^2$	$M\Omega^2$

1.8.4 MSM for random base excitations

The MSM may also be employed to calculate the response of structures to random base excitations. To do this, Equation [16] needs to be modified [17]:

$$S_i = H_{ij}^* H_{ji} S N_l \beta_{OP} \tag{17}$$

where, H^* is the complex conjugate of H. The inputs and outputs now represent spectral densities (in units of quantity squared per Hz) where as β_{OP}

represents a table of quantity conversions similar to those of Table 1.2. Table 1.3 summarizes the new quantity conversions for random vibration.

Table 1.3 Random Vibration Quantity Type Conversions, β [12]

S/S$_i$	**Displacement**2/ Hz**	**Velocity**2/ Hz**	**Acceleration** 2/Hz**	**G**2/Hz**
Displacement**2/ Hz	$M^2\Omega^4$	$M^2\Omega^6$	$M^2\Omega^8$	$M^2\Omega^8/g$
Velocity**2/Hz	$M^2\Omega^2$	$M^2\Omega^4$	$M^2\Omega^6$	$M^2\Omega^6/g$
Acceleration**2/ Hz	M^2	$M^2\Omega^2$	$M^2\Omega^4$	$M^2\Omega^4/g$
G**2/Hz	gM^2	$g\,M^2\Omega^2$	$g\,M^2\Omega^4$	$M^2\Omega^4$

Finally, a variance, or mean response, E may be calculated by [18]:

$$E_i = \sqrt{\int_{\Omega_1}^{\Omega_2} S_i d\Omega} \tag{18}$$

1.9 Objectives of the Study

The motivation of this research is to analyze the effect of thermal aging oriented mechanical property degradation for different percentages of *Ag* on electromigration oriented failure of flip-chip SAC solder joint. It also addresses the effect of different thicknesses for thermally long aged solder joint and applied random vibration on electromigration failure concern. The objectives of the present work can be summarized as follows:

(i) To develop a 3D finite element model of a Flip-Chip C4 (Controlled Collapse Chip Connection) SAC Solder joint and validate the model by comparing the calculated results with that obtained from the experimental investigations for the similar Flip-Chip SAC Solder joints available in literature.

(ii) To study the variation of solder mass diffusion flux for different isothermal solder aging conditions (0-20 days) at 100 - 125°C.

(iii) To observe the variation of solder mass diffusion flux with the variation of *Ag* percentages from 1% to 4% in the solder material under different thermal aging conditions mentioned in (ii).

(iv) To obtain the stress distribution in solder joint due to electromigration process and predict the Time to Failure (TTF) of Flip-Chip SAC solder joint under different thermal aging conditions mentioned in (ii) and for different *Ag* percentages mentioned in (iii).

(v) To observe the effects of Intermetallic Compound (IMC) formed in the solder material on the void propagation in thermally long aged Flip-Chip SAC solder joint.

(vi) To study the variation of solder mass diffusion flux under random vibration of the component with different thermal aging conditions mentioned in (ii) and the variation of *Ag* percentages mentioned in (iii).

CHAPTER 2

Literature Review

Electromigration or electrotransport, is a term used to describe the mass transport occurring in a conductor under an applied direct electric field. The study of electromigration has been pursued in solid as well as liquid metallic systems [13]. Electromigration phenomena have been studied for a long time. From this study on mass transport of impurities in molten metals, the significance of the interaction between atoms and moving charge carriers was underlined. In the 1950s, the first systematic studies of electromigration, based on the correlation between the direction of the current flow and the material transport, were presented by Seith and Wever [14]. By measuring the mass transport of a series of solid alloys and plotting it in a phase diagram, they observed that the direction of transport varies with the sign of the charge carriers, i.e. electrons or holes, in the specific alloy phase. They also introduced the "marker motion" technique, now called vacancy flux method, which permits to measure the electromigration-induced mass transport using the displacement of an indentation on a metal wire [15]. These experiments prompted the concept of an "electron wind" to account for the induced mass transport. The first mathematical formulations of the electromigration driving force have been derived independently by Fiks [16] and Huntington and Grone [17]. These authors treated the electron wind force by developing a "ballistic" approach based on the semiclassical collision process between mobile point defects and charge carriers. The investigations demonstrated the possibility of using electromigration to probe the interaction of moving atoms and charge carriers directly. All these theoretical ideas stimulated considerable technological interest during the 1960s in experimental studies on electromigration in integrated circuits. In the late 1960s, Blech and Sello [18] discovered that electromigration in aluminum thin films could be a leading source of failure in planar semiconductor ICs. In the late 1980s and 1990s, the introduction of pure copper-based interconnects took place. Copper was proposed because of its lower electrical resistivity and, therefore, much lower sensitivity to electromigration than aluminum [19]. Apart from this, ambient temperature plays a

decisive role in case of electromigration oriented failure [20]. Electromigration process is inherently a mass diffusion process in which the grain boundary diffusion is the most significant source of mass transfer. That's the reason for which above a critical temperature this mass diffusion due to grain boundary diffusion is not much visible in SAC305 solder joints [21]. In parallel to the development of the interconnect technology, new aspects of electromigration physics were introduced to the modeling. Different models of electromigration failure phenomenon for VLSI interconnections, based on the electromigration stress-induced voiding, were carried out [22-23]. Furthermore, a new class of models based on the void surface evolution theory was initiated in the mid-1990s [24-27]. Different mechanisms are found in the literature to simulate the void formation mechanism due to electromigration [28-31]. These mechanisms include Atomic Flux Divergence or AFD method, Atomic Density Integral or ADI method etc. Being AFD method erroneous and limited in case studies [32], ADI technique is applied in this study.

A common alloy in the industry that has replaced *SnPb* solder is tin-silver-copper (*SnAgCu*) or SAC. Alongside with this, shift from lead based solder joints to lead free solder joints caused reduction in environmental pollution from electronic package production. With the adoption of this new material, research has been conducted to understand the lifetime of these joints under extreme current and temperature conditions. Nevertheless, Thermal aging causes significant reduction in structural properties of SAC solder material [33]. Numerous analyses have been conducted to even determine the effect of thermal aging at extreme conditions [34-36]. These findings are very important for the high temperature point of application such as Automotive or higher altitude point of application such as Aircraft on board electronic packages [37].These degradation of structural properties such as elastic modulus and ultimate strength are the consequences of microstructure evolution. In real life applications, solder joints are supposed to be continuously exposed to aging during service. It has been well documented that the microstructure, mechanical response, and failure behavior of solder materials are constantly evolving under such circumstances [38-40].

Isothermal aging effects have been reported earlier in literature to lower the strength of solder joints. The mechanical response of solder joints to external loading can be different from the bulk solders due to the presence of fine microstructure, grain orientation (single grain/ multigrain), and the presence of intermetallic compounds at joint boundaries [41-42].

It had been previously reported by Li et al. [43] that 20% shearing strength reduction of BGA solder joints after 240 hours of aging at room temperature. A 10% shearing strength reduction has been observed by Lee et al. [44] for the BGA packages just after 3 days room temperature aging. Chilton et al. [45] witnessed a 15% fatigue strength reduction of *Sn-Pb* (Lead-Tin) solder joints of a SMD test package which were aged for 60 days at room temperature. Li et al. [46] studied the elevated temperature aging effects on flip-chip packages with SAC solders. They have shown that the shear strength of solder bumps subjected to aging at 80°C decreased gradually with aging. Also for the aging temperatures 150 and 175°C, the degradation of shear strength of the bumps was much faster. Yang et al. [47] showed pre-aging oriented bump dissolution of *SnAg* solder joint has impact on electromigration oriented void formation. Although, multiple analyses on the eletromigration have been performed in the past, effect of thermal aging oriented mechanical property degradation on electromigration has remained unexplored. Effect of variation of stress-strain behavior of SAC material on electromigration oriented failure is to be investigated in this current study. These changes in microstructure could even possibly affect mass diffusion rate which is the goal of our current study. Additionally, intermetallic compound formation is one of the consequences of thermal aging. However, very few works are reported on the combined effect of microstructure evolution and IMC formation on electromigration oriented failure.

Change of *Ag* percentage plays a deterministic role in material properties of lead free solder joint. Zhang et al. [42] investigated the relationship between elevated temperature isothermal aging and the long-term thermal reliability of fine-pitch packages with *Sn*–1.0*Ag*–0.5*Cu* (SAC 105), *Sn*–3.0*Ag*–0.5*Cu* (SAC 305), and 63*Sn*–

Pb solder ball interconnects. Significant cycle lifetime degradation was observed with aging for both SAC105 and SAC305 in different packages. Ma et al. [48] showed microstructural change and mechanical property variation for different percentage of SAC alloys at different thermal aging conditions. Che et al. [49] analyzed and recorded mechanical properties of SAC solder with the variation of *Ag* percentage at different strain rate. However, few works have been found on the effect of *Ag* percentage on electromigration oriented failure.

A large portion of research on high cycle fatigue is concerned with predicting the fatigue life of electronic components exposed to a sinusoidal vibration. Chen et al. [50] combined the vibration failure test, FEA, and theoretical formulation for the calculation of the electronic components fatigue life under sinusoidal vibration loading. Perkins and Sitaraman [51] used linear sweep vibration test to characterize the fatigue failure for ceramic column grid array (CCGA). Yang et al. [52] characterized the dynamic properties of a plastic ball grid array (PBGA) assembly with a sweep sine excitation. Although, many researches have been conducted on the effect of vibration on the fatigue life of electronic packages, the effects of vibration on electromigration oriented failure with aging and *Ag* percentage remained unexplored.

CHAPTER 3

Finite Element Modeling

This chapter discusses the finite element modeling for the *Cu*-SAC-*Cu* interconnections.

3.1 Electromigration Analysis

In this study, a Flip Chip C4 SAC solder joint of diameter of 120 μm with two copper conductors at the ends of solder joint of dimension of 135 μm× 60 μm× 10 μm is modeled for analysis. The solder joint has a vertical height of 60 μm. The dimensions are selected from Lin et al. [53] from a similar flip chip solder joint. A single solder joint is analyzed for the simulation purpose to reduce computational cost as electrical current has quite similar effect on all the solder joints in case of electromigration failure [54].

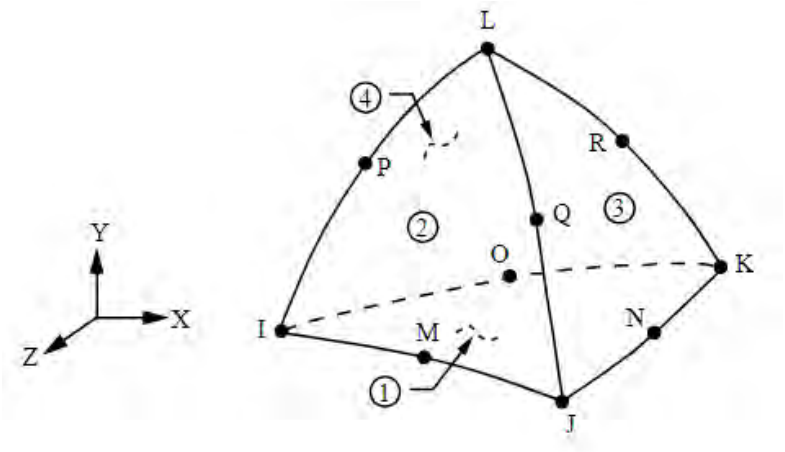

Figure 3.1 Thermal-Electric Coupled Field Element Geometry [55]

For the current analysis, thermal-electric couple field element has been selected as shown in Figure 3.1. The element has ten nodes with up to five degrees of freedom per node. Structural capabilities include elasticity, plasticity, hyperelasticity, viscoelasticity, viscoplasticity, creep, large strain, large deflection, stress stiffening effects, and prestress effects. It also has mixed formulation capability for simulating deformations of nearly incompressible elastoplastic materials, and fully

incompressible hyperelastic materials. In addition to thermal expansion, structural-thermal capabilities include the piezocaloric effect in dynamic analyses. The Coriolis effect is available for analyses with structural degrees of freedom. The diffusion expansion effect is available for analyses with structural and diffusion degrees of freedom. The element selected in this analysis is tetragonal in shape. 55068 elements are used to conduct the finite element modeling of the *Cu* conductor and *SAC* solder geometry model.

The simulation procedure deals with the application of electrical current through a *Cu* conductor, a SAC solder joint and finally leaves through another *Cu* conductor. Both ends of the *Cu* conductor are required to be properly constrained electrically as shown in Figure 3.2 to pass electrical current through left end of the top *Cu* conductor and leave through right end of the bottom *Cu* conductor. At first, a geometrical model of flip chip SAC solder joint using the dimensions stated earlier is created using finite element solver interface. This geometrical model is then fitted with appropriate material properties of *Cu* and SAC solder materials as found from literature. Copper is modeled as linear elastic material whereas SAC material is modeled as elastic plastic material using Multilinear isotropic hardening. Both Cu and SAC material are fitted with migration model [55] properties from electromigration properties which will be mentioned later in this chapter. Later, electrical and structural constraints are applied on the geometrical model as appropriate boundary conditions as shown in Figure 3.2 and 3.3. In this analysis symmetric model is considered and half of the solder joint is taken into account to reduce computation cost and time.

The analysis is considered as isothermal to observe the effect of mechanical property degradation on stress migration and resultant mass diffusion. Isothermal temperatures of 100°C and 125°C are selected to evaluate the effect of ambient temperature on solder joint electromigration life. The selection of these temperatures is of great significance as grain boundary diffusion rate, which is the main source of mass diffusion, is predominant at such higher temperatures. A variation of current density from 2.7×10^{7} A/m^{2} to 1.4×10^{8} A/m^{2} is applied on the solder joint to observe the effect of current density on the mass diffusion and plastic work per volume. It has been found out from the literatures that electromigration oriented failure is mostly

visible at such values of current density. Finally, literature data obtained for different aging conditions ranging from 0 day to 20 days are used to determine the effect of microstructure coarsening and subsequent mechanical property degradation on electromigration oriented failure in flip chip solder joint.

In this analysis, an electromigration analysis is done considering unaged SAC solder material for *Ag* percentage of 3% (which is the most commercially available lead free solder material) at an electrical current density of 2.7×10^{7} A/m^{2} . Then, the electrical current density is varied from 2.7×10^{7} A/m^{2} to 1.4×10^{8} A/m^{2} to reveal the impact of electrical current density on electromigration oriented diffusion flux and verify the validity of the study. Later, isothermal aging duration is increased from 0 day to 20 day in order to investigate the effect of thermal aging oriented material property degradation in electromigration of SAC solder joint. Along with this, electromigration experimentation temperature is changed to verify the diffusion flux variation with the change of temperature. Finally, the *Ag* percentage is varied from 1% to 3% to detect the effect of *Ag* percentage on electromigration diffusion flux of SAC solder joint.

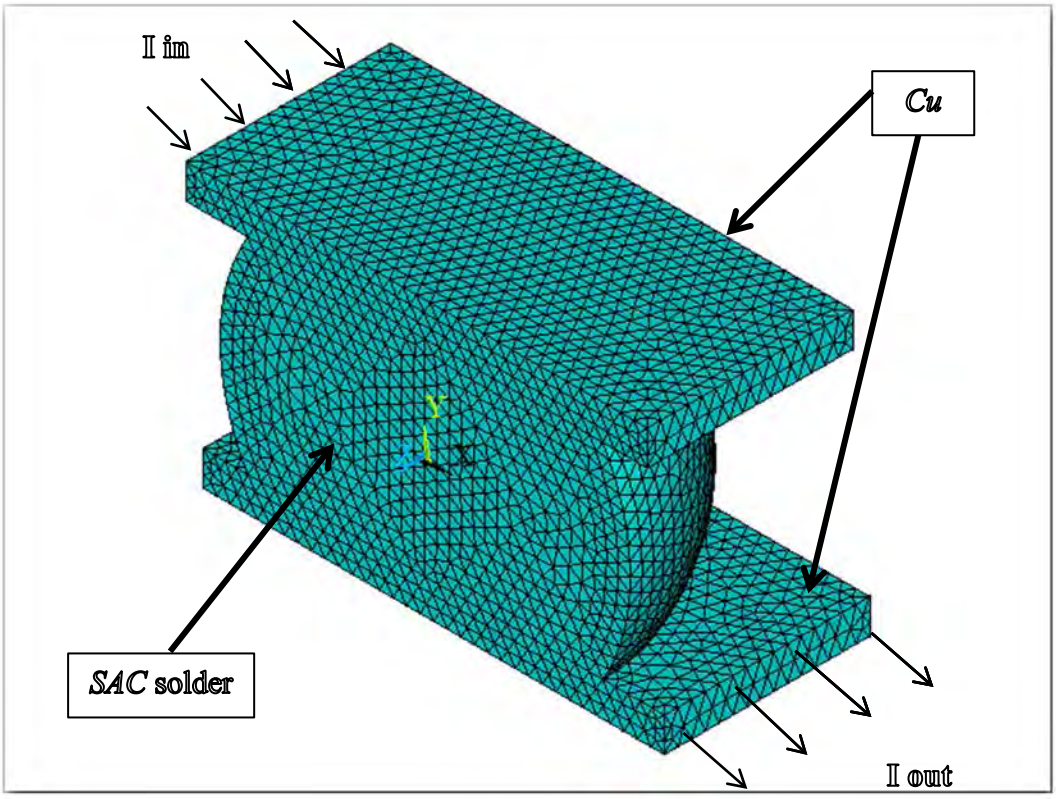

Figure 3.2 Finite Element Model of Analysis Geometry Showing Current Conduction Path

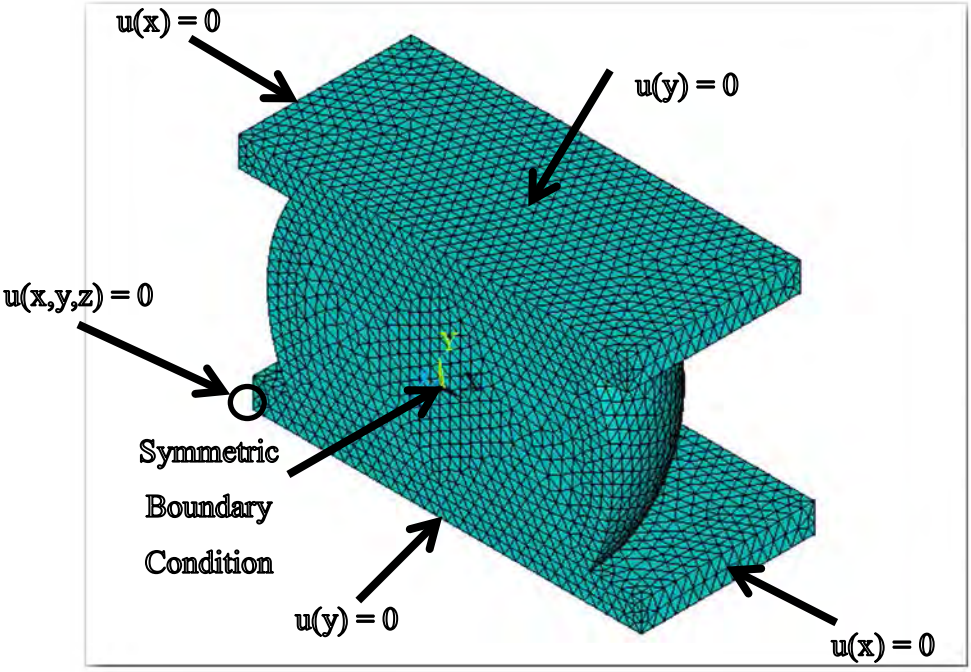

Figure 3.3 Finite Element Model of Analysis Geometry Showing Structural Constraints [56]

3.2 Material Models

Copper is modeled as linear elastic material whereas SAC material is modeled as elastic plastic material using Multilinear isotropic hardening. Proper constraint for geometrical model is applied and for the consideration of symmetry, only half of the solder joint is taken into account for analysis.

3.2.1 Multilinear isotropic hardening

Rate-independent plasticity can be defined by the irreversible straining process that occurs in a material when a cut-off level of stress is reached. As the plastic strains are supposed to develop instantaneously, it is considered to be time independent. Theory of Plasticity provides a mathematical relationship that symbolizes the elastoplastic response of a material when load is applied. There are

three ingredients in the rate-independent plasticity theory: the yield criterion, flow rule and the hardening rule [50].

3.2.2 Yield criterion

The yield criterion defines the stress level of the initiation of yielding. For multi-component stresses, this criterion is dependent on the individual components of stress, which can be interpreted as an equivalent stress σ_e:

$$\sigma_e = f(\{\sigma\}) \tag{17}$$

where, $\{\sigma\}$=stress vector

$$f(\{\sigma\}) = \sigma_y \tag{18}$$

When the equivalent stress equals a material yield parameter σ_y, the material will develop plastic strains. If σ_e is less than σ_y, the material is elastic and the stresses will develop according to the elastic stress-strain relations. It is mentionable that the equivalent stress can never exceed the material yield as plastic strains would develop instantaneously in this case. As a result it will reduce the stress to the material yield. The stress space as shown in Figure 3.4 is known as the yield surface and any stress state inside the surface is elastic, that is, they do not cause plastic strains.

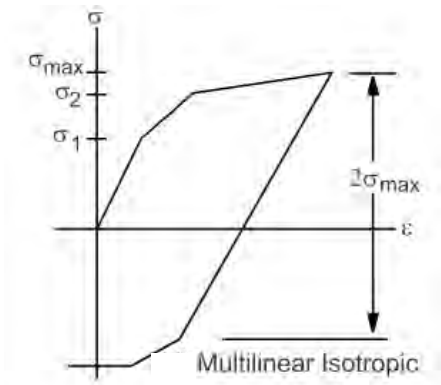

Figure 3.4 Yield surface for Multilinear Isotropic Hardening Model

3.2.3 Flow rule

The flow rule determines the direction of plastic straining and is given as:

$$\{\partial \varepsilon_{pl}\} = \lambda \left\{\frac{\partial Q}{\partial \sigma}\right\} \tag{19}$$

where,

λ = plastic multiplier (which determines the amount of plastic straining)

Q = function of stress termed the plastic potential (which determines the direction of plastic straining). If Q is the yield function, the flow rule is termed associative and the plastic strains occur in a direction normal to the yield surface.

3.2.4 Hardening rule

The hardening rule is defined by the changing of the yielding surface with progressive yielding, so that the stress states for subsequent yielding can be formed. Two hardening rules can be found from the literature: work (or isotropic) hardening and kinematic hardening. In work hardening, the yield surface remains centered about its initial centerline and expands in size as the plastic strains develop. For materials with isotropic plastic behavior this is termed isotropic hardening and is shown in Figure 3.5.

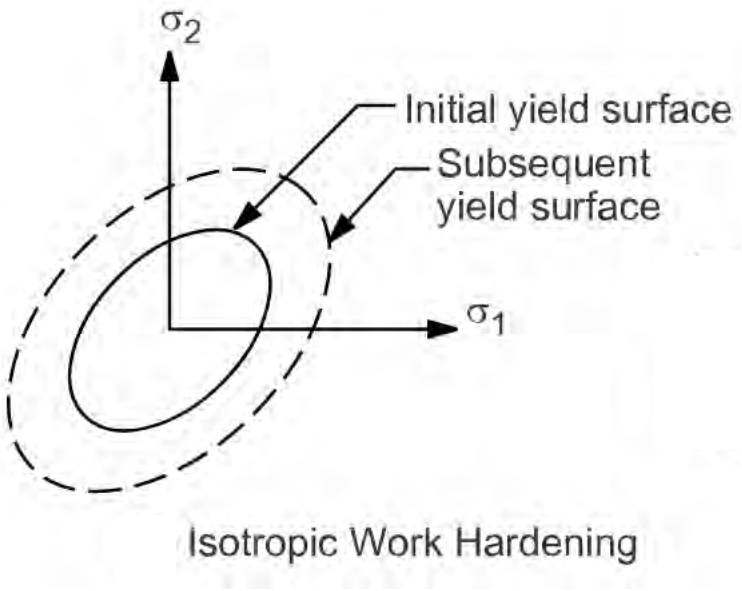

Figure 3.5 Stress States for Isotropic Hardening Model

3.3 Mechanical Properties

3.3.1 Mechanical properties of SAC solder material

As stated earlier, all the mechanical properties are taken for thermal aging temperature of 100°C and uniaxial tensile testing temperature of 100°C and 125°C.

SAC material provides unique properties based on it's *Ag* percentage as well as aging time along with aging and testing temperatures. These material properties

are collected from Motalab et al. [56] and are shown in Figure 3.6. All the mechanical properties of SAC material are tested at a strain rate of $0.001s^{-1}$.

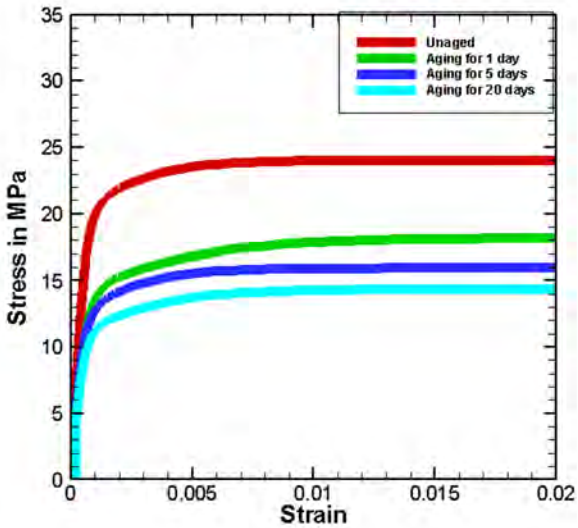

(a)

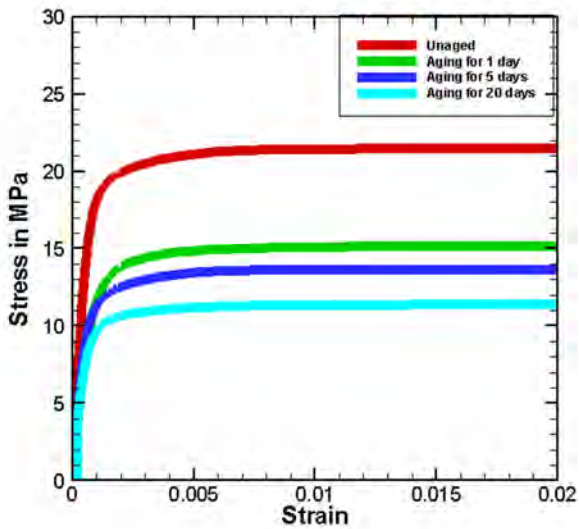

(b)

Figure 3.6 Mechanical properties of SAC 305 solder material at different isothermal aging conditions at 100°C and uniaxial tensile testing temperatures of (a) 100 °C and (b) 125°C [56]

After summarizing those data from the figures shown above, stress-strain data set for multilinear isotropic hardening input is shown in Table 3.1-3.3.

Table 3.1 Stress- Strain Behavior of SAC305 under isothermal aging at temperature of 100°C and uniaxial tensile testing done at temperature of 100°C

Aged at T= 100°C and Tested at T=100°C		No Aging	1 Day Aging	5 Day Aging	20 Day Aging
Strain Rate	Strain	Stress(MPa)	Stress(MPa)	Stress(MPa)	Stress(MPa)
10^{-3} s^{-1}	0	0	0	0	0
	0.00054545	15.6453	10.2387	10.3093	9.0809
	0.0010303	20.1157	13.7212	12.9071	11.3253
	0.0023637	22.2144	15.5452	14.4472	12.6175
	0.0045714	23.3927	16.6565	15.44	13.5951
	0.02	24.0561	18.1756	15.9685	14.379

Table 3.2 Stress- Strain Behavior of SAC305 under isothermal aging at temperature of 100°C and uniaxial tensile testing done at temperature of 125°C

Aged at T= 100°C and Tested at T=125°C		No Aging	1 Day Aging	5 Day Aging	20 Day Aging
Strain Rate	Strain	Stress(MPa)	Stress(MPa)	Stress(MPa)	Stress(MPa)
10^{-3} s^{-1}	0	0	0	0	0
	0.00054545	14.2129	8.441	9.0585	7.7374
	0.0010303	18.3128	11.8058	11.4372	9.7845
	0.0023637	20.1742	14.1079	12.7285	10.7733
	0.0045714	21.0313	14.6973	13.3863	11.1589
	0.02	21.4712	15.1662	13.6751	11.3923

Table 3.3 Elastic Modulus of SAC305 under isothermal aging at 100°C and uniaxial tensile testing done at temperature of 100°C and 125°C

Aging Time	Elastic Modulus, E in GPa (Aged at T=100°C and Tested at T=100°C)	Elastic Modulus, E in GPa (Aged at T=100°C and Tested at T=125°C)
No Aging	28.69	26.06
1 Day Aging	20.77	18.48
5 Day Aging	18.90	16.61
20 Day Aging	16.65	14.19

Similarly, Material properties of SAC105 and SAC205 are collected from Che et al. [57] and Lall et al. [58].

3.3.2 Mechanical properties of copper

Copper has been considered as linear elastic material. So, elastic property such as young's modulus and poissons ratio is suitable enough to define mechanical property of *Cu* material. Mechanical behavior found for Copper from literature is listed in Table 3.4.

Table 3.4 Elastic Properties of Copper

Material	Elastic Modulus, E_x	Poissons Ratio, ϑ
Cu	127 GPa	0.35

3.3.3 Mechanical properties of intermetallic compounds

Mechanical behavior found for intermetallic compounds is listed in Table 3.5.

Table 3.5 Elastic Properties of IMCs

Material	Elastic Modulus, E_x	Poissons Ratio, ϑ
Cu_3Sn	132 GPa	0.31

Intermetallic compound (IMC) is a brittle material. For such reason, only elastic properties are sufficient enough to define IMC materials. In this study, Cu_3Sn

is used as IMC material layer as this compound is mostly found in the IMC layer under electromigration experimentation.

3.4 Basic equations for electromigration

Electromigration is, as termed earlier, a diffusion controlled mass transport process in interconnects [45]. The time-dependent evolution equation of the local atomic density caused by an applied current is the mass balance (continuity) equation,

$$\nabla \cdot \mathbf{q} + \frac{\partial c}{\partial t} = 0 \tag{20}$$

where, c is the normalized atomic density (NAD), $c = C/C_0$, C is the actual atomic density and C_0 is the initial (equilibrium state) atomic density in the absence of a stress field, t is the time and $\boldsymbol{q}$ is the total normalized atomic flux. The driving forces of atomic flux may include electron wind, temperature gradient, hydrostatic stress gradient and atomic density gradient; thus,

$$\begin{aligned}\mathbf{q} = \mathbf{q}_{\mathrm{Ew}} + \mathbf{q}_{\mathrm{Th}} + \mathbf{q}_{\mathrm{S}} + \mathbf{q}_{\mathrm{C}} &= \frac{cD}{k_B T} eZ^* j\rho - \frac{cD}{k_B T} Q^* \frac{\nabla T}{T} - \frac{cD}{k_B T} \Omega \nabla \sigma_m - D\nabla c \\ &= c \cdot \mathbf{F}(\nabla T, \nabla \sigma_m, j, \ldots) - D\nabla c,\end{aligned} \tag{21}$$

where, k is Boltzmann's constant, e is the electronic charge, Z^* is the effective charge which is determined experimentally, T is the absolute temperature, ρ is the resistivity which is calculated as $\rho = \rho_0\big(1 + \alpha(T - T_0)\big)$, where α is the temperature coefficient of the metallic material, ρ_0 is the resistivity at T_0, j is the current density vector, Q^* is the heat of transport, Ω is the atomic volume, $\sigma_m = (\sigma_1 + \sigma_2 + \sigma_3)/3$ is the local hydrostatic stress, where $\sigma_1, \sigma_2, \sigma_3$ are the components of principal stress, D is the effective atom diffusivity, $D = D_0 \exp(-E_a/kT)$, where E_a is the activation energy, D_0 is the effective thermally activated diffusion coefficient. For the EM evolution equation (Equation 20) on any enclosed domain V with the corresponding boundary Γ, the atomic flux boundary conditions of a metal interconnects can be expressed as

$$q \cdot n = q_0 \quad on\ \Gamma \tag{22}$$

For blocking boundary condition,

$$q_0 = 0 \quad on\ \Gamma \tag{23}$$

At the initial time, the normalized atomic density is assumed to be

$$c_0 = 1. \tag{24}$$

The above equations and boundary conditions constitute the boundary value problem that governs the atomic transport during EM. This boundary value problem must be solved accurately in order to adequately describe the continuous atom redistribution and to capture the realistic kinetics of void nucleation and growth as a function of the interconnect architecture, segment geometry, material properties and stress conditions.

3.4.1 Electromigration evolution method

3.4.1.1 Atomic density integral algorithm

In general, atom redistribution, caused by kinds of EM driving forces, tends to bring the atomic system to quasi-equilibrium (steady state). Depending on the particular solder bump geometry, material properties and applied electrical current, voids may be nucleated somewhere at the interface of *Cu* pad and solder bump. The nucleated void affects current density, temperature and mechanical stress distributions around the void; hence, it changes the local atomic fluxes in the void vicinity and leads to further void evolution. Equation (20) describes the atom density evolution at any point of the considered segment characterized by the given current density **j**, T, gradients of temperature and stress. Thus, to obtain a complete solution of the problem, we should determine in coupled manner the evolution of the current, temperature and stress distributions in the considered segment, caused by continuous atom density redistribution. We assume that the establishment of a new equilibrium in the current, temperature and stress distributions is immediate, but the process of atom migration is slow. Therefore, we can obtain the current, temperature and stress by the steady-state solutions. After we obtain the current, temperature, stress and atomic density distribution in an incremental step, the atomic density redistribution needs to be solved based on equation (20) in the next step. In the finite element method, we seek an approximation solution for equation (20) to develop a new local simulation algorithm for the local atomic density in a solder bump. The first step is to

multiply the time-dependent EM evolution equation with a weighted residual function w and integrate over the enclosed domain V based on the vector identity by applying the Gauss-Ostrogradsky divergence theorem to the product of the scalar function w and the atomic flux vector field:

$$\int_V w(\nabla \cdot \boldsymbol{q} + \dot{c})dV = \int_V w\dot{c}dV + \int_V w \cdot (\nabla \cdot \boldsymbol{q})dV = \int_V w\dot{c}dV - \int_V \frac{\partial w}{\partial \boldsymbol{n}} \cdot \boldsymbol{q}dV + \int_\Gamma w \cdot (\boldsymbol{q} \cdot \boldsymbol{n})d\Gamma = 0 \tag{25}$$

From equation (25) with considering the atomic flux boundary condition of equation (22),

$$\int_V w\dot{c}dV - \int_V \frac{\partial w}{\partial \boldsymbol{n}} \cdot \boldsymbol{q}dV = -\int_\Gamma wq_0 d\Gamma \tag{26}$$

Next, we assume that

$$c = \sum_{j=1}^{n} \psi_j c^j, \quad \dot{c} = \sum_{j=1}^{n} \psi_j \dot{c}^j \tag{27}$$

and $w = \psi_i$ (for Galerkin method), where ψ_i is the shape function of the element.

After element discretization, the matrix form of equation (26) can be written as equation (27)

$$[\boldsymbol{M}]\{\dot{c}\} + [\boldsymbol{K}]\{c\} = \{\boldsymbol{Y}\}, \tag{28}$$

where the mass matrix [**M**] is independent of time, the stiffness matrix [**K**] will remain constant in an incremental step where we assume that the current density **j** and the local hydrostatic stress σ_m are not varied (i.e., both are constants) in the current incremental step, {**Y**} is the known term.

For an eight-node element e with volume Ve, mass matrix [**M**] and stiffness matrix [**K**] can be discretized as

$$[\boldsymbol{M}]_{ij}^e = \int_{Ve} \psi_i \psi_j dV_e = \sum_{k=1}^{8} \psi_i(\xi_k, \eta_k, \zeta_k)\psi_j(\xi_k, \eta_k, \zeta_k)J_k w_k,$$
$$[\boldsymbol{K}]_{ij}^e = \int_{Ve} \left[-\left(\frac{\partial \psi_i}{\partial \boldsymbol{n}} \cdot \boldsymbol{F}\right)\psi_j + D\frac{\partial \psi_i}{\partial \boldsymbol{n}} \cdot \nabla \psi_j\right] dV_e, \tag{29}$$

Where $[\boldsymbol{M}]_{ij}^e$ and $[\boldsymbol{K}]_{ij}^e$ are discretized forms of mass matrix [**M**] and stiffness matrix {K} respectively, ψ_i and ψ_j are shape function.

Furthermore, $[\boldsymbol{K}]_{ij}^e$ can be described as:

$$[\boldsymbol{K}]_{ij}^{e} = \int_{Ve}\left[-\left(\frac{\partial\psi_i}{\partial\boldsymbol{n}}\cdot\boldsymbol{F}\right)\psi_j + D\frac{\partial\psi_i}{\partial\boldsymbol{n}}\cdot\nabla\psi_j\right]dV_e = \int_{Ve}\left[-\left(\frac{\partial\psi_i}{\partial x}\cdot F_x + \frac{\partial\psi_i}{\partial y}\cdot F_y + \frac{\partial\psi_i}{\partial z}\cdot F_z\right)\psi_j + D\left(\frac{\partial\psi_i}{\partial x}\cdot\frac{\partial\psi_j}{\partial x} + \frac{\partial\psi_i}{\partial y}\cdot\frac{\partial\psi_j}{\partial y} + \frac{\partial\psi_i}{\partial z}\cdot\frac{\partial\psi_j}{\partial z}\right)\right]dV_e = \int_{Ve}[-G+H]dV_e = \sum_{k=1}^{8}[-G(\xi_k,\eta_k,\zeta_k) + H(\xi_k,\eta_k,\zeta_k)]J(\xi_k,\eta_k,\zeta_k)W_k \tag{30}$$

where,

$$F_x = \frac{D}{kT}Z^*e\rho j_x - \frac{D}{kT}Q^*\frac{1}{T}\frac{\partial T}{\partial x} - \frac{D}{kT}\Omega\frac{\partial\sigma_m}{\partial x},$$

$$F_y = \frac{D}{kT}Z^*e\rho j_y - \frac{D}{kT}Q^*\frac{1}{T}\frac{\partial T}{\partial y} - \frac{D}{kT}\Omega\frac{\partial\sigma_m}{\partial y},$$

$$F_z = \frac{D}{kT}Z^*e\rho j_z - \frac{D}{kT}Q^*\frac{1}{T}\frac{\partial T}{\partial z} - \frac{D}{kT}\Omega\frac{\partial\sigma_m}{\partial z},$$

$$G(\xi_k,\eta_k,\zeta_k) = \left(\frac{\partial\psi_i}{\partial x}\cdot F_x + \frac{\partial\psi_i}{\partial y}\cdot F_y + \frac{\partial\psi_i}{\partial z}\cdot F_z\right)\psi_j,$$

$$H(\xi_k,\eta_k,\zeta_k) = D\left(\frac{\partial\psi_i}{\partial x}\cdot\frac{\partial\psi_j}{\partial x} + \frac{\partial\psi_i}{\partial y}\cdot\frac{\partial\psi_j}{\partial y} + \frac{\partial\psi_i}{\partial z}\cdot\frac{\partial\psi_j}{\partial z}\right)$$

The most commonly used local iteration scheme for solving the above equation is the α -family of approximation method in which a weighted average of the time derivatives at two consecutive time steps is approximated by linear interpolation of the values of the variable at two steps:

$$(1-\alpha)\dot{c}_{t_i} + \alpha\dot{c}_{t_i+1} = \frac{c_{t_{i+1}} - c_{t_i}}{\Delta t},\ \ for\ \ 0 \le \alpha \le 1. \tag{31}$$

In this work, α = 0.5 is used. Such method is called the Crank-Nicolson scheme which is stable and has the accuracy order of $O((\Delta t)^2)$. It follows from Equations [27] and [29] with considering the incremental step

That

$$([\boldsymbol{M}] + \alpha\Delta t[\boldsymbol{K}])\{c_{t_{i+1}}\} = ([\boldsymbol{M}] - (1-\alpha)\Delta t[\boldsymbol{K}])\{c_{t_i}\} + \{\overline{\boldsymbol{Y}}\}_{i,i+1}, \tag{32}$$

where,

$$\{\overline{\boldsymbol{Y}}\}_{i,i+1} = (1-\alpha)\Delta t\{\overline{\boldsymbol{Y}}\}_{t_i} + \alpha\Delta t[\boldsymbol{M}]\{\overline{\boldsymbol{Y}}\}_{t_{i+1}} \tag{33}$$

Thus, the normalized atomic density c in the (i+1)th step can be obtained based on Eq. (33) in terms of the corresponding value in the i-th step. Since the initial atomic density $c_0 = 1$ is known, the above equations provide the solution to c at any time step. In this study, the blocking boundary condition ($\mathbf{q}\cdot\mathbf{n} = 0$) is considered so $\{\overline{\boldsymbol{Y}}\}_{i,i+1} = \{0\}$.

3.4.1.2 Simulation approach of EM induced void evolution

The damage induced by electromigration appears as voids. Lifetime and failure location in a solder bump can be predicted by means of numerical simulation of the process of void incubation, initiation and growth. The changes in current density and temperature distribution due to void growth need be taken into account in simulation. The computation procedure of EM induced void evolution based on ADI (Atomic Density Integral) algorithm is shown in Figure 3.7. It has been assumed that there is a critical atomic density for void initiation c^*_{min}. When c is less than or equal to c^*_{min}($c \leq c^*_{min}$), the void will appear or grow. Conversely, when the normalized atomic density c is greater than or equal to c^*_{max}($c \geq c^*_{max}$), a hillock will be generated. The values of c^*_{min} can be obtained from experiments. The criterion cited here is based on test data [60], for solder alloys $c^*_{min} = 0.85$. Another failure criterion caused due to electromigration is short circuit caused by the hillock formation at the anode end of the solder and *Cu* pad interface. In this study, hillock location could be detected from the maximum amount of mass accumulation at the interface. However, in this analysis, failure caused from hillock formation is neglected as it has been found from the literature that electromigration lifetime calculated from void formation is shorter compared to lifetime calculated from hillock formation criterion. For such reason, void formation is considered more severe reason of failure under electromigration of solder joint.

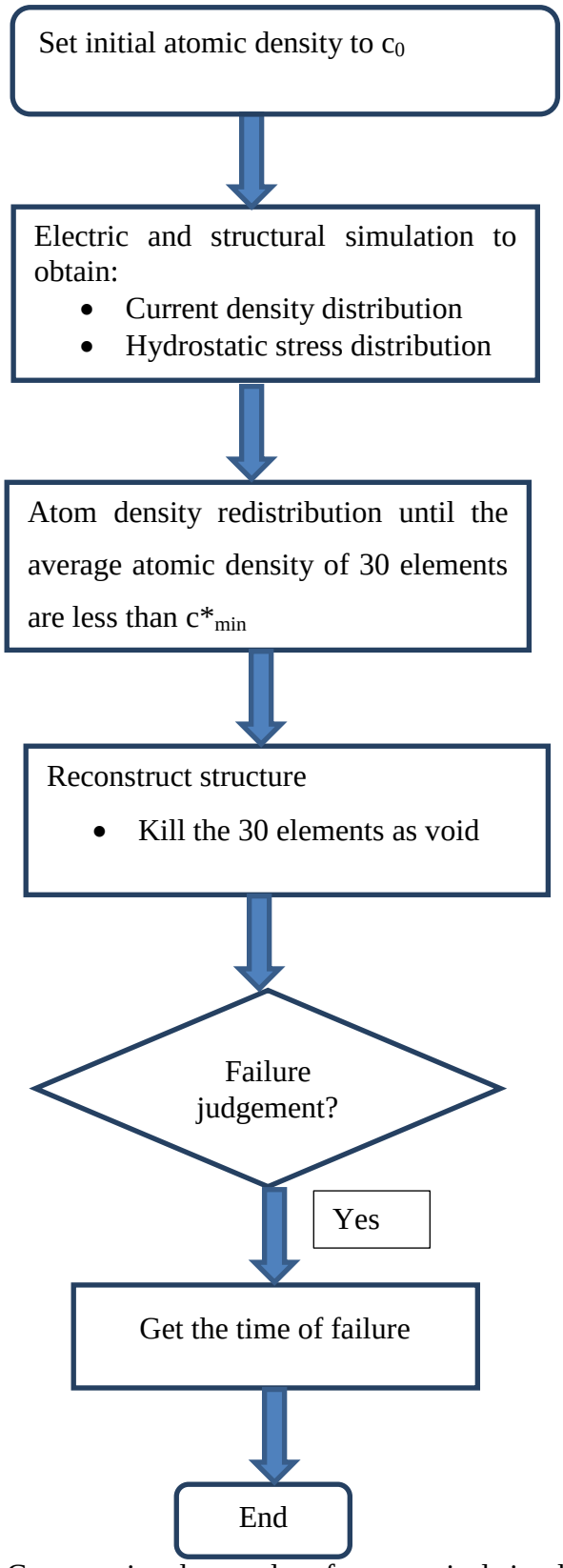

Figure 3.7 Computational procedure for numerical simulation of the EM evolution: void growth period [59]

In the simulation procedure of the void growth period, once the average atomic density value of the elements is less than the critical atomic density for void initiation c^*_{min}, the corresponding elements will be killed ("element death") and the structure, presented in Figure 3.8, needs to be reconstructed. To achieve the "element death" effect, "killed" elements aren't actually remove. Instead, it deactivates them by reducing the element material attribute, such as the elastic modulus and resistivity, by a factor of 1.0e-6.

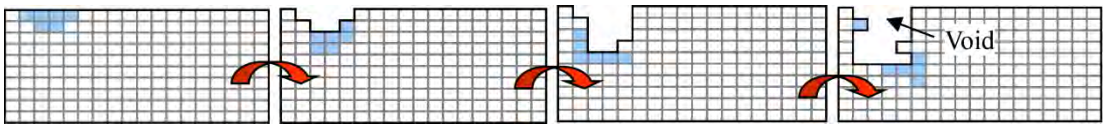

Figure 3.8 Schematic process flow of void evolution [59]

In the semiconductor industry for a FCBGA solder bump failure criterion, a 15% increment in electrical resistance of the bump is usually considered EM failure. This criterion is used in the study to get the final TTF.

3.5 Electromigration Properties

Electromigration properties of Cu, SAC and IMCs are listed as shown below. These properties are collected from [61-63].

Table 3.6 Basic Electromigration Properties

Parameter	Units	*Cu*	SAC	Cu_3Sn
Activation Energy, E_A	eV	-	0.8	-
Activation Energy, E_A	J/K-mole	210	-	83.91
Effective Charge Number, Z^*	-	-4	-23	-24.5
Diffusivity (pre-exponent), D_0	m^2/s	7.8e-5	4.1e-5	3.2e-6
Electrical resistivity, ρ_0@135°C	Ω.m	2.33e-8	17.4e-8	8.93e-8
Thermal Expansion Coefficient, α	1/K	17.1e-6	23e-6	23e-6
Atomic Volume, Ω	m^3/atom	1.182e-29	2.71e-29	2.71e-29

Electromigration properties of all SAC materials are considered similar for this study as these properties are not quite available from literature.

3.6 Simulation Methodology for Random Vibration Analysis

Combined electromigration and random vibration analysis deals the application of displacement power spectrum density on the center nodes of the base of solder joint to determine the response of the solder joint. Solid 227 element is incapable of dealing with vibration analysis. For such purpose, vibration analysis is executed using Solid 187 element capable of dealing with vibration analysis. After selecting the element, geometrical model similar to the electromigration analysis is meshed with Solid 187 element. Center nodes of the geometrical model are kept fixed to determine the natural frequencies of first few modes of the model. Modal analysis is the process of characterizing the dynamic characteristics of a structure in terms of its modes of vibration, that is, its natural frequencies, mode shapes, and modal damping ratios. These modal parameters can be determined from a set of frequency response functions acquired by exciting the structure and measuring its response at various points on its surface. These natural frequencies are used to determine the response of the model while subjected to random vibration. After determination of natural frequencies, previously fixed nodes are selected as the base nodes and acceleration PSD as shown in Figure 3.9 is applied on those base nodes for excitation purpose. Magnitude of acceleration PSD is selected in such a manner so that first few natural frequencies could not be found out within certain range to avoid resonance. Acceleration PSD is a plot of power spectrum density of acceleration with the variation of frequency. Constant damping ratio has been selected to be 2% as found from literature. After the random vibration analysis of the solder joint, Solid 187 element is turned off and Solid 227 element is used for further electromigration simulation. Electrical current is applied to the model and similar electromigration routine has been followed to determine the effect of random vibration on electromigration oriented failure. Complete simulation methodology is illustrated in Figure 3.10. Stresses induced from random vibration analysis are imposed on the geometrical model.

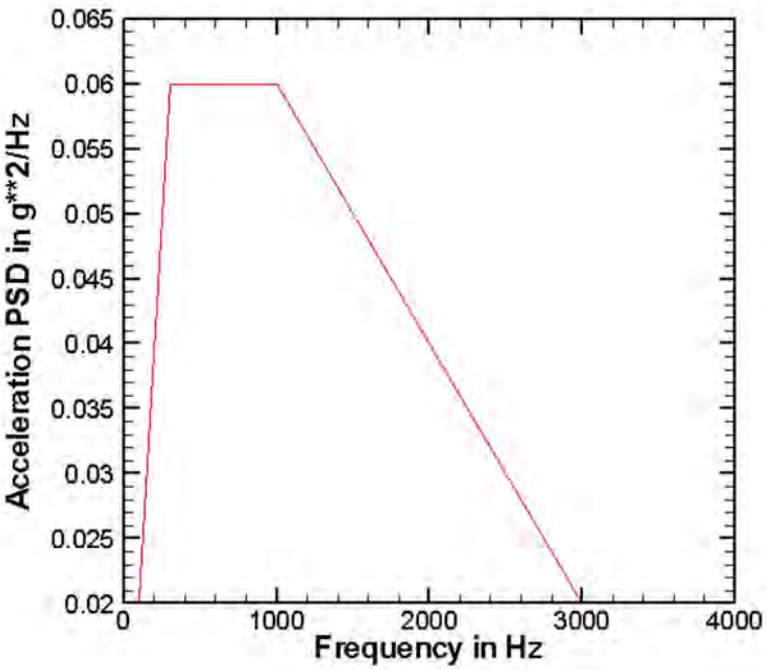

Figure 3.9 Applied acceleration PSD profile

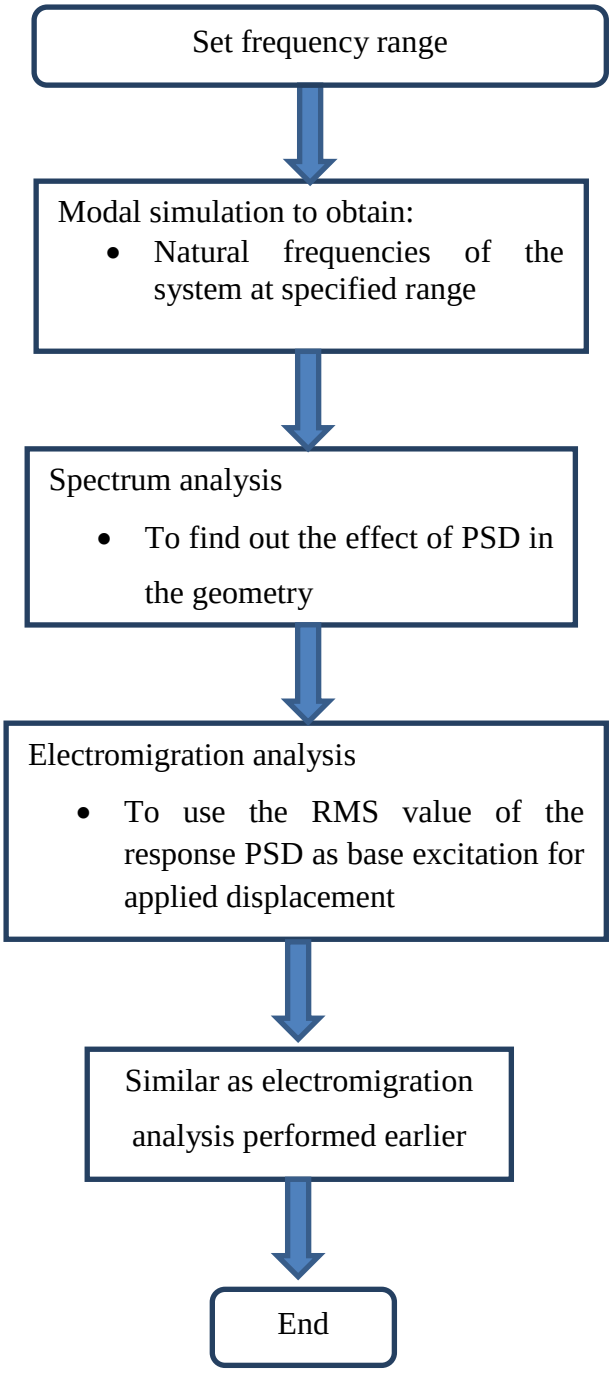

Figure 3.10 Computational procedure for combined electromigration and random vibration simulation of the solder joint

CHAPTER 4
Results and Discussions on Electromigration Analysis

This chapter discusses the electromigration results and associated reliability obtained for the *Cu*-SAC-*Cu* interconnections. The solder joints were subjected to high density electrical current and investigation of parameters relevant to the thesis objectives are recorded under higher temperature appropriate for electromigration.

4.1 Current Density Distribution in the Solder Joint

Figure 4.1(a) shows the current density distribution of a flip-chip SAC305 solder joint for current stressing of 100 hr at input current of 0.01A at a temperature of 100°C. It is observed that the initial current density is maximum (2.76×10^{7} A/m^{2}) at the left end interfacial portion of solder joint and upper *Cu* pad from where current enters the solder joint as well as the right end interfacial portion of solder joint and lower *Cu* pad from where current leaves the solder joint. Those two junctions act as the most critical location where electron accumulation is most severe due to the sharp change of geometry. This location is mostly known as “Current Crowding Zone” and this phenomenon is known as “Current Crowding Effect”. This initial current density distribution is entirely independent of material property degradation caused by thermal aging of SAC305 solder material found in this current study.

Figure 4.1(b) shows the vector plot of the current density distribution of a flip-chip SAC305 solder joint for current stressing of 100 hr at input current of 0.01A at a temperature of 100°C. It needs to be mentioned that peak value of vector plot is smaller compared to the peak value of the contour plot. It is only for the reason to contrast the maximum current conduction zone more definitively.

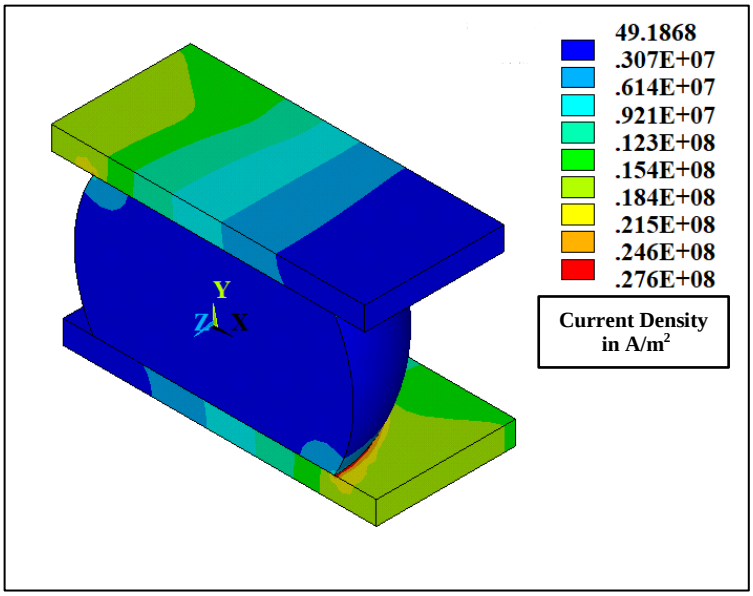

(a)

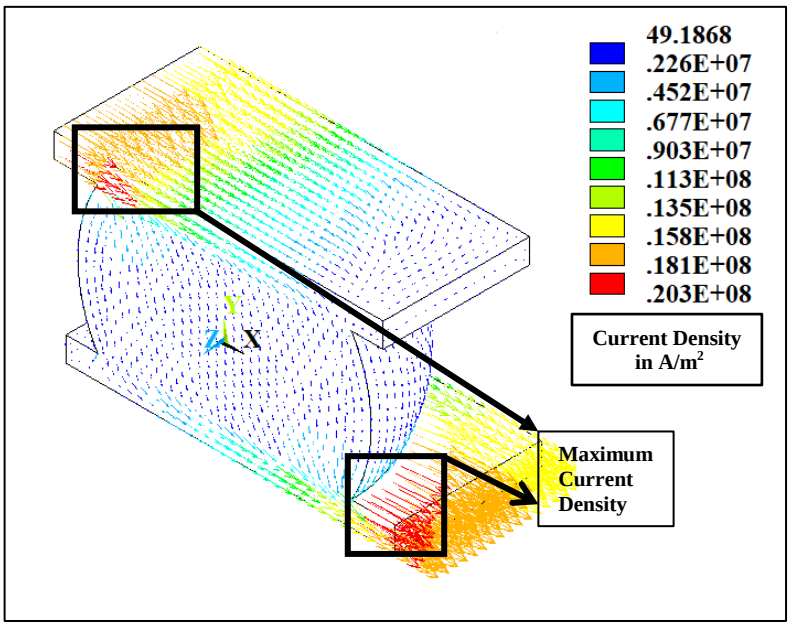

(b)

Figure 4.1 Current density distribution of a flip-chip SAC305 solder joint for current stressing of 100 hr at input current of 0.01A at a temperature of 100°C (a) Contour Plot and (b) Vector Plot

This variation in electrical current is the sole function of geometry of the solder joint and *Cu* pad interface. However, initial electrical current density varies linearly with the variation of electrical current which is verified from the plot of maximum current density variation with electrical current as shown in Figure 4.2. Electrical current density is by definition the electrical current per unit normal area. It is further observed in Figure 4.2 that the maximum electrical current density that occurs at the time of failure at solder joint seems to be function of some other parameters such as material properties etc. That is the reason for which electrical current density at the time of failure vary in a different manner compared to initial current density with the variation of electrical current. The maximum current density is observed at the bottom interface of *Cu* and SAC material where the voids coalesce to form an open circuit. This localized current density further amplifies void formation process.

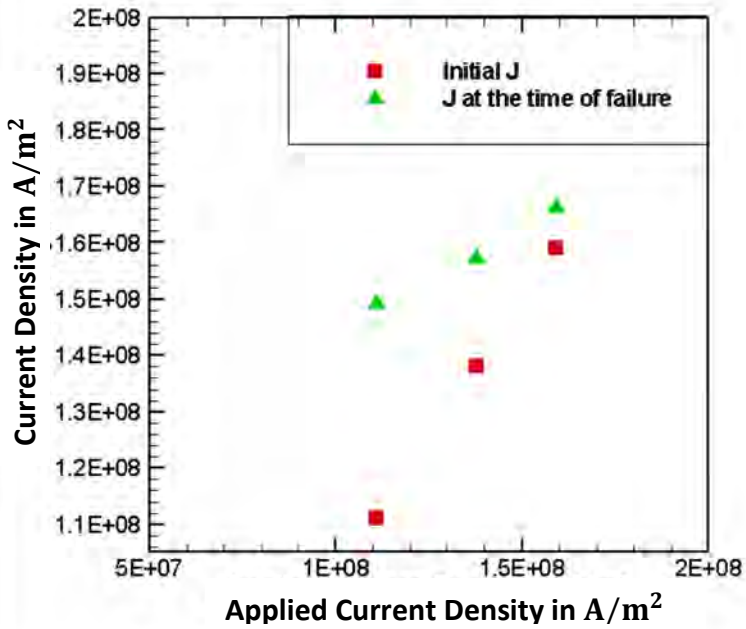

Figure 4.2 Variation of maximum initial current density (*j*) and maximum current density (*j*) at the time of failure as a function of electrical current of a flip-chip SAC305 solder joint

4.2 Effects of Current Density

4.2.1 Effects of current density on diffusion flux

The process by which, charge carriers (electrons or holes) in a semiconductor moves from a region of higher concentration to a region of lower concentration is called diffusion. The diffusion current density is directly proportional to the concentration gradient. Concentration gradient is the difference in concentration of electrons or holes in a given area. If the concentration gradient is high, then the diffusion current density is also high.

Figure 4.3 shows the maximum normalized concentration diffusion flux (normalized concentration per unit area) of a SAC305 solder joint under applied electrical current. The figure reveals that mass diffusion flux increases non-linearly with the increment of conduction current density as increased electrical current enhances more electrons to pass through the solder joint and cause subsequent mass flux.

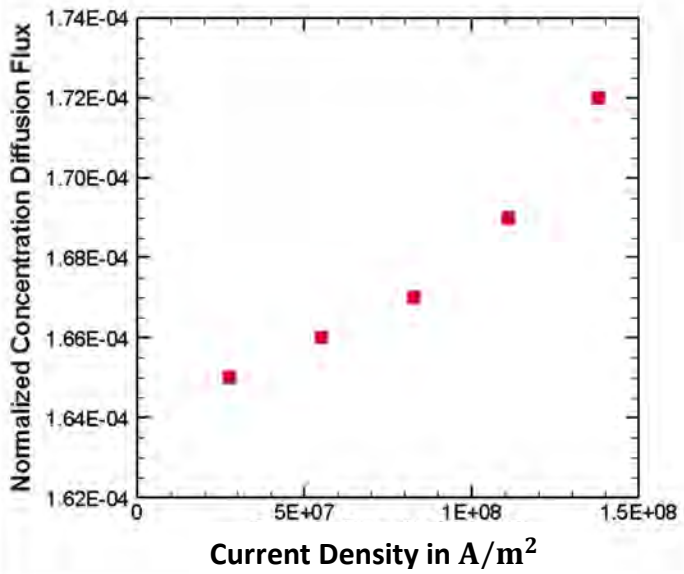

Figure 4.3 Variation of diffusion flux with applied current density for unaged SAC 305 solder joint

4.2.2 Effects of current density on plastic work per volume (PLWK)

A specimen accumulates plastic work whenever it is subjected to external loads and undergoes plastic deformation due to the presence of constraints. In this current study as stated earlier, it has been confirmed to possess plastic deformation of the model under the application of electrical current. This plastic deformation is caused by the stress generated by the stress migration due to electromigration and due to the external constraints applied on the model. Figure 4.4 shows the PLWK distribution of a flip chip SAC solder joint subjected to electrical current of 0.01A under isothermal pre-aged condition. This plot reveals that maximum PLWK occurs at the corner edges of the solder joint at which the electrical current enters and leaves the solder joint. Those are the critical locations where void formation is most prominent due to the current crowding effects. Most of the region of the solder joint is somehow showing no sign of PLWK generation. The cause of such distribution can be explored by the movement of electron through the solder joints. Electrons tend to pass through the minimal resistance zones of the solder joint and thus get crowded at the interfaces. And that's the prime cause of absolutely zero PLWK at significant portion of space in solder joint.

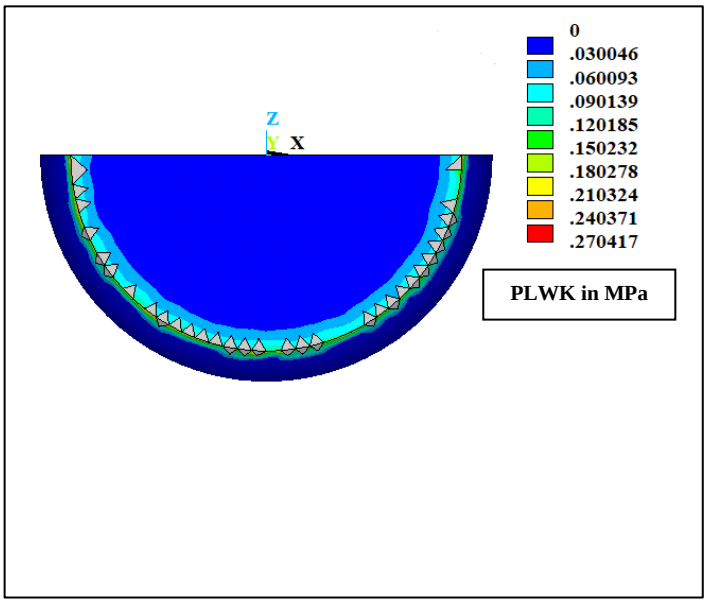

(a)

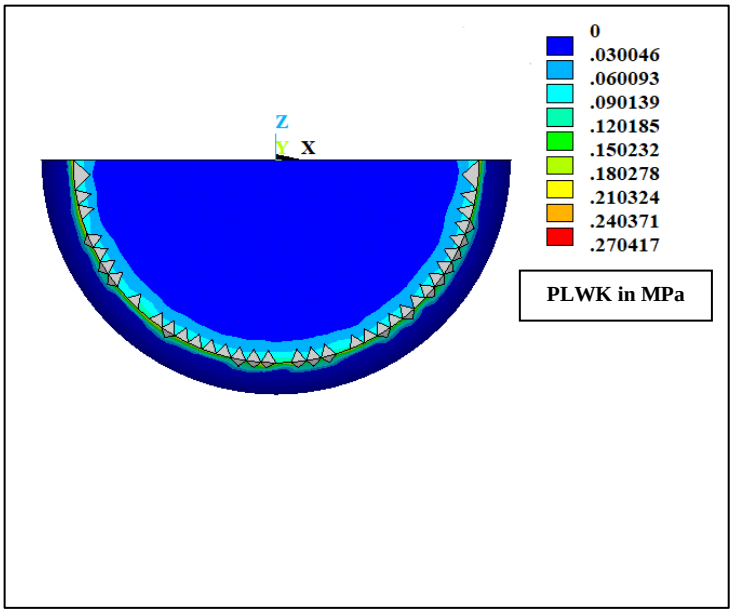

(b)

Figure 4.4 Plastic Work per Volume distribution (PLWK) of a flip-chip SAC305 solder joint for current stressing of 100 hr at an input current density of (a) 2.76×10^7 A/m^2 (b) 8.28×10^7 A/m^2 at an experimentation temperature of 100°C for unaged condition

Figure 4.4(a) and 4.4(b) contrasts between PLWK distribution of two solder joints subjected to same aging condition but different electrical currents applied on the solder joint. It can be observed from those two plots that both of the solder joints PLWK distribution is actually similar except the numerical values that is attained in each of the cases. Higher amount of PLWK is observed in case of input current, I=0.03A. This finding can be explained in terms of stress migration as more electron transports more amount of mass from cathode side to anode side. That's why more accumulation of mass takes place at the anode side transported from the cathode side. Thus, about 10% more tensile and compressive stresses occur at the interfaces of solder joint and *Cu* pads. Figure 4.5 shows the variation of maximum diffusion flux with electrical current density. The plot reveals that PLWK is increased with the increment of current density.

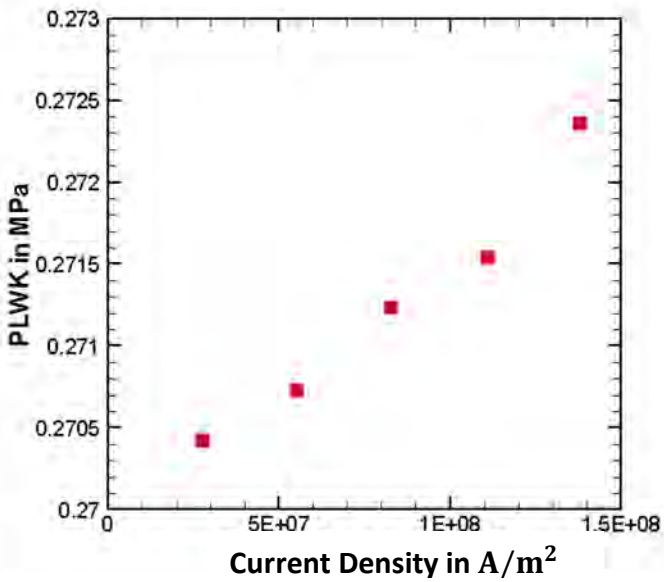

Figure 4.5 Maximum PLWK at different value of current density at unaged condition at experimentation temperature of 100°C for SAC305 solder material

4.3 Effects of Ambient Temperature

4.3.1 Effects of ambient temperature on diffusion flux

Ambient temperature plays a significant role on diffusion flux distribution of SAC solder joint. Figure 4.6 shows the normalized concentration diffusion flux distribution for unaged SAC305 solder joint at elevated temperature of 100°C and 125°C. As the plot reveals, with the increment of solder joint ambient temperature from 100°C to 125°C, diffusion flux increases about 6-8 times. Atomic mobility term is mathematically represented as $exp(\frac{-E_A+\Omega\sigma_H}{RT})$ as mentioned from Arrhenius law. From this expression it can be observed that with the increment of temperature, atomic mobility increases which in turn increases the atomic diffusivity of the component materials present in the electronic packages. As the expression varies exponentially with the increment of temperature, electromigration oriented mass diffusion increases exponentially.

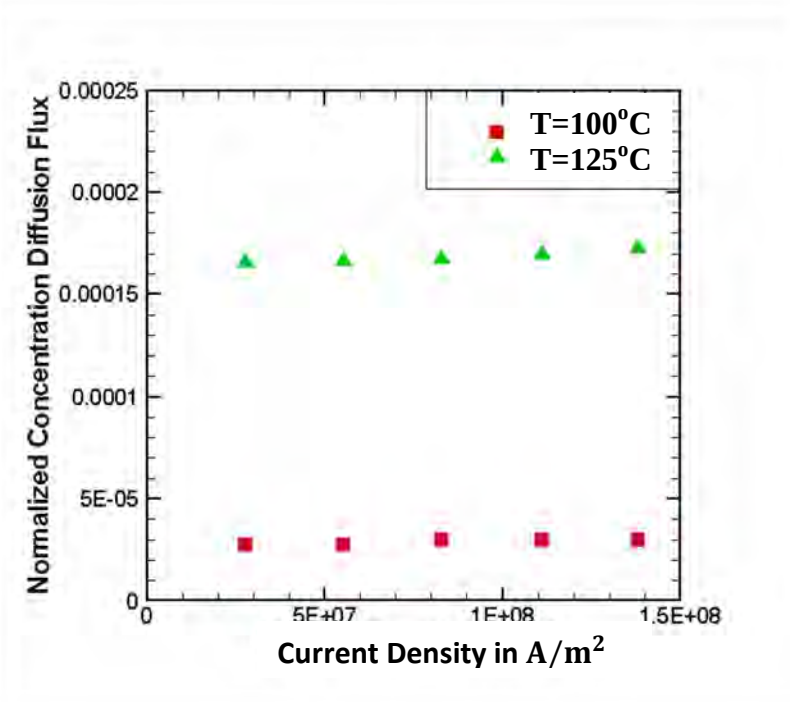

Figure 4.6 Maximum diffusion flux at different value of current density at unaged condition for different values of ambient temperature for SAC305 solder material

Accordingly, whenever the solder joint temperature increases above 100°C, grain boundary diffusion becomes prominent in solder joints. Diffusivity of metal ions gets increased exponentially due to the increment of temperature. Due to this reason, the metallic ions diffuse more rapidly in those cases where ambient temperature is elevated. Therefore for the solder joints subjected to higher temperature are more prone to failure due to electromigration [55].

4.3.2 Effects of ambient temperature on PLWK

Ambient temperature plays an important role in electromigration oriented failure. It can reduce time to failure of a solder joint subjected to electromigration significantly. Figure 4.7(a) and Figure 4.7(b) compares two flip chip solder joints subjected to same electrical current of 0.03A under unaged conditions but experimented at elevated temperatures of 100°C and 125°C for grain boundary diffusion. Comparison of those two cases shows that Magnitude of plastic work dissipation is quite higher in case of higher value of temperature. Figure 4.8 shows

maximum PLWK at different values of electrical current densities at different ambient temperatures. The plot reveals that with the increment of ambient temperature, PLWK increases significantly.

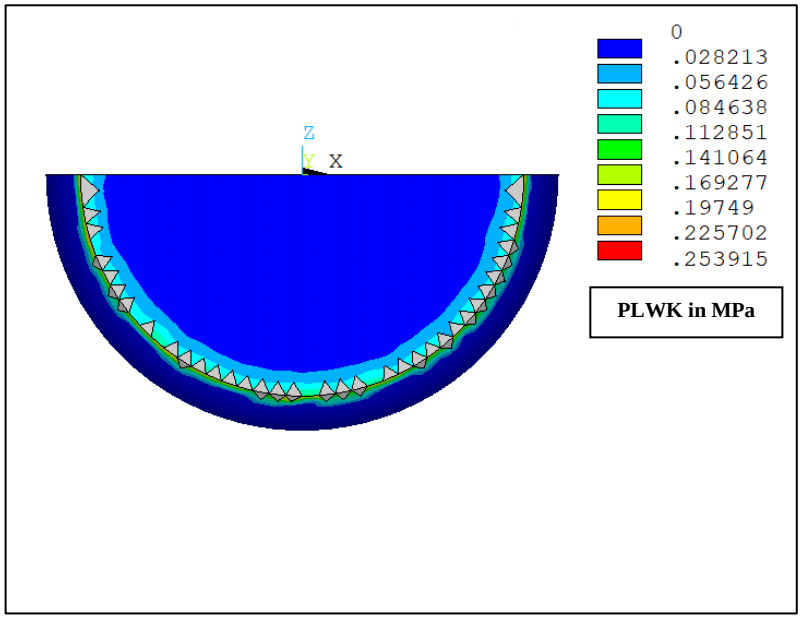

(a)

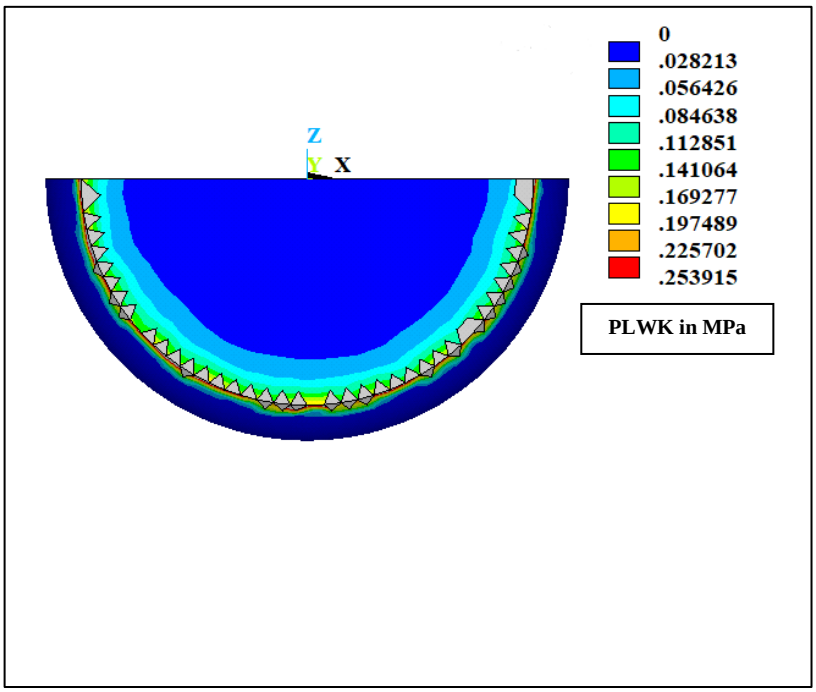

(b)

Figure 4.7 Plastic Work per Volume distribution (PLWK) of a flip-chip SAC305 solder joint for current stressing of 100 hr at input current density of 8.28×10^7 A/m^2 at an experimentation temperature of (a) 100°C and (b) 125°C at unaged condition

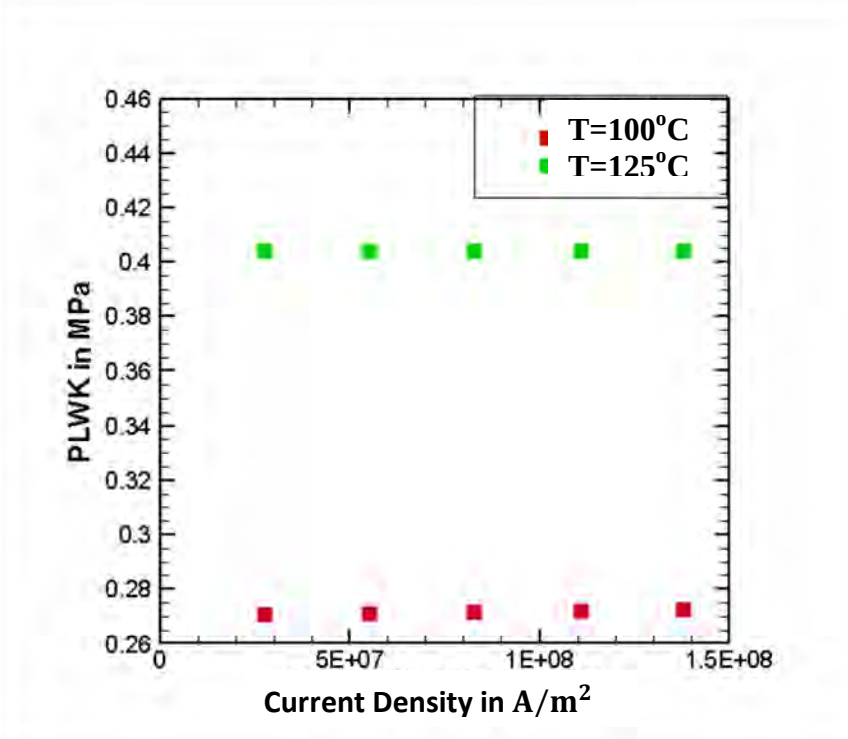

Figure 4.8 Maximum PLWK at different value of current density at unaged condition for different values of ambient temperature for SAC305 solder material

4.4 Effects of Thermal Aging

4.4.1 Effect of thermal aging on diffusion flux

Figure 4.9(a) shows the variation of maximum diffusion flux at the current crowding region with the current density can be observed under various aging conditions subjected to different electrical current for 100 hr at 100°C. This distribution shows that diffusion flux has a proportional relation with the electrical current density meaning more electron passing through the SAC solder joint.

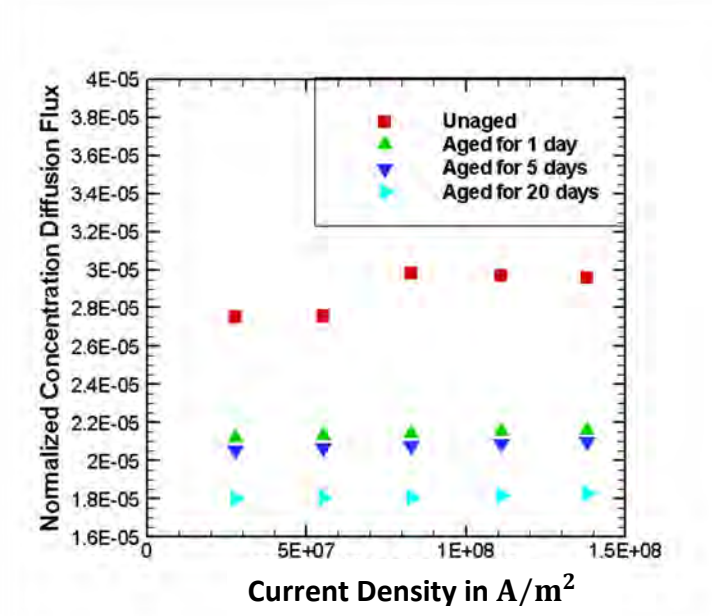

(a)

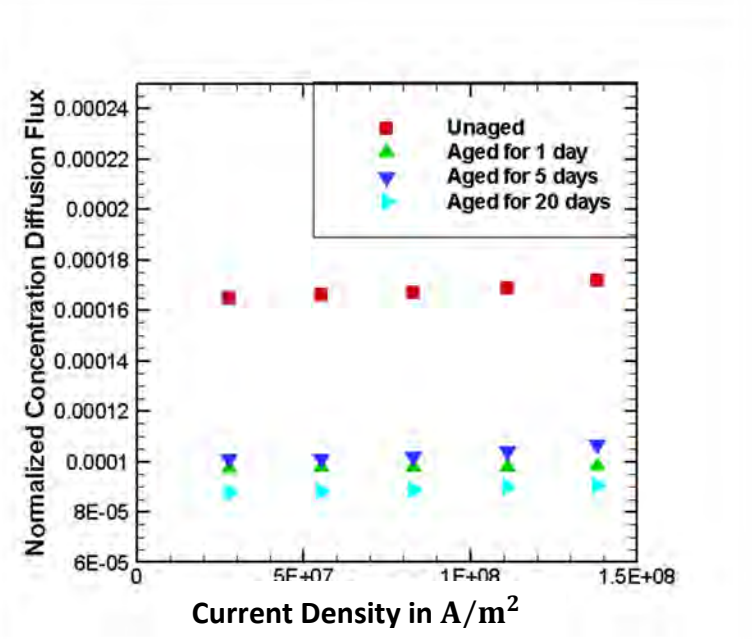

(b)

Figure 4.9 Variation of diffusion flux with electrical current density at different thermal aging conditions of a flip-chip SAC305 solder joint for current stressing of 100 hr at an electromigration temperature of (a) 100°C and (b) 125°C

From Figure 4.9(a), it can be observed that with the increment of aging time from 24 hour to 480 hour, the maximum diffusion flux decreases by approximately 20%. The cause of such reduction can be explained in terms of dislocation along the grain boundary and it's impact on grain boundary diffusion rate. It is reported in literature that increment in aging time reduces grain boundary area which in turn reduces mass diffusion flow of *Sn* in SAC solder matrix. Additionally, from Figure 4.9(b) increased amount of diffusion flux can be observed at higher electromigration temperature (125°C) due to the increased amount of kinetic energy obtained due to electron movement at higher temperature. So, it can be concluded that pre aging of solder significantly reduces the diffusion flux of solder joint. Figure 4.10 shows the diffusion flux distribution at I=0.03A at different aging conditions for a SAC305 solder joint are observed. These plots reveal that diffusion flux is the most critical at the junction between *Cu* pad and the solder joint.

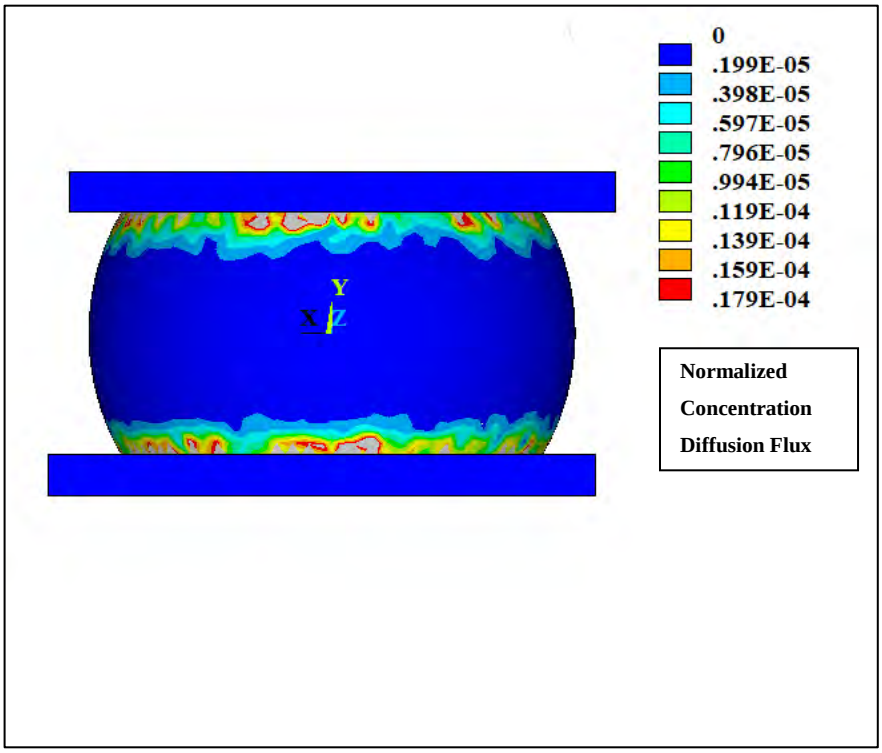

(a)

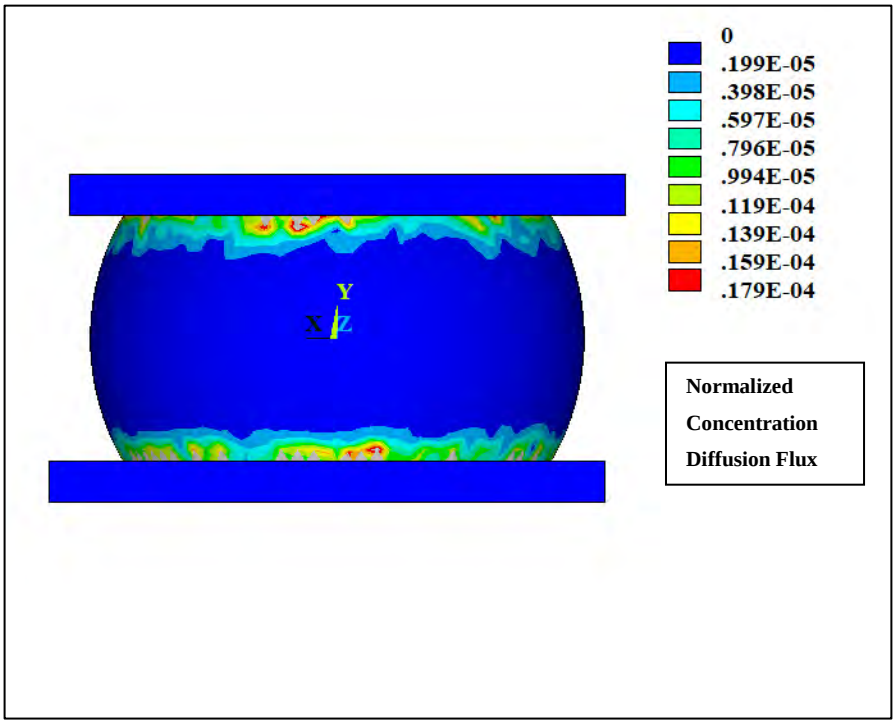
0
.199E-05
.398E-05
.597E-05
.796E-05
.994E-05
.119E-04
.139E-04
.159E-04
.179E-04
Y
X
Z
Normalized
Concentration
Diffusion Flux

(b)

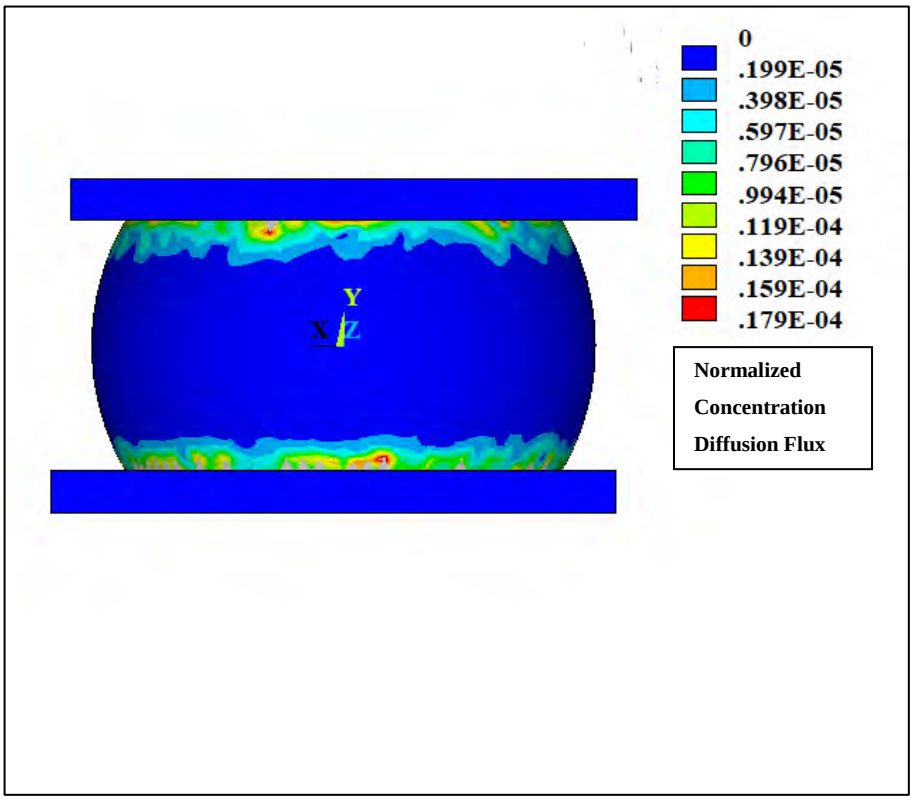
0
.199E-05
.398E-05
.597E-05
.796E-05
.994E-05
.119E-04
.139E-04
.159E-04
.179E-04
Y
X
Z
Normalized
Concentration
Diffusion Flux

(c)

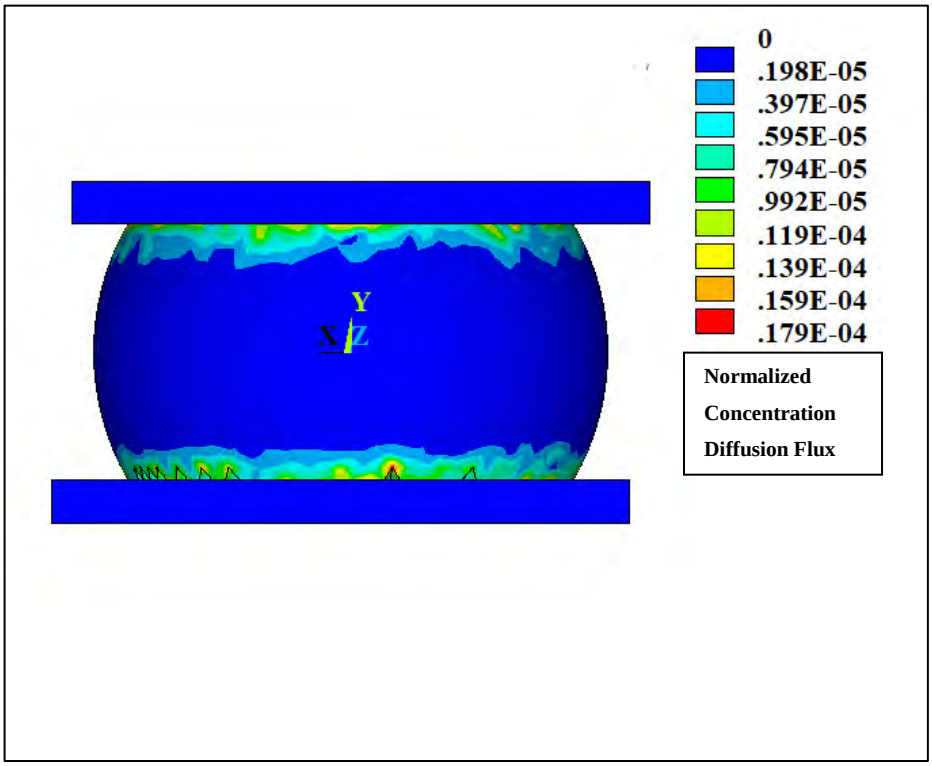

(d)

Figure 4.10 Diffusion Flux distribution at electrical current density of 8.28×10^7 A/m^2 of a flip-chip SAC305 solder joint for current stressing of 100 hr at electromigration temperature of 100°C at aging duration of (a) 0 day, (b) 1 day, (c) 5 days and (d) 20 days

These plots reveal that diffusion flux is the most critical at the junction between *Cu* pad and the solder joint. This is due to the presence of flux divergence caused by the current crowding and interfacial geometry between *Cu* pad and SAC solder joint. Additionally, from these Figures, effect of aging condition on electromigration oriented mass diffusion for same electrical current and experimentation time can be observed. Normalized concentration diffusion flux reduced from 2.77×10^{-5} $\mu m^{-2}s^{-1}$ to 2.14×10^{-5} $\mu m^{-2}s^{-1}$ after the first day of isothermal aging at 100°C which is about 23% reduction from the unaged value. However, the normalized concentration diffusion flux reduced by 28% and 36% from the unaged value for 5 and 20 days of aging respectively. It suggests the diffusion flux changes dramatically during the first few days of aging and then slows down with longer aging times.

4.4.2 Effects of thermal aging on PLWK

As stated earlier, thermal aging deteriorates mechanical properties (both elastic and plastic structural properties) of SAC305 solder interconnects. Actually, any type of change in electromigration induced stress is a direct consequence of change in microstructure as found from the literature [65]. In case of thermal aging, a significant change in the microstructure of SAC solder material is observed which affects the electromigration oriented mass diffusion in turn. Here, in this study, thermal aging symbolizes isothermal aging maintained at a constant temperature of $100^{o}C$ in which SAC solder material undergoes microstructure evolution. Additionally, thermal aging causes coarsening of microstructures in SAC solder materials. Boundary of Ag_3Sn and Cu_6Sn_5 intermetallic compounds gets detached from each other and *Sn* based granules get coarsened [66]. This coarsening of *Sn* based granules is the prime source of deterioration of mechanical properties in SAC materials. These coarsening causes to reduce the resistance of SAC material to deform plastically when loaded. This property degradation can affect electromigration oriented diffusion significantly.

From Figure 4.11 it can be observed that maximum value of PLWK reduces approximately 43% whenever aging time is increased from 0 day to 20 days. Now the cause of such reduction in PLWK can be explained from the point of view of diffusion in metallic ion. Whenever aging causes degradation in elastic and plastic properties of SAC305 materials, this degradation directly affects the diffusion pattern of these materials. At a high temperature, the diffusion process is predominantly governed by the grain boundary diffusion process of SAC305 material. Fundamentally thermal aging causes degradation of SAC305 material by coarsening its *Sn*-rich grain and reducing the amount of grain boundary of Ag_3Sn and Cu_6Sn_5 present. However, this physical change advertently proves beneficiary to the electromigration as reduction in grain boundary area causes reduction in grain boundary diffusion rate required for electromigration to occur [65]. For such reason, the reduction in PLWK is observed and subsequent failure from electromigration is somehow delayed by the inclusion of thermal aging. However, the question regarding the optimum period of isothermal thermal aging time is yet to be answered.

It has been observed from the current study that the change in PLWK is not much severe from 1 day aging to several days of aging. Figure 4.12 shows the variation of maximum PLWK as a function of current density at various aging conditions. This plot signifies that the change in the value of PLWK is quite extreme for the comparison between unaged and aging time of 1 day. After that sharp decrease of approximately 30% in value of PLWK, only 3% and 14% decrease are observed for the increment of aging time from 1 day to 5 days and 20 days respectively. So, it seems that thermal aging oriented property degradation rate gets slower at longer aging times.

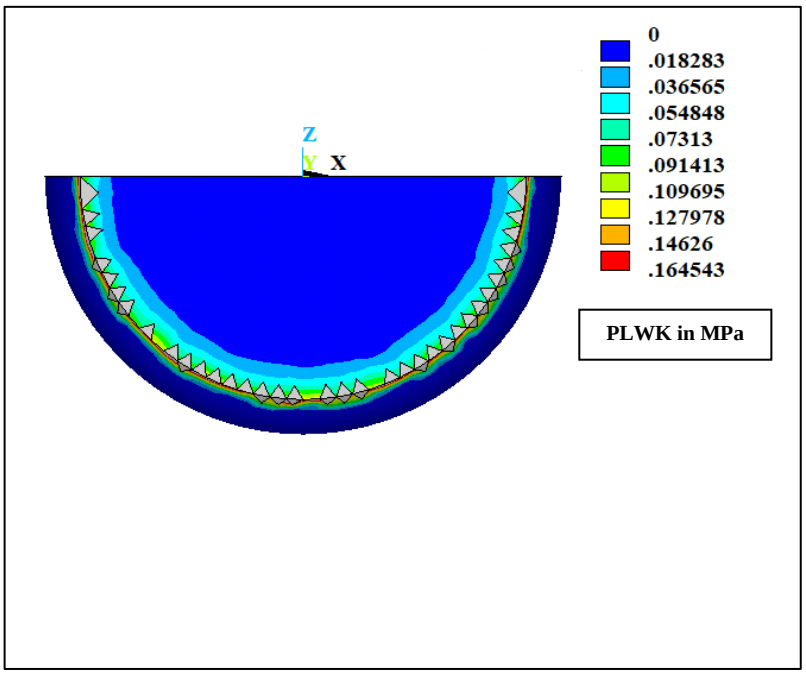

(a)

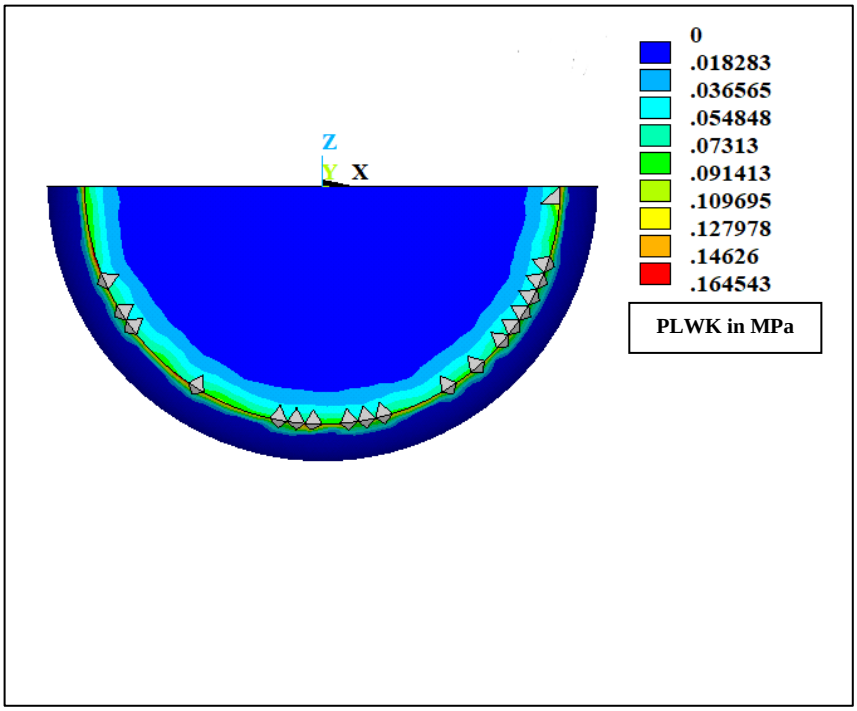
Z
Y
X
0
.018283
.036565
.054848
.07313
.091413
.109695
.127978
.14626
.164543
PLWK in MPa

(b)

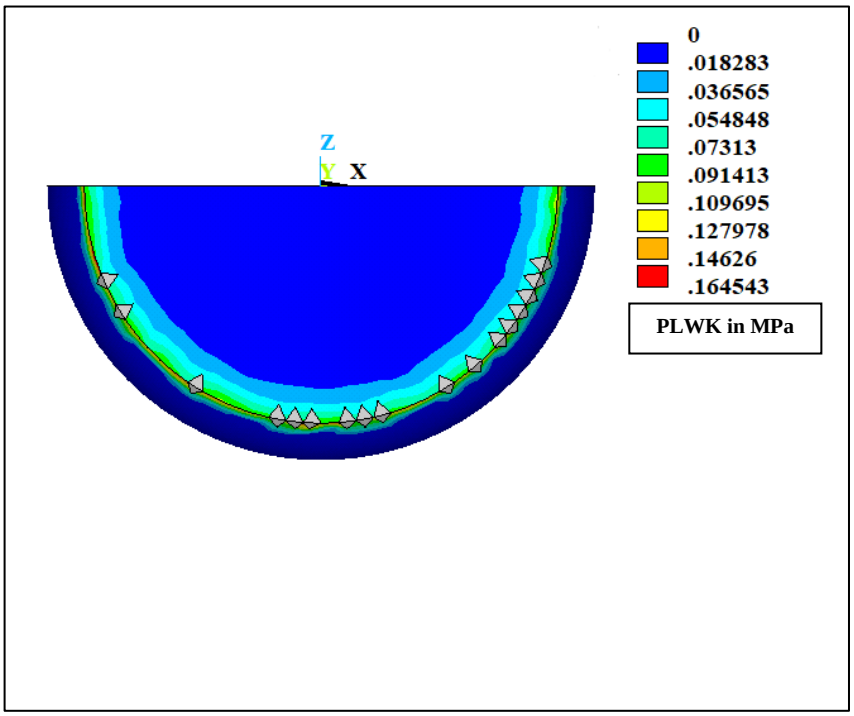
Z
Y
X
0
.018283
.036565
.054848
.07313
.091413
.109695
.127978
.14626
.164543
PLWK in MPa

(c)

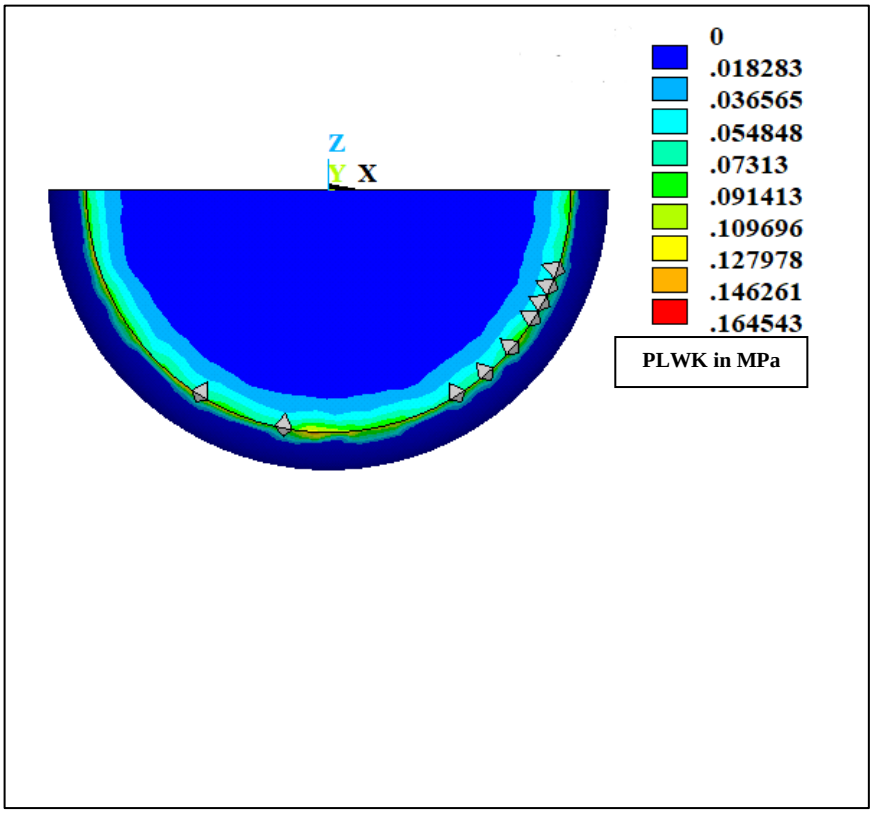

(d)

Figure 4.11 Plastic Work per Volume distribution (PLWK) of a flip-chip SAC305 solder joint for current stressing of 100 hr at input current density of 8.28×10^7 A/m^2 at a temperature of 100°C for isothermal aging period of (a) 0 day, (b) 1 day, (c) 5 days and (d) 20 days

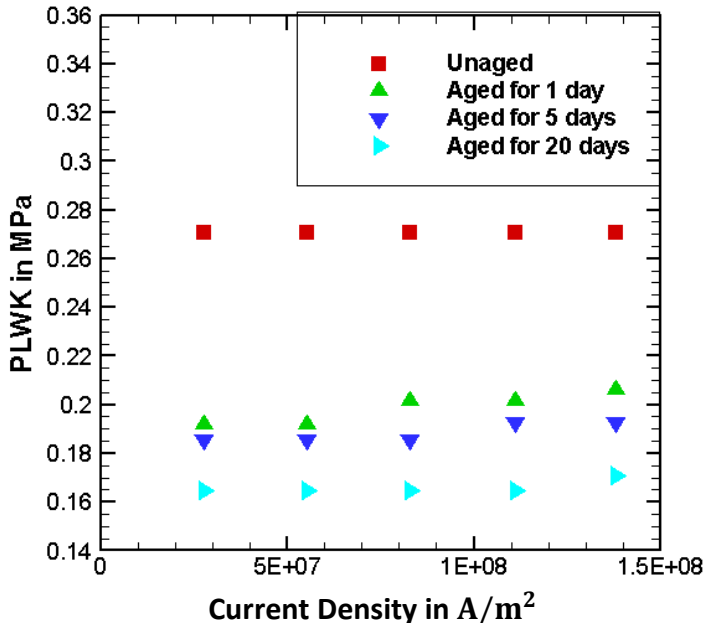

Figure 4.12 Maximum Plastic Work per Volume (PLWK) of a flip-chip SAC305 solder joint for current stressing of 100 hr at different values of input current at a temperature of 100°C for isothermal aging for different aging conditions.

4.5 Effects of *Ag* percentage

4.5.1 Effects of *Ag* percentage on diffusion flux

Ag percentage plays an important role in mass diffusion through SAC solder joint. With an increment in the amount of *Ag* from 1% to 3% while keeping the *Cu* content same in SAC material, significant improvement in mechanical strength of solder material takes place. This improvement in mechanical strength as well as elastic modulus is the consequence of the grain boundary thickening due to the formation of Ag_3Sn at the grain boundaries. These thick grain boundaries actually dominate the grain boundary diffusion in SAC solder joint material. With the increment in Ag_3Sn with increased amount of *Ag,* mass diffusion rate due to electromigration increases significantly. As observed from Figure 4.13, diffusion flux increases about 70% and 100% when *Ag* content is increased from 1% to 2% and 3% respectively. Suh et al. [67] studied the effects of bulk properties under impact tests for the SAC alloys with different *Ag* content, showing that the bulk properties of SAC alloys have profound effects on high-strain rate fracture resistance. Lowering *Ag* content was found to be highly effective in increasing bulk

compliance and plastic energy dissipation ability, resulting in performance enhancement in drop testing. Che et al. [64] showed that variation in structural properties of SAC solder joint materials are merely a function of their *Ag* percentage present in SAC material which directly influences the microstructure of the SAC material. In case of increased amount of *Ag* in SAC material, Ag_3Sn and Cu_6Sn_5 intermetallic is formed in a significant amount which act as a boundary and suppresses to resist any sort of plastic deformation in SAC material of higher *Ag* percentage.

The overall reliability, however, can be greatly affected by the amount and size of the Ag_3Sn intermetallic in the microstructure. This structure of Ag_3Sn is significant as it can also affect mechanical properties negatively. The large Ag_3Sn intermetallic is generally believed to be detrimental in both crack initiation and propagation, with numerous studies having attributed failure in SAC305 solder to large plate-like Ag_3Sn intermetallics under impact and thermal cycling stimuli [68-70]. These effects become more critical when the solder volume becomes smaller, e.g. flip-chip solder bumps.

From Figure 4.14, variation of electromigration oriented mass diffusion in terms of *Ag* percentage is summarized for study. The plot reveals that diffusion flux is the maximum for the *Ag* percentage of 3%. This finding can be explained in terms of mass diffusion caused by thickening of grain boundary with increased amount of Ag_3Sn produced from the increased *Ag* content present in SAC alloy as shown in Figure 4.15. This increment in *Ag* percentage in turn increases mechanical strength and results better stress-strain relationship. However, electromigration oriented mass diffusion is prominent in case of the microstructures where the grain boundary area is maximum and causes more diffusion through the disorder propagating along the grain boundaries. Figure 4.16 shows the variation of diffusion flux with the variation of aging time for different *Ag* percentages.

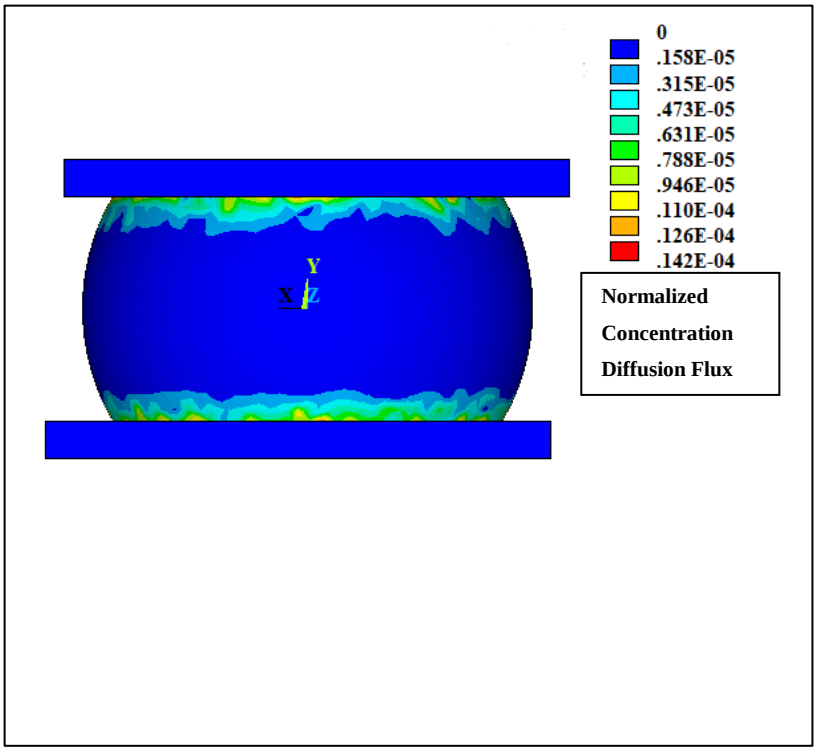
0
.158E-05
.315E-05
.473E-05
.631E-05
.788E-05
.946E-05
.110E-04
.126E-04
.142E-04
Normalized
Concentration
Diffusion Flux
Y
X
Z

(a)

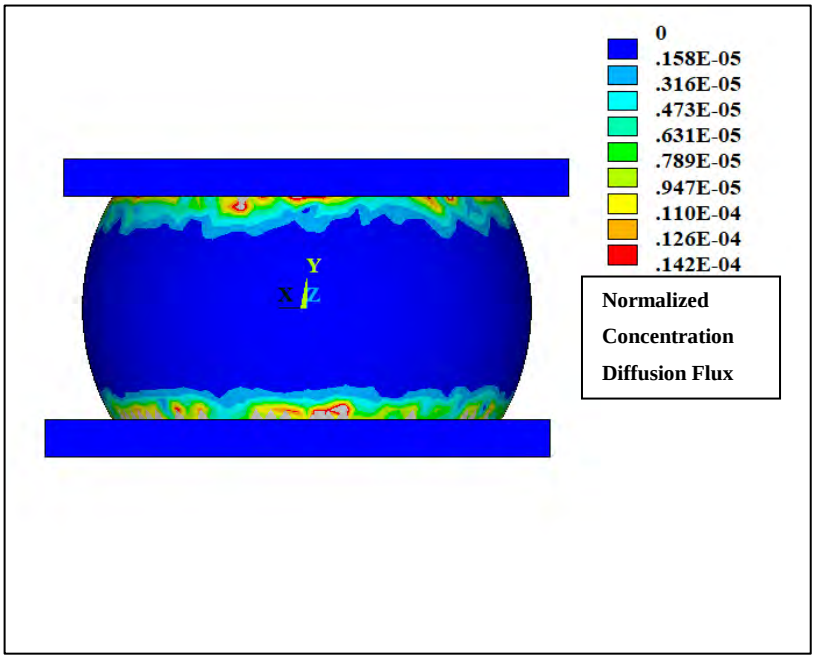
0
.158E-05
.316E-05
.473E-05
.631E-05
.789E-05
.947E-05
.110E-04
.126E-04
.142E-04
Normalized
Concentration
Diffusion Flux
Y
X
Z

(b)

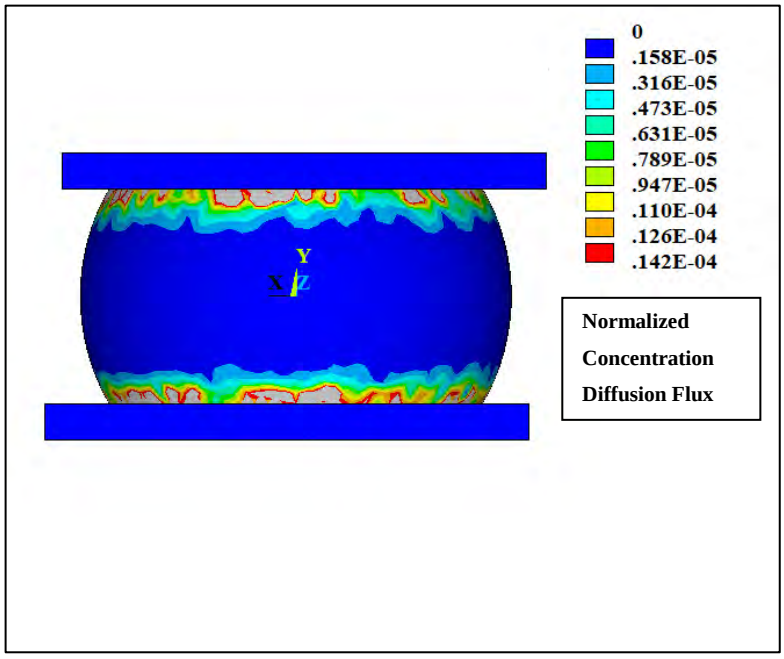

(c)

Figure 4.13 Diffusion Flux distribution at electrical current density of 8.28×10^7 A/m^2 of a flip-chip SAC solder joint for current stressing of 100 hr at electromigration temperature of 100°C at unaged condition for *Ag* percentage of (a) 1%, (b) 2% and (c) 3%

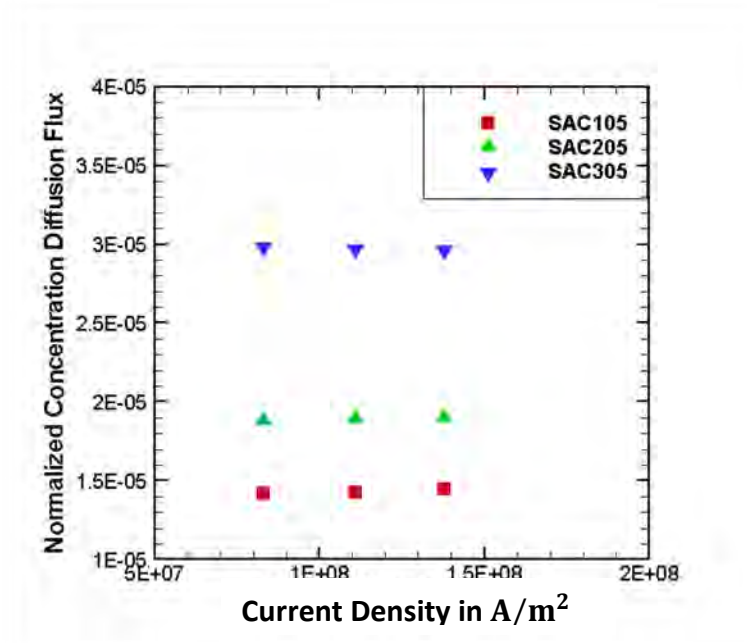

(a)

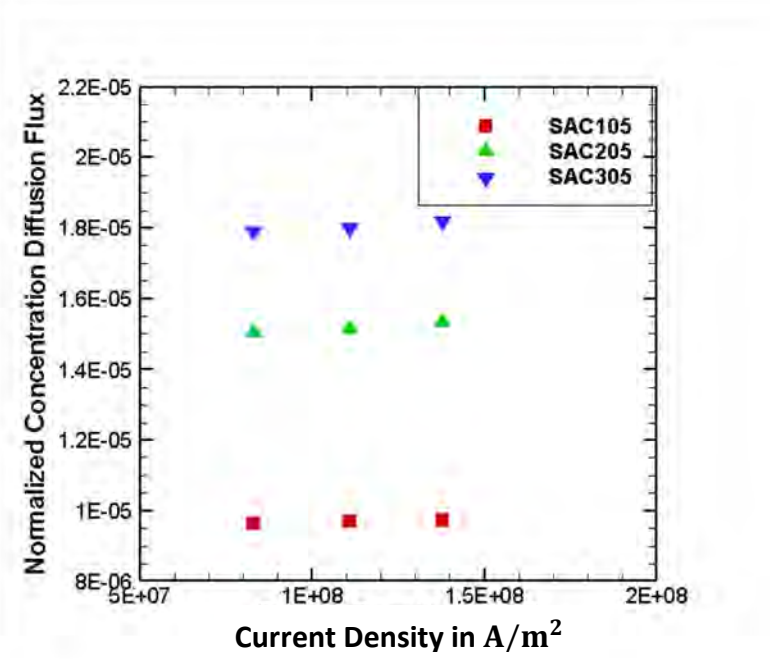

(b)

Figure 4.14 Variation of diffusion flux with electrical current density of a flip-chip SAC solder joint for current stressing of 100 hr at an electromigration temperature of 100°C at thermal aging duration of (a) 0 hour and (b) 480 hours

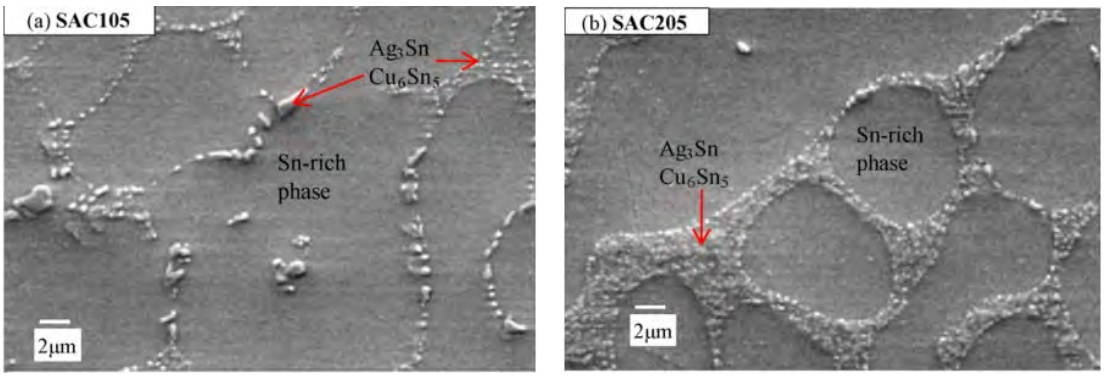

(a) (b)

Figure 4.15 SEM images of the microstructure of SAC solders a) SAC105 and b) SAC205 [71]

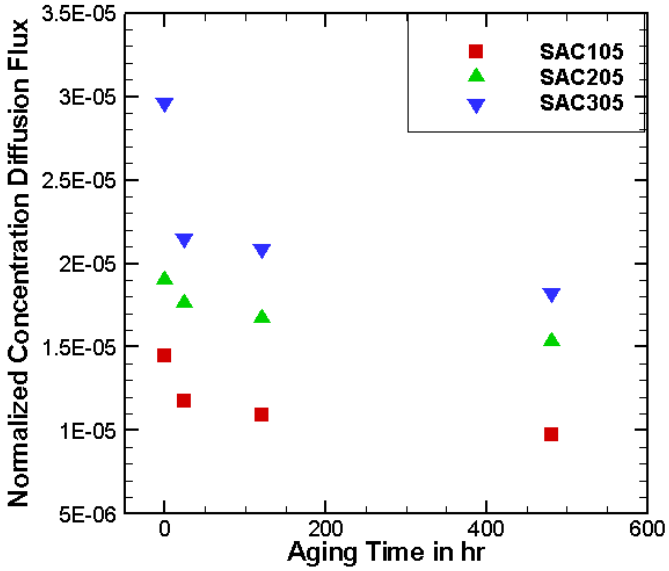

Figure 4.16 Variation of diffusion flux with the variation of *Ag* percentages of SAC material at different isothermal aging conditions at 100°C

4.5.2 Effects of *Ag* percent*age* on PLWK

Ag percentage in SAC solder material plays a significant role in the determination of mechanical property of SAC material. In this study, variation of electromigration oriented mass diffusion is observed with the variation of *Ag* percentage. All the mechanical properties used in this study is collected from Che et al. [64].

Figure 4.17 shows that mechanical property improvement due to the addition of *Ag* in SAC material actually reduces the electromigration performance of a flip-chip SAC solder joint. Here, Inclusion of *Ag* from 1% to 2% has increased the PLWK upto 50% whereas it has risen about 120% if the *Ag* content is 3% of the SAC composition. It is due to the increased amount of Ag_3Sn formed from the presence of increased amount of *Ag*. So it can be definitely stated that increased *Ag* percentage reduces electromigration life of SAC solder joint. The reason behind the findings is that more diffusion takes place with increased *Ag* percentage which creates more voids meaning increment of local stresses which in turn increases PLWK.

In Figure 4.18, PLWK is plotted against various current densities for different percentages of *Ag* content. From this plot, it could be acknowledged that *Ag* percentage variation affects PLWK of a SAC solder joint under electrical current significantly. This maximum PLWK is observed for the SAC305 solder material where *Ag* percentage is kept 3%. Actually, better mechanical or structural properties ensure better strength or resistance at thermal cycling and experimentation of shear stress of these solder joints. However, this improvement in mechanical property reduces electromigration resistant performance tremendously as found in the study. Figure 4.19 shows the variation of PLWK with the variation of aging time for different *Ag* percentages.

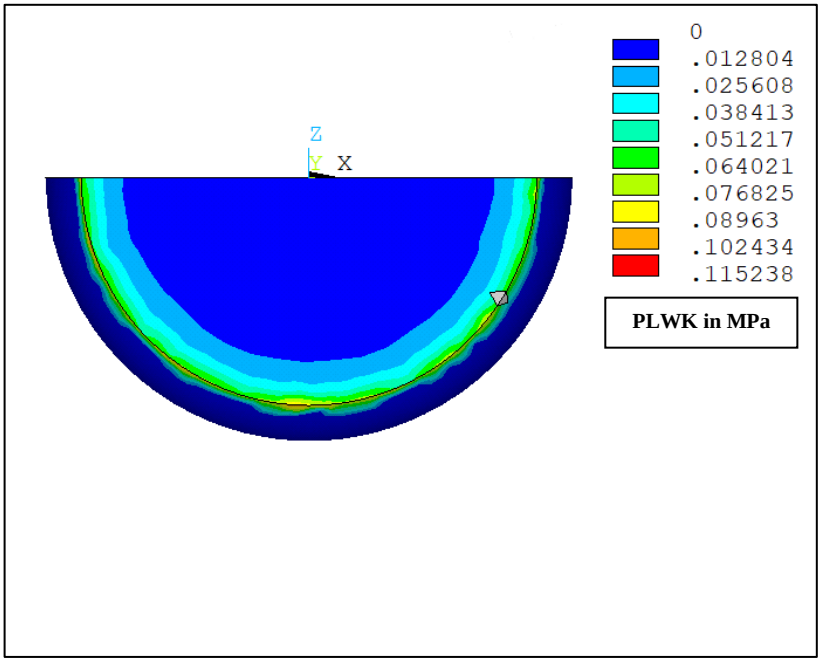

(a)

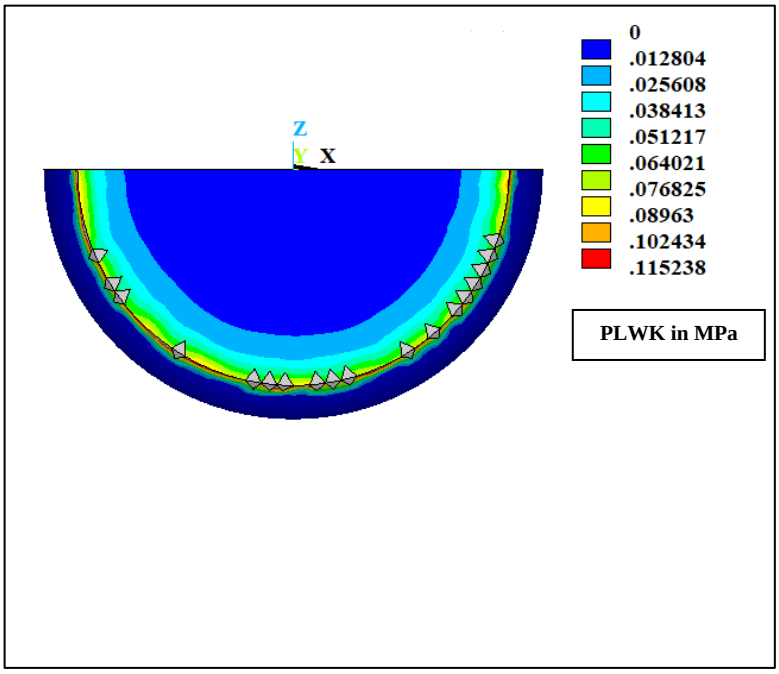

(b)

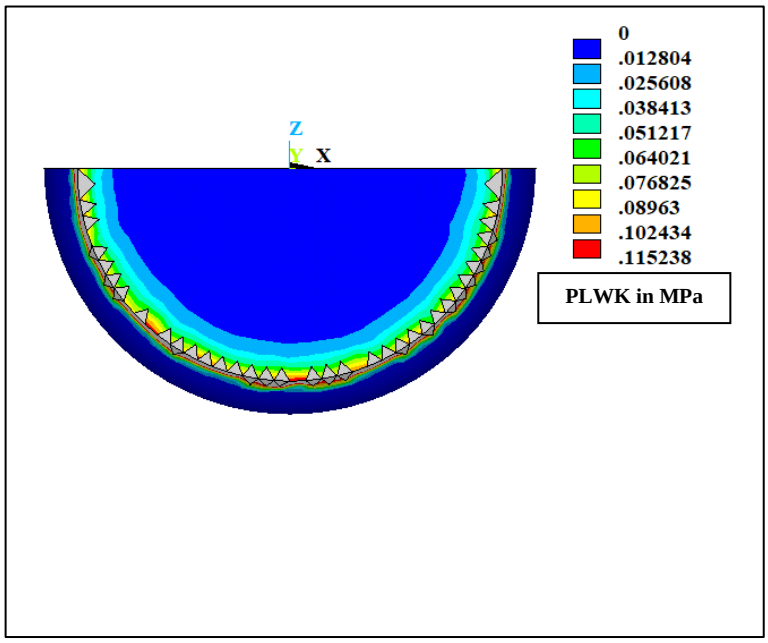

(c)

Figure 4.17 PLWK Distribution at electrical current of I=1.11 × 10^8A/m^2 A of a flip-chip SAC solder joint for current stressing of 100 hr at an electromigration temperature of 100°C for unaged condition for *Ag* percentage of (a) 1% , (b) 2% and (c) 3%.

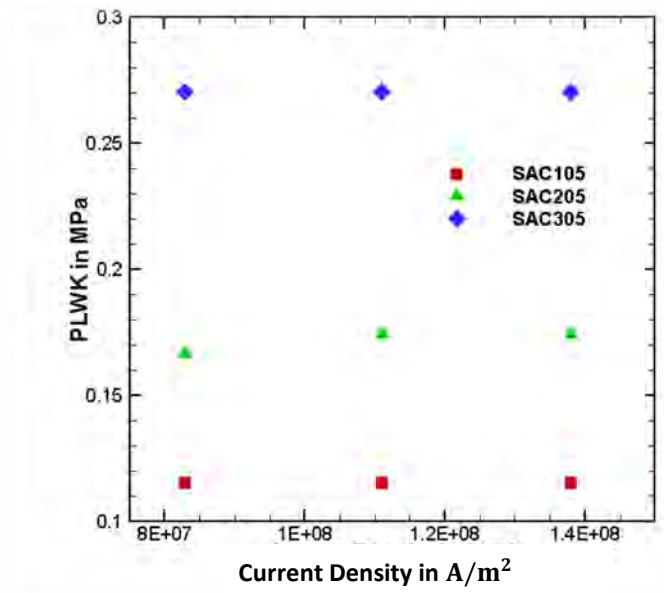

(a)

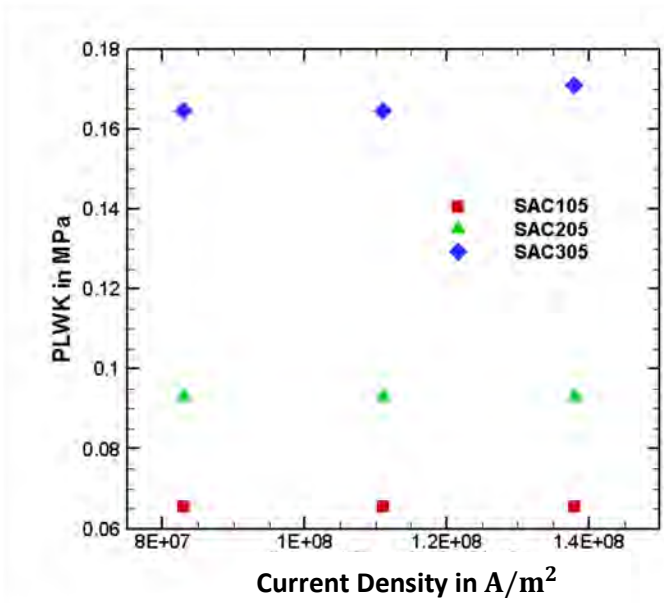

(b)

Figure 4.18 Variation of PLWK with electrical current density at different *Ag* percentage of a flip-chip SAC solder joint for current stressing of 100 hr at an experimentation temperature of 100°C for an aging period of (a) 0 hour and (b) 480 hour at 100°C

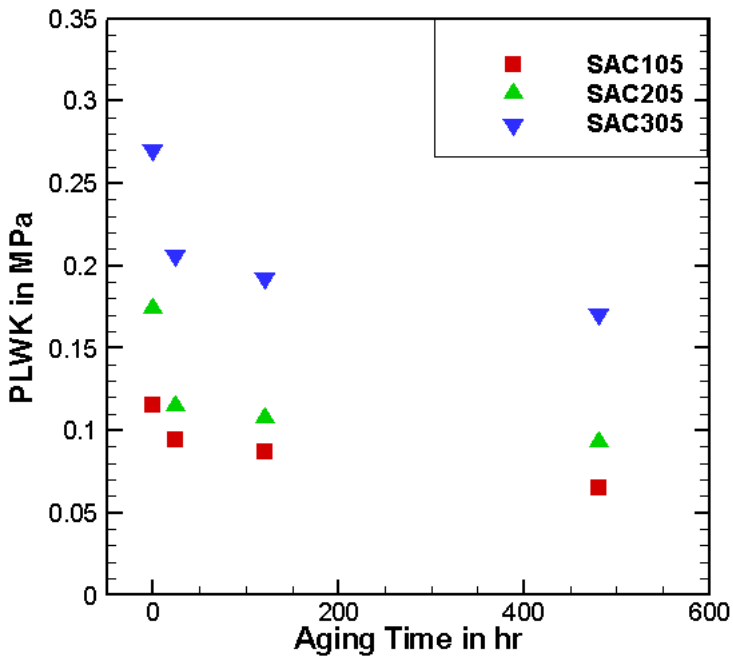

Figure 4.19 Variation of PLWK with the variation of *Ag* percentages of SAC material at different isothermal aging conditions at 100°C

4.6 Effects of Thermal Aging on Hydrostatic Pressure

Hydrostatic pressure is the most important parameter in electromigration oriented void formation and subsequent failure due to those voids. Positive value of hydrostatic pressure symbolizes tensile stress which defines void formation and subsequent open circuit formation whereas negative value of hydrostatic pressure symbolizes compressive stress which defines hillock formation as well as failure due to short circuit formation. In the study, failure by void formation only has been considered as it is the prime concern according to the literature. Figure 4.20 shows a comparative picture for hydrostatic pressure distribution of a SAC305 solder joint under applied electrical current. As, the material property degrades and softening takes place due to the effect of thermal aging, hydrostatic pressure just drops from about 24 MPa to 10.6 MPa when it is aged for 480 hour at 100°C and with testing temperature of 100°C.

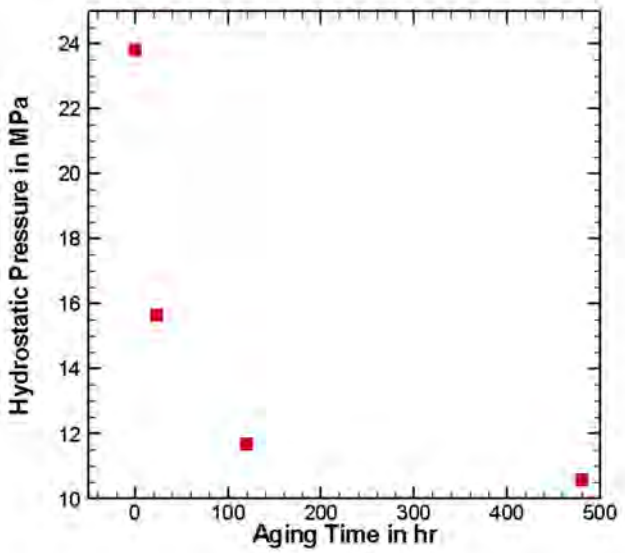

(a)

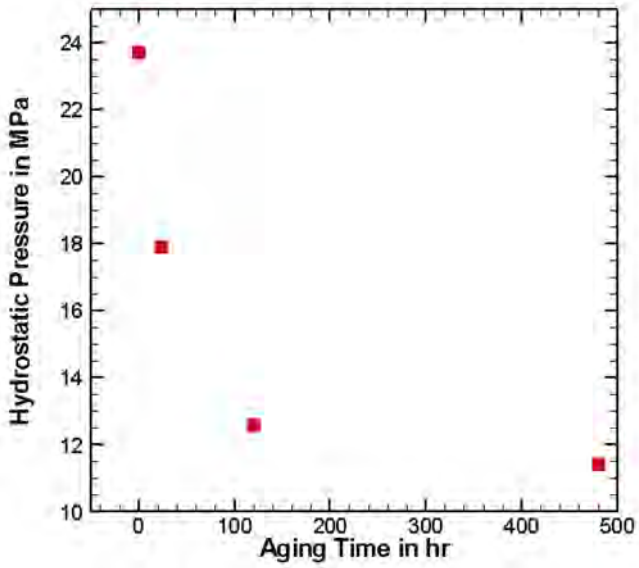

(b)

Figure 4.20 Maximum value of hydrostatic pressure of a flip-chip SAC305 solder joint for current stressing of 100 hr at an input current density of 2.76×10^{7} A/m^{2} at an experimentation temperature of (a) 100°C and (b) 125°C for different aged sample

With the increase of temperature to 125°C, hydrostatic pressure increases at different period of aging time. This increase in hydrostatic pressure contributes to the increase in PLWK by increasing stress induced diffusivity and causes subsequent electromigration failure due to stress induced voiding.

4.7 Effects of Thermal Aging on Electromigration Life

Electromigration oriented life or Time to Failure (TTF) is calculated for different isothermal aging conditions under applied electrical current density of 1.11×10^{8}A/m^{2} - 1.6×10^{8}A/m^{2} as shown in Figure 4.21. This captures the scenario that thermal aging causes a significant increase in electromigration life by decreasing the mass diffusion caused by grain boundary diffusion. For an increment in electrical current of 0.01A, electromigration life has increased about 5% which can be identified by the small increase as well as dependence of electromigration life on applied electrical current. For different aging conditions, time to failure has changed significantly. In case of changing isothermal aging time from 0 day to 1 day, electromigration life has approximately been doubled due to the microstructure evolution caused by thermal aging. However, prolonged aging causes to slow down the effect of thermal aging and subsequent resistance to electromigration failure. For such reason, electromigration life has increased only around 20% in case of increment in thermal aging time from 5 days to 20 days. Effect of *Ag* percentages on electromigration life is shown in Figure 4.22.

Electromigration lifetime of solder joint is calculated using iterative killing scheme of elements whose normalized concentration falls below 0.85. At first, a geometrical model is subjected to applied electrical current for current stressing and then checked whether void formation criterion has been fulfilled to kill an element. Whenever 30 elements attain the void formation criterion, those elements are killed and atomic density redistribution occurs to incorporate the effect of dead elements on the increment of electrical current density. This simulation takes place until the resistance of the overall solder joint model gets increased by 15% of the initial

resistance. The time taken to cause such change of resistance is marked as the time to failure (TTF) of the solder joint.

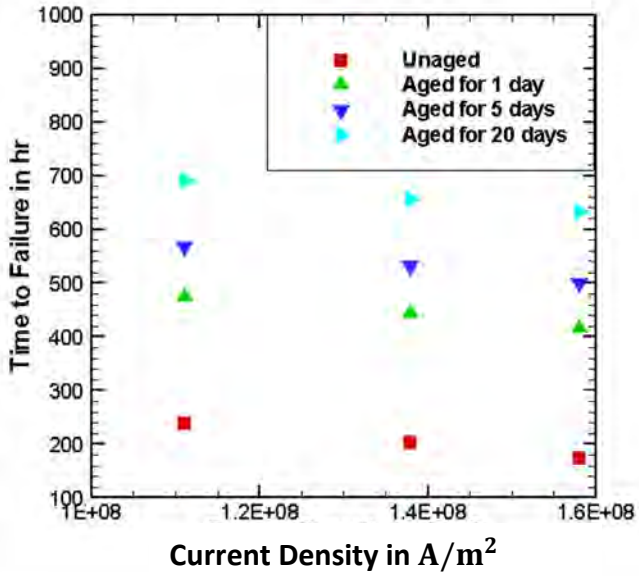

Figure 4.21 Estimated Electromigration Life of SAC305 solder joint under different currents at different aging conditions at aging temperature of 100°C

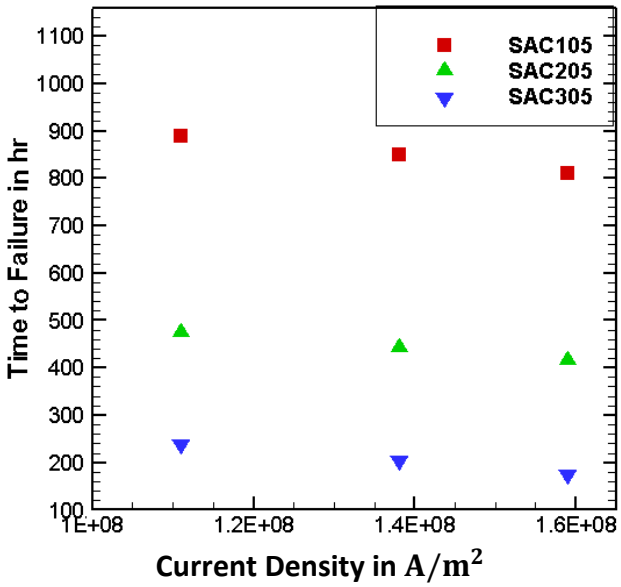

Figure 4.22 Estimated Electromigration Life of SAC solder joint under different currents at unaged condition at different *Ag* percentages

As at an elevated temperature, grain boundary diffusion process is the most dominant one for mass diffusion, this reduction in grain boundary area and coarsening of *Sn*- based microstructure causes increment in electromigration life. This reduction in grain boundary is governed by the values of elastic modulus as well as the stress strain properties of the SAC solder material under different thermal aging conditions. Due to the coarsening of microstructure of *Sn*-rich SAC solder material, structural property degrades significantly. This degradation in structural property affects the stress migration and subsequent mass diffusion in SAC solder joint. Thus, thermal aging plays an important role in case of increasing electromigration life of a SAC305 solder joint.

4.8 Effect of IMC Formation on Thermally Long Aged Solder Joints

Intermetallic compound (IMC) is a layer of thin metal formation composed of bulk solder material and *Cu*. This layer plays a significant role in determination of electromigration life of a SAC solder joint. Figure 4.23 shows the finite element model that is studied to analyze the impact of IMC layer on electromigration. This IMC layer has a comparatively lower value of diffusivity compared to bulk solder joint material. Thus, this layer prohibits grain boundary diffusion of solder material to propagate through solder geometry. It acts as a diffusion barrier in case of electromigration oriented mass diffusion. For such reason, formation of IMC layer with thermal aging has a positive impact on electromigration life of a SAC solder joint.

Figure 4.24 and Figure 4.25 shows the variation of PLWK with the variation of IMC content in solder joint material. Analysis of these Figures revealed that PLWK reduced from 0.27 MPa to 0.17 MPa (about 35%) with the inclusion of thermal aging as well as small amount (2 micron) of IMC in the solder joint. Additionally, it dropped to 0.16 MPa (about 43% compared to unaged solder) with the inclusion of 4 micron of IMC layer with the solder joint. The IMC layer thickness used in the study has been selected from Chowdhury et al. [72] considering dependence of electrical current density on IMC layer thickness.

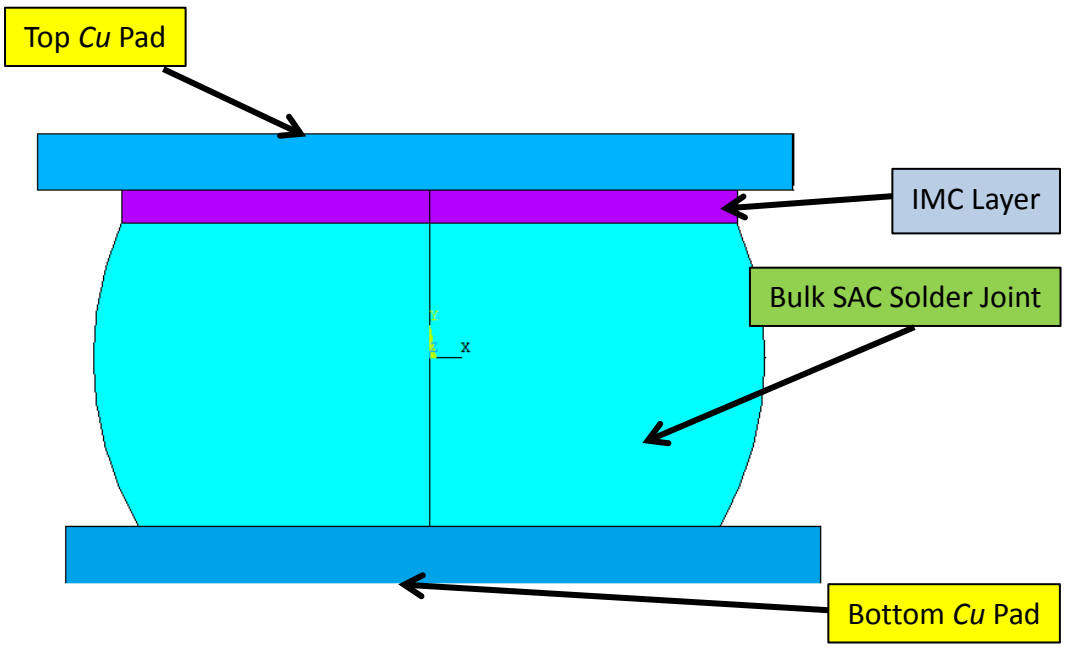

Figure 4.23 Finite element model of SAC solder joint with IMC

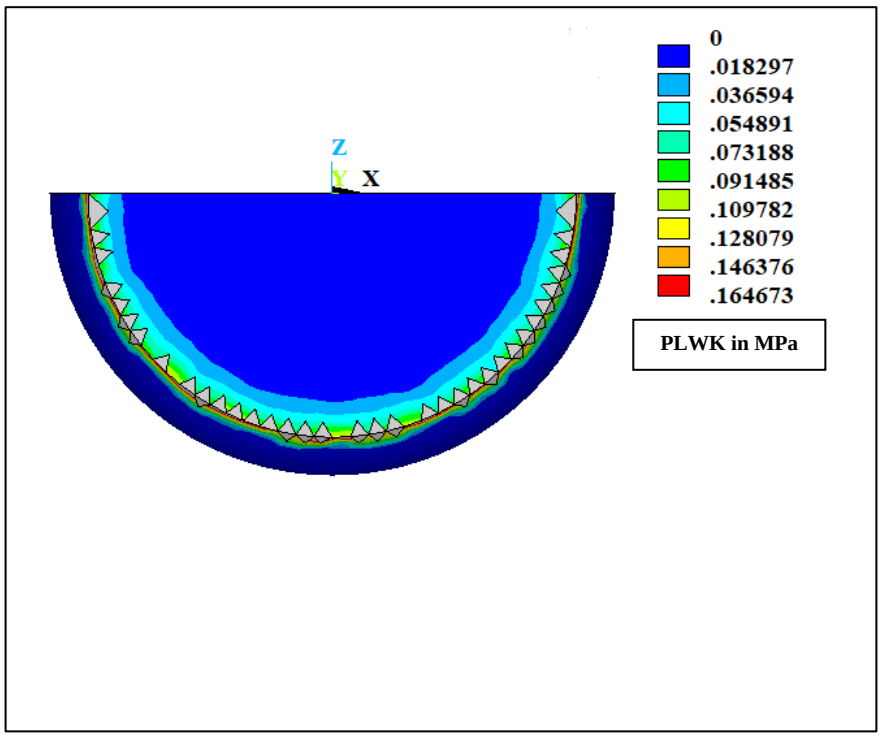

(a)

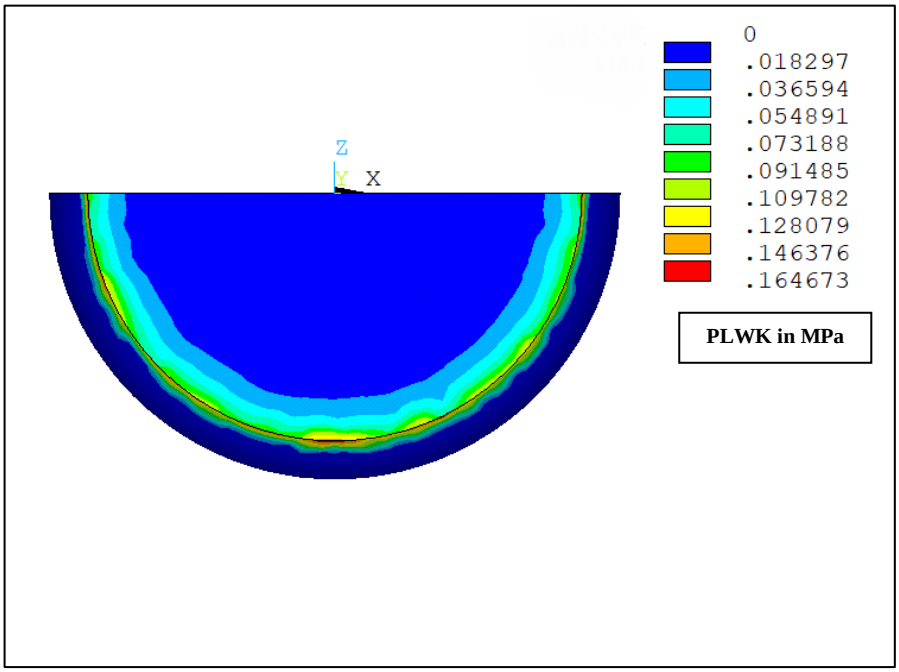

(b)

Figure 4.24 Plastic Work per Volume distribution (PLWK) of a flip-chip SAC305 solder joint for current stressing of 100 hr at input current density of 8.28×10^7 A/m^2 at a temperature of 100°C for isothermal aging period of (a) 0 day without IMC and (b) 180 days with 4 micron IMC layer

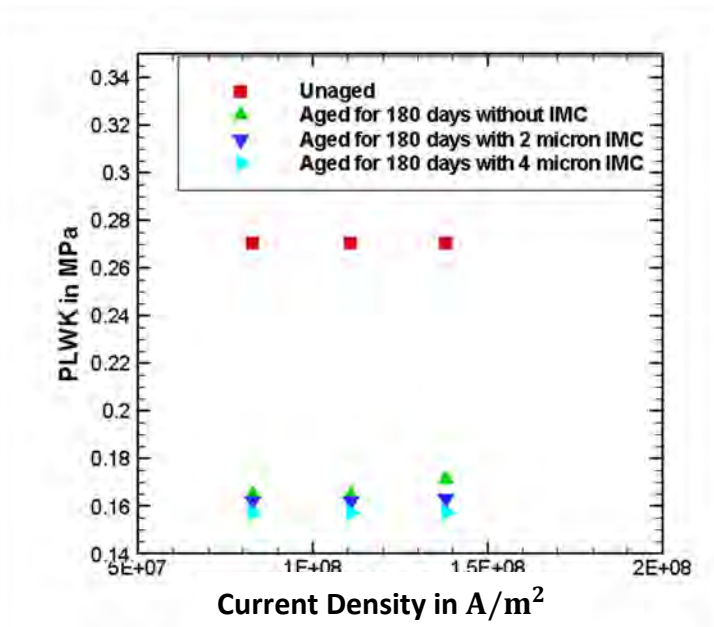

(a)

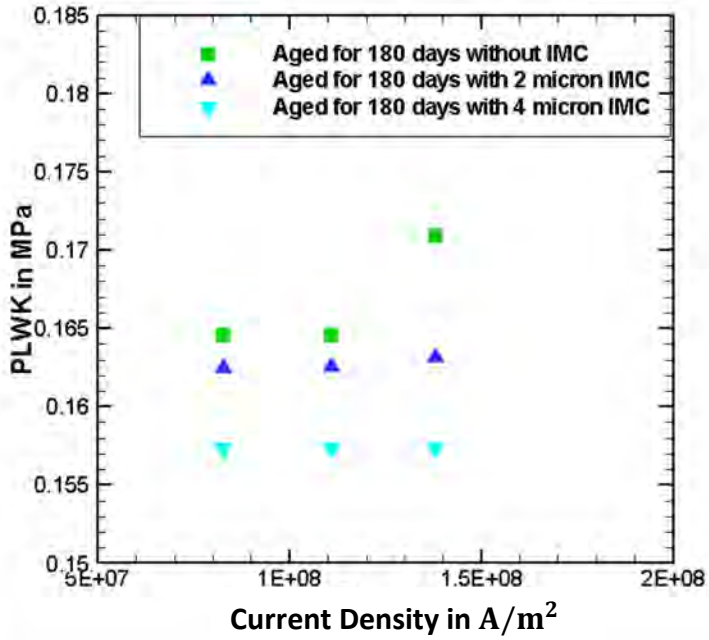

(b)

Figure 4.25 Maximum Plastic Work per Volume (PLWK) of a flip-chip SAC305 solder joint for current stressing of 100 hr at different values of input current at a temperature of 100°C for isothermal aging for different aging conditions (a) comparing unaged and aged conditions and (b) aged portions enlarged

Figure 4.26 contrasts between the distributions of diffusion flux in SAC solder joint with no IMC and with 4 micron of IMC. It shows that diffusion flux is significantly lower at most of the region of the SAC solder joint. Intermetallic compounds such as Cu_3Sn and Cu_6Sn_5 are essentially present in SAC solder joints under thermal aging conditions subjected for a long length of time. These IMC materials are brittle in structural properties as compared to bulk solder materials. For such reason, they have been modeled as linear elastic materials whose properties are enlisted earlier. This brittle layer of IMC blocks the electromigration oriented mass diffusion at the interface of the solder and *Cu* pads. As a result, Diffusion rate decreases and subsequent reduction in PLWK occurs. Being linear elastic in nature, IMC layer shows no inelastic work dissipation as similar to the *Cu* pad in previous studies. Such findings result that IMC layer has positive impact on the resistance to electromigration oriented failure.

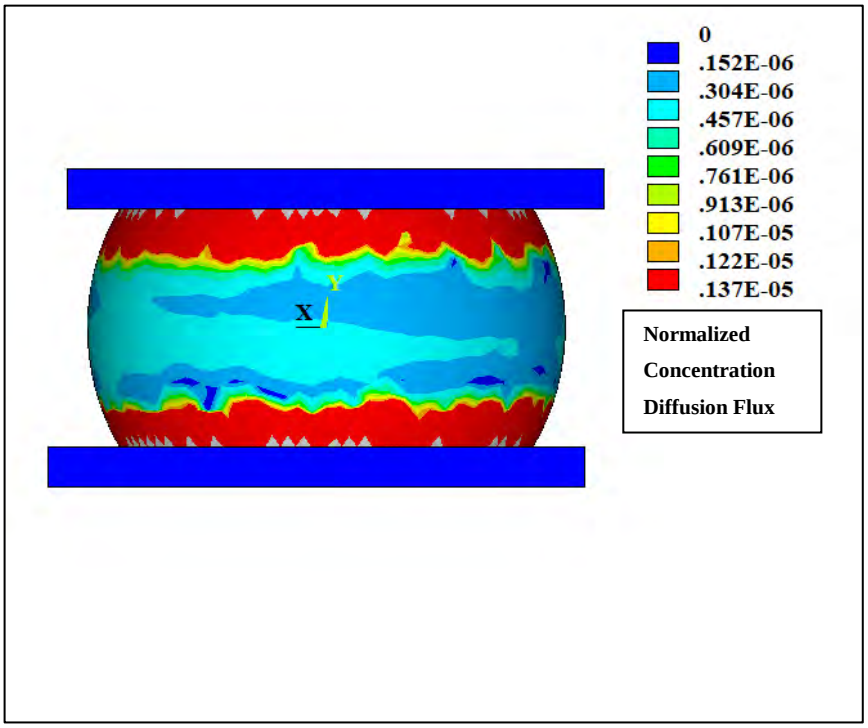
0
.152E-06
.304E-06
.457E-06
.609E-06
.761E-06
.913E-06
.107E-05
.122E-05
.137E-05
Normalized
Concentration
Diffusion Flux
Y
X

(a)

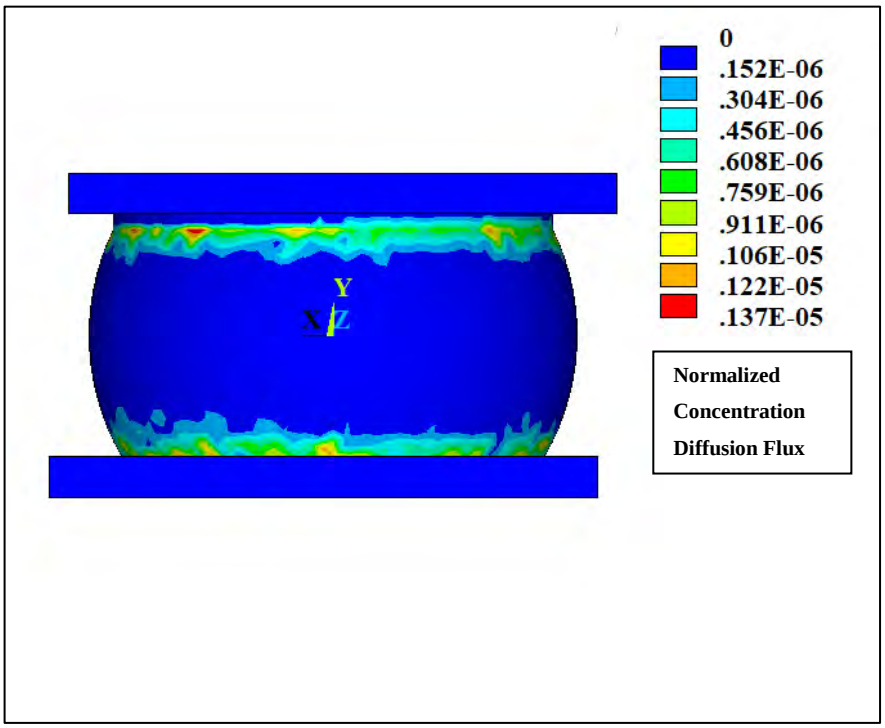
0
.152E-06
.304E-06
.456E-06
.608E-06
.759E-06
.911E-06
.106E-05
.122E-05
.137E-05
Normalized
Concentration
Diffusion Flux
Y
X
Z

(b)

Figure 4.26 Diffusion flux distribution of a flip-chip SAC305 solder joint for current stressing of 100 hr at input current density of 8.28×10^{7} A/m^2 at a temperature of 100°C for isothermal aging period of (a) 0 day and (b) 180 days with 4 micron IMC

In this study, a single layer of intermetallic compound has been placed between top *Cu* pad and SAC solder joint. In real life applications, IMC layers are usually present at both of the interfaces of the SAC solder joint. For simplification, IMC has been incorporated only at the top interface. However, accountancy of such layers in both side of the solder joint will actually further reduce the diffusion flux and subsequent PLWK more significantly compared to the single layer of IMC.

4.9 Numerical Validation

Finite element model used in this current study is validated using experimental results obtained from Lin et al. [55]. For this validation purpose, a *SnPb* solder joint has been subjected to a current density of 2×10^4 A/cm^2 at an elevated temperature of 100°C similar to the applied electrical current mentioned in the paper as shown in Figure 4.27. The solder joint of this experiment has a similar diameter of approximately 120 μm, bump height of 60 μm as well as the *Cu* conductor thickness is of 12 μm. Under such applied currents and geometrical configuration, the time to failure (TTF) of this C4 *SnPb* solder joint was found to be 95 minutes.

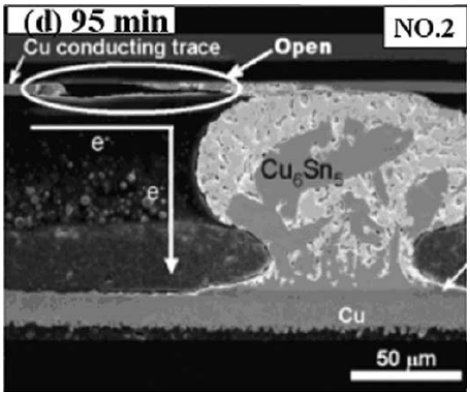

Figure 4.27 Microstructure evolution in the No. 2 joint. Electrons flowed from the chip side to the substrate side. The nominal current density was 2×10^4 A/cm^2 and the environmental temperature was 100°C [55].

The finite element model of this research has been used to predict the TTF of the *SnPb* solder joint (similar to the study done by Lin et al. [55]). For this purpose, the properties of *SnPb* solder material have been used from Wang et al. [63] (Table 4.1). The same electrical current of 2×10^4 A/cm^2 and temperature of 100°C have been used. The TTF found from the FEA study is 104 minutes which is close to the experimental result of 95 minutes. The simulation model is shown in Figure 4.28.

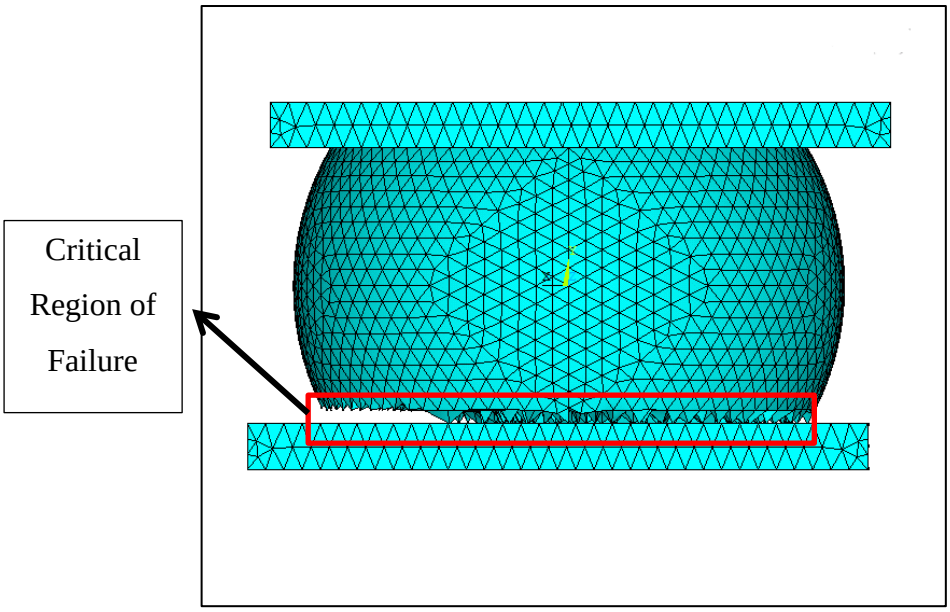

Figure 4.28 Simulation Model capturing failure of *SnPb* solder joint

Table 4.1 Electromigration and Mechanical Parameter of *SnPb* Solder Joint [63]

Parameter	Units	*SnPb*
Activation Energy, E_A	eV	0.8
Activation Energy, E_A	J/K-mole	-
Effective Charge Number, Z^*	-	-33
Diffusivity (pre-exponent), D_0	m^2/s	9.69e-5
Electrical resistivity, ρ_0@135°C	Ω.m	15.5e-8
Thermal Expansion Coefficient, α	1/K	24e-6
Atomic Volume, Ω	m^3/atom	2.48e-29
Elastic Modulus	GPa	30.8
Poisson's Ratio	-	0.4

4.10 Grid Independence Test

Grid independence study has been done to establish consistency in the finite element results with the variation of element numbers and shown in Figure 4.29. Simulation study has been done for element size ranging from 10000-150000 elements. However, value of selected parameter doesn't change significantly with the number of elements after certain meshing is selected. That concludes that this analysis is mesh independent. Detail contour plot regarding mesh independence test is shown in Figure A.4.

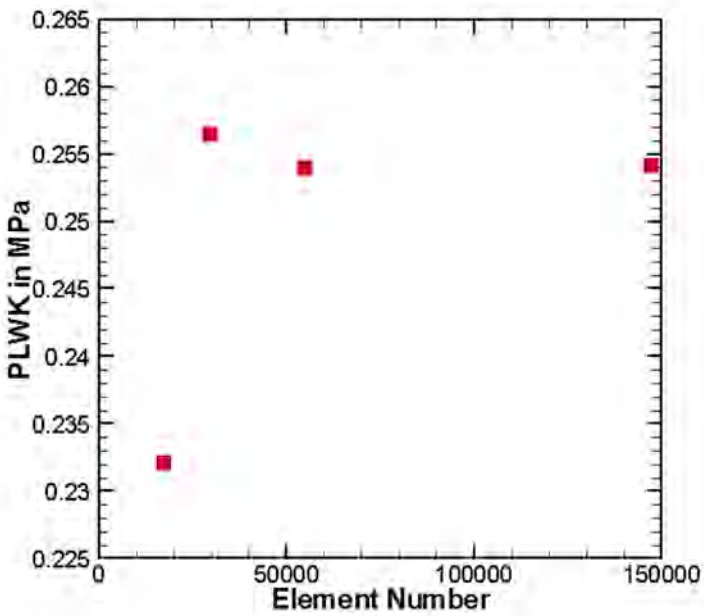

Figure 4.29 Variation of PLWK with element number for a flip-chip SAC305 solder joint for current stressing of 100 hr at applied current of 2.76×10^{7} A/m^{2} at a temperature of 100°C for unaged condition

CHAPTER 5
Electromigration Analysis with Random Vibration

In order to analyze the failure of the solder joint, the modal analysis and random vibration analysis are conducted by using the finite element analysis following electromigration analysis process described earlier.

5.1 Modal Shapes of SAC Solder Joint

In this study, a SAC solder joint connected by two *Cu* pads is subjected to an acceleration power spectrum density first, and then subjected to electrical current to observe the combined effect of random vibration and electromigration. Random vibration is introduced in this study in the form of base excitation. This base excitation causes the base to get displaced randomly in the vertical direction normal to the base face of the solder joint.

Figure 5.1 shows the modal shapes of the SAC solder joint under small displacement necessary for simple harmonic motion to occur. In this study, this modal displacement and modal frequencies are utilized to calculate displacement of the solder joint under applied random vibration using mode superposition method. Using this method, the dynamic response of a structure can be approximated by a superposition of a small number of its eigenmodes. The frequency range of the applied PSD has been selected in such a way that resonance will not occur. Variation of modal shapes at different aging times has been shown in Figures A.1-A.3.

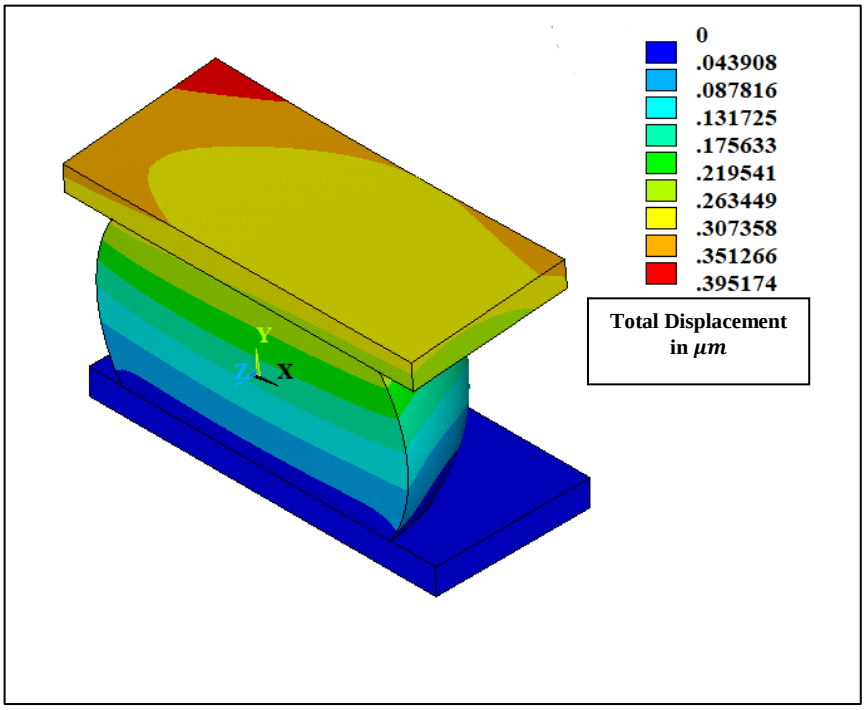
0
.043908
.087816
.131725
.175633
.219541
.263449
.307358
.351266
.395174
Total Displacement
in μm
Y
Z
X

(a)

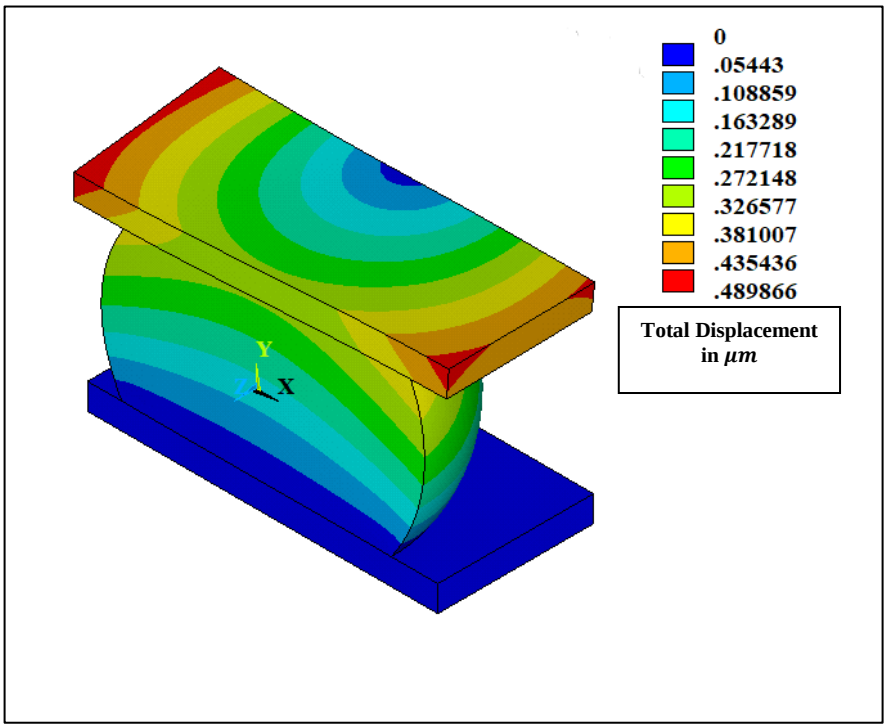
0
.05443
.108859
.163289
.217718
.272148
.326577
.381007
.435436
.489866
Total Displacement
in μm
Y
Z
X

(b)

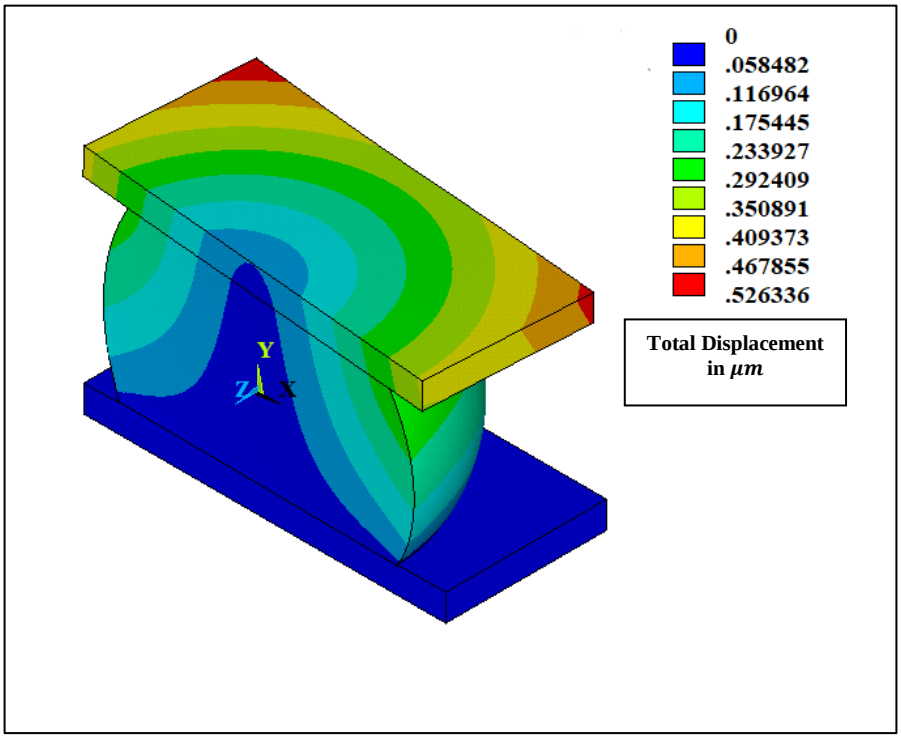
0
.058482
.116964
.175445
.233927
.292409
.350891
.409373
.467855
.526336
Total Displacement
in μm
Y
Z
X

(c)

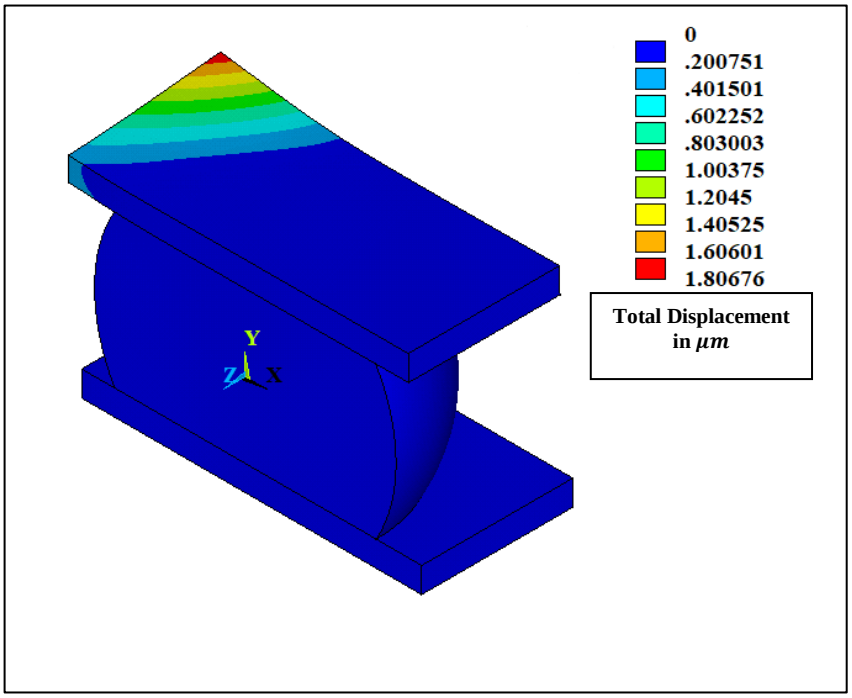
0
.200751
.401501
.602252
.803003
1.00375
1.2045
1.40525
1.60601
1.80676
Total Displacement
in μm
Y
Z
X

(d)

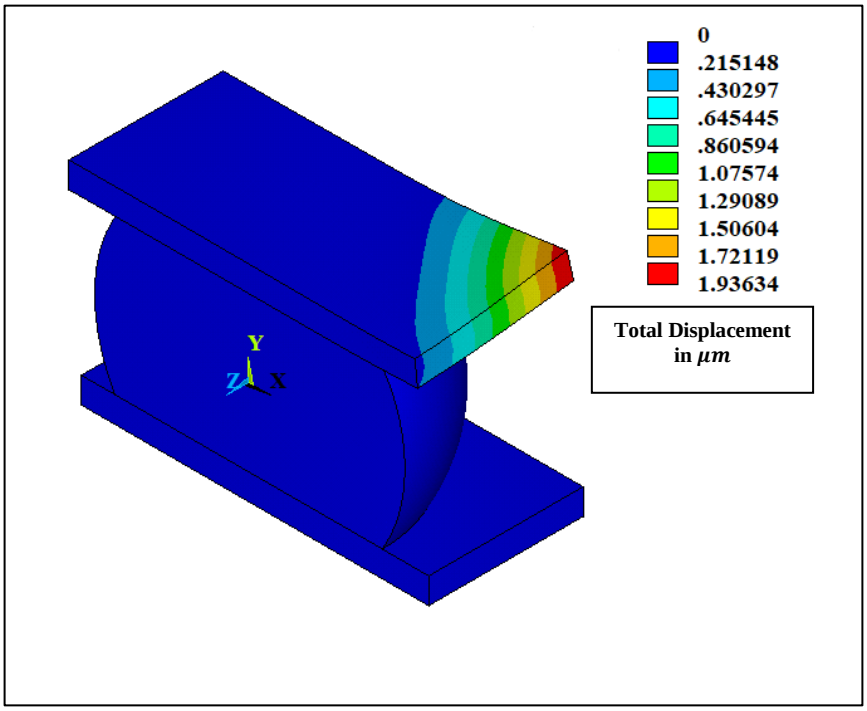

(e)

Figure 5.1 Modal shapes for SAC305 solder joint under base constraint with natural frequencies of (a) 18.7543 Hz, (b) 24.0477 Hz, (c) 25.7506 Hz, (d) 36.3911 Hz and (e) 42.1848 Hz at unaged condition

5.2 Effect of Random Vibration on Electromigration

5.2.1 Effect of random vibration on diffusion flux

As the top surface remains constrained due to the presence of other components (for example: die, epoxy material, substrate etc.) present above the solder joint, it gets stressed more rigorously compared to pure electromigration case. During the application of random vibration in SAC solder joint, RMS value of the response PSD of applied displacement is imposed on the base of the solder joint. Figure 5.2 compares between the diffusion flux distributions of SAC solder joints for unaged condition. SAC solder joint subjected to random vibration shows approximately 80% higher diffusion flux compared to the pure electromigration mode result. The cause of such increment in diffusion flux is the stress evolution posed due to applied displacement of response PSD from random vibration.

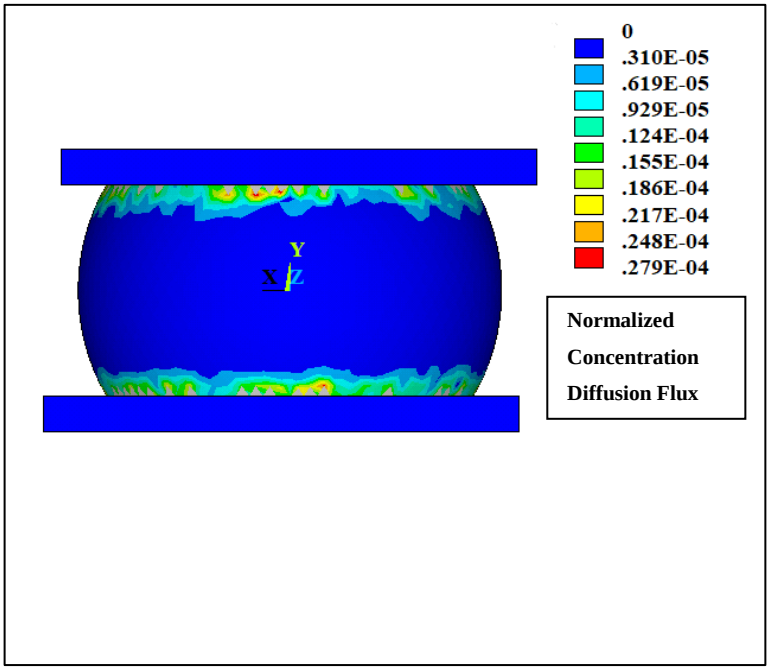

(a)

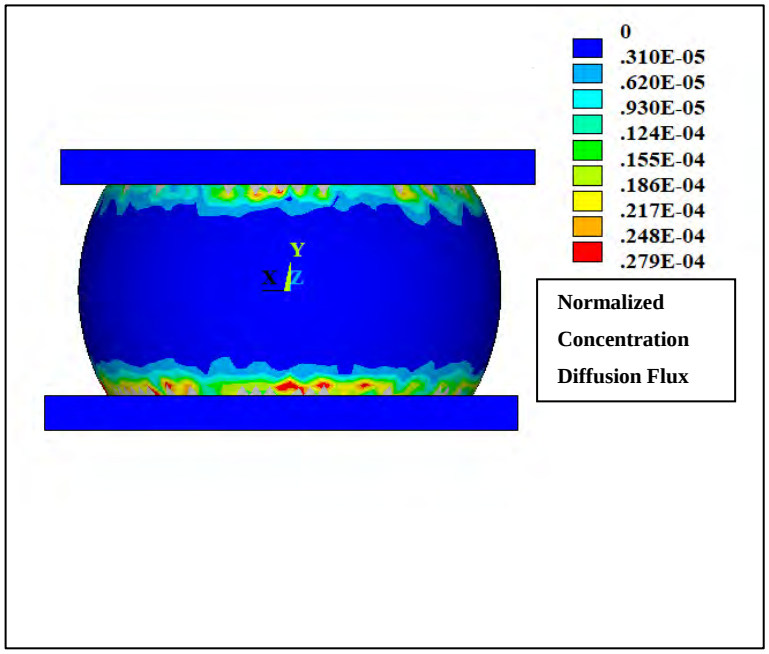

(b)

Figure 5.2 Diffusion flux distribution of a flip-chip SAC305 solder joint for current stressing of 100 hr at applied current density of 1.11×10^{8} A/m^{2} at a temperature of 100°C for unaged condition under (a) the effect of electromigration only and (b) combined random vibration and electromigration effect

5.2.2 Effect of random vibration on PLWK

Analysis shows that failure occurs near the base surface due to the presence of the base excitation and greater compression near the base surface. From Chen et al. [75], it has been acknowledged that random vibration oriented failure pattern is somehow different from the failure pattern due to electromigration. Electromigration oriented failure is mainly void based failure whereas random vibration oriented failure is crack formation based failure. So, it could be estimated that combined mode failure pattern is the summation of void propagation and crack propagation in the weakest zone.

From Figure 5.3, it can be observed that the maximum PLWK attained in case of combined mode is significantly higher compared to the pure electromigration mode. The magnitude of PLWK in combined mode is approximately 150% higher compared to the pure electromigration mode result. Similar findings were obtained by Wang et al. [76]. The cause of such change is due to the acceleration PSD value selected for this study and subsequent stress imposed on the solder joint due to applied vibration.

Whenever void is formed in the solder joint, crack propagation may become dominant in the nearest zone of that void. This plot revealed that PLWK decreases in similar fashion with the increment in aging time.

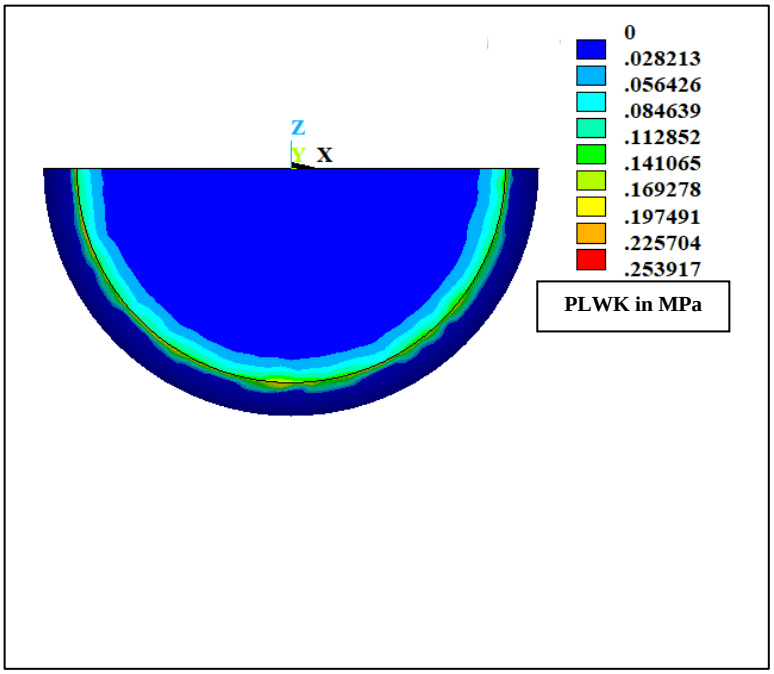

(a)

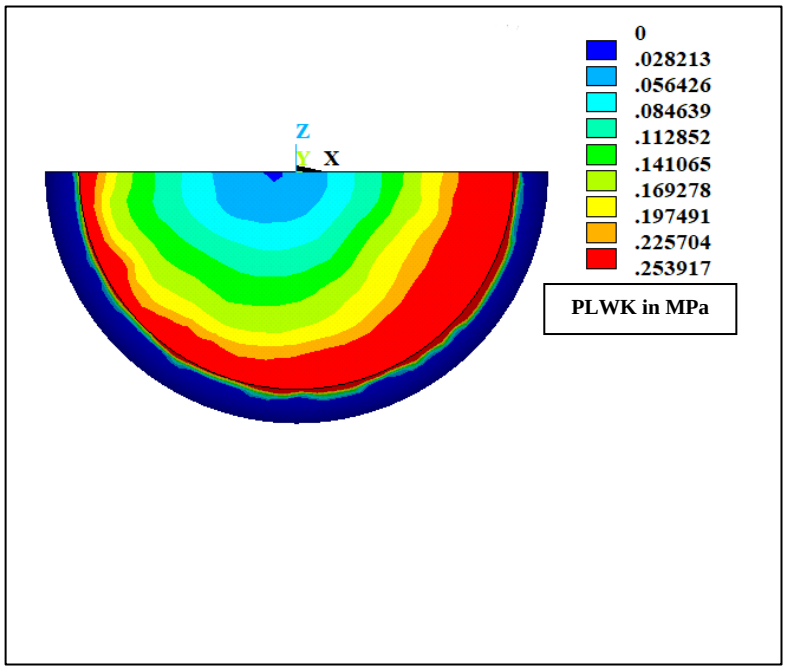

(b)

Figure 5.3 PLWK distribution of a flip-chip SAC305 solder joint for current stressing of 100 hr at applied current density of 1.11×10^{8} A/m^{2} at a temperature of 100°C for unaged condition under (a) electromigration effect only and (b) combined random vibration and electromigration effect

5.2.3 Effect of thermal aging on electromigration with random vibration

Effect of thermal aging and random vibration on the electromigration oriented failure has been studied in this section. It has been found that diffusion flux and PLWK decrease with the increment of the aging time. Figure 5.4 shows that the diffusion flux reduces by approximately 70% as aging time is increased up to 480 hour. Similarly, from Figure 5.5, it is obtained that the PLWK also reduces by approximately 180% for the same level of aging. It is due to the effect of applied stress caused by the PSD imposed on the solder joint.

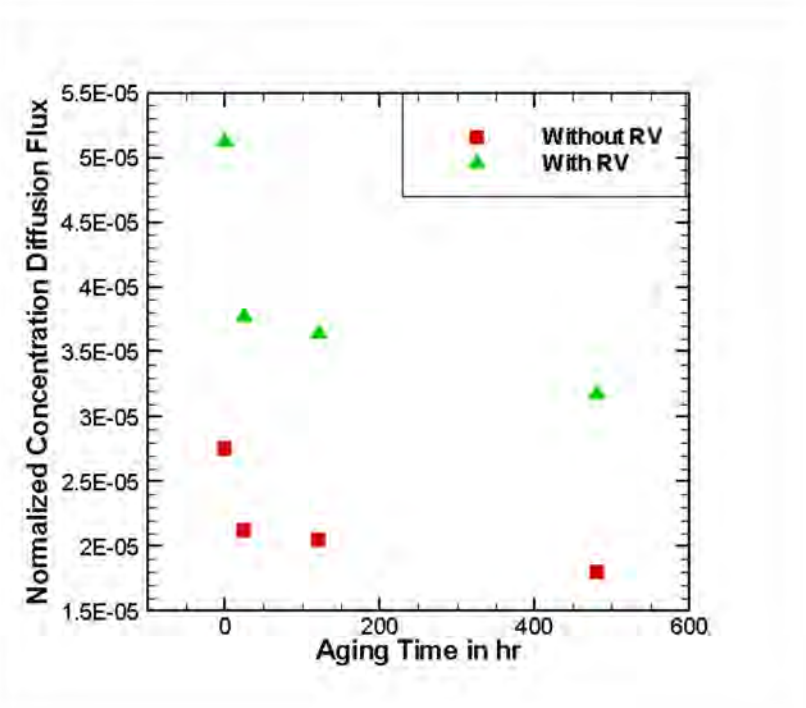

Figure 5.4 Variation of maximum diffusion flux at applied current density of 1.11×10^{8} A/m^{2}at a thermal aging temperature of 100°C and experimentation temperature of 100°C for thermal aging duration of 0 hour to 480 hours of SAC305 solder with and without applied random vibration

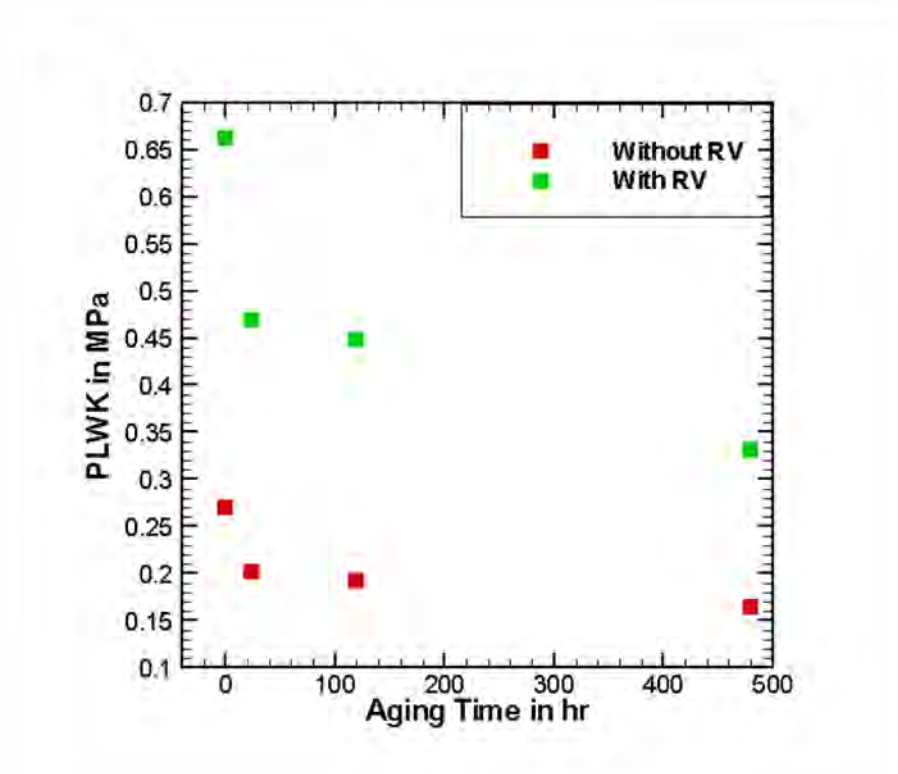

Figure 5.5 Variation of the maximum value of PLWK at current density of 1.11×10^{8} A/m^{2} at a thermal aging temperature of 100°C and experimentation temperature of 100°C for different thermal aging durations with and without applied random vibration.

5.2.4 Effect of *Ag* percentage on electromigration with random vibration

Effect of *Ag* percentage and random vibration on the electromigration oriented failure has been studied in this section. It is observed from Figure 5.6 that the diffusion flux is increasing with the increment of the *Ag* percentage in the SAC solder material. As the *Ag* percentage is increased from 1% to 3%, the diffusion flux changes by approximately 80%. Similarly, the PLWK has increased about 200% due to the change of Ag percentage from 1% to 3% as shown in Figure 5.7. So, it can be stated that effect of random vibration is more severe in SAC solder joints containing higher percentage of *Ag*.

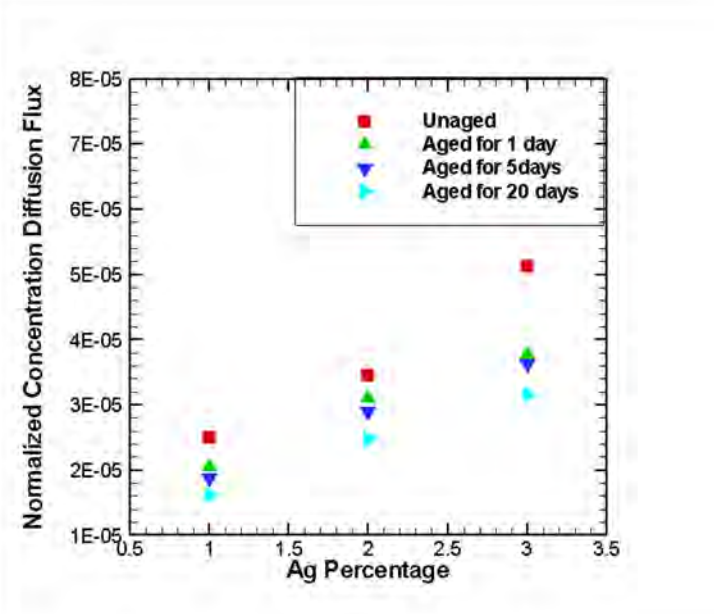

Figure 5.6 Variation of the maximum value of diffusion flux at density of 1.11×10^{8} A/m^{2} at a thermal aging temperature of 100°C and experimentation temperature of 100°C for thermal aging duration of 0 hour and 480 hour for different *Ag* percentages under applied random vibration

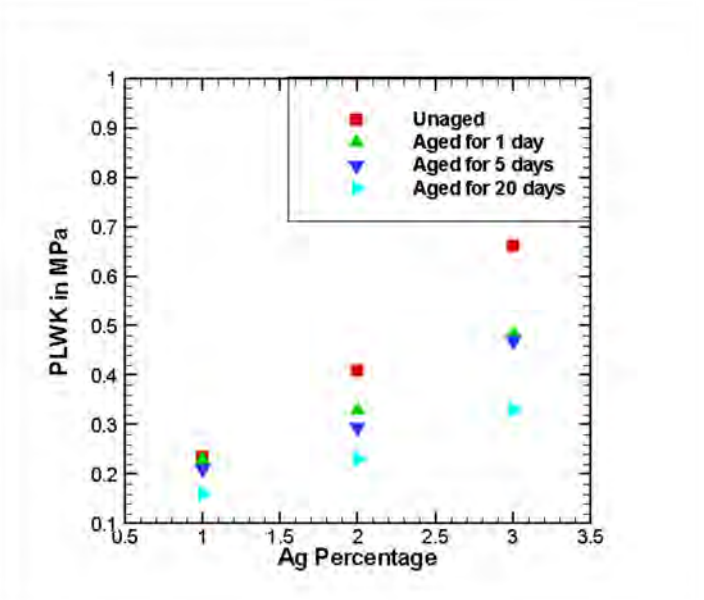

Figure 5.7 Variation of the maximum value of PLWK at density of 1.11×10^{8} A/m^{2} at a thermal aging temperature of 100°C and experimentation temperature of 100°C for thermal aging duration of 0 hour and 480 hour for different *Ag* percentages under applied random vibration

As known from the theory of random vibration, both the input and output result are defined in terms of probability. In this study, all the results are presented in terms of 1-σ nodal solution results. As PSD diagram has a mean along zero line, the standard deviation calculated from the PSD gives RMS value of the results. It means that there is 68.37% probability that the actual results are above the findings showed in the results. According to the theory of random vibration, the 3-σ results are 3 terms of the 1- σ results and there is 99.28% probability that the actual results are above the findings showed in the results.

CHAPTER 6

Conclusions

6.1 Conclusions

The main objectives of the thesis are to observe the impact of the thermal pre-aging on electromigration oriented failure of electronic packages, effects of *Ag* percentage on electromigration and combined effect of electromigration and random vibration oriented failure on flip-chip SAC solder joints using suitable mechanical and electromigration properties of SAC solder materials. Main conclusions of this study are summarized as follows:

- A 3-D finite element model of the flip-chip SAC solder joint has been developed in a commercial finite element solftware. Simulation of electromigration has been done at an electrical current of I=0.01A to 0.05A for a current stressing period of 100 hr.
- In the study, critical location of SAC solder joint has been found at the interfaces of *Cu* pad and SAC solder joint which is termed as the "Current Crowding Zone" as found from the literature. It has been found that diffusion flux has a proportional relation with the electrical current density. Furthermore, with the increment of current density from 2.7×10^{7} A/m^{2} to 1.4×10^{8} A/m^{2}, about 5% increase in diffusion flux is observed through SAC solder joint material.
- It has been observed from the analysis that the diffusion flux and PLWK decreases dramatically by 23% and 30% respectively after the first day of aging from the corresponding unaged values. These findings conclude that thermal aging has a positive impact on electromigration oriented reliability concern.
- Variation of SAC solder joint electromigration life with *Ag* percentage showed that with the increment of *Ag* content in SAC solder materials, the diffusion rate also increases, which in turn increases the electromigration oriented damage accumulation. Therefore, SAC 105 shows lower PLWK compared to SAC 205 and SAC 305.

- It has been shown in the study that the inelastic energy dissipation for SAC 305 solder joint decreases by 30-35 % when the IMC thickness is increased to 4 micron from the unaged condition in absence of intermetallics. So there is strong influence of IMC layer on electromigration life.
- The analysis of random vibration showed that about 150% increase in inelastic energy dissipation and 80% increase in diffusion flux are observed for an input power spectrum density as shown in Figure 3.9. This concludes that random vibration reduces electromigration life of a solder joint and could be considered as a serious reliability concern.
- This research will enable us to realize the effects of thermal aging, *Ag* percentage and random vibration on the electromigration related mass diffusion in Flip-Chip SAC solder joints. Deliverables of this research could be expected to determine the optimum pre-aging time and *Ag* percentages for superior component design and thus to optimize the solder joint reliability of Flip-Chip Packages. Such informations may be proved fruitful for electronic packaging industries for designing reliable and cost effective electronic components.

6.2 Limitations of the Work

- Due to unavailability of experimental data for SAC405 at elevated temperature of aging as well as unavailability of data for uniaxial tensile test at elevated temperature for SAC405, it wasn't possible to incorporate the simulation for SAC405. However, based on *Ag* percentage and results from SAC105, SAC205 and SAC305, it is possible to predict the behavior of the SAC405 solder material under applied electrical current and combined electromigration and random vibration mode.
- Due to unavailability of data, some diffusion properties of intermetallic compound are considered similar to the bulk solder joint material. As, the experimental data was not available for such type of study, it became necessary to assume those data for simulation. However, A comparison

between maximum PLWK for different values of pre diffusion exponent for SAC105 considering lattice and grain boundary diffusion is provided in Figure A.5 showing about only 0.1% change in PLWK values.

- As the TTF calculation is a highly time consuming process with existing computational resources, electromigration life for SAC105 and 205 couldn't be calculated in this study.

6.3 Recommendation for Future Works

- Effects of SAC solder joint dimensions (i.e. lengths, widths and thicknesses of different layers) on electromigration life may be studied using the FEA.
- Failure of electronic packages is a combination of different modes of failure such as electromigration, thermal cycling, drop testing, random vibration etc. These modes of failure cumulatively affect the solder joint more devastatingly compared to any of them in a single mode. In this study, only combination of random vibration and electromigration has been observed. However, failure by the collective impact of all of those failure modes could be a topic of great interest for future researchers in this field.
- The coupling between electromigration oriented failure subjected to thermal aging and mechanical property degradation caused due to thermal aging could be an interesting topic for future analysis.

References

[1] Li, Y., Wong, C. and Lu, D., (2009), *Electrical Conductive Adhesives with Nanotechnologies*, Springer, Germany.

[2] Tu, K. N., "Reliability challenges in 3D IC packaging technology." *Microelectron. Reliab.,* vol. 51, no. 3 pp. 517-523, 2011.

[3] Khan, N., Rao, V.S., Lim, S., We, H.S., Lee, V., Zhang, X., Liao, E.B., Nagarajan, R., Chai, T.C., Kripesh, V. and Lau, J.H., "Development of 3-D silicon module with TSV for system in packaging" in *2010 IEEE Transactions on Components and Packaging Technologies*, Vol. 33, Mar. 2010, pp. 3-9.

[4] Hsieh, M.C. and Yu, C.K., "Thermo-mechanical simulations for 4-layer stacked IC packages," in *EuroSimE 2008 -International Conference on Thermal, Mechanical and Multi-Physics Simulation and Experiments in Microelectronics and Micro-Systems*, April 2008, pp. 1-7.

[5] Yu, A., Lau, J.H., Ho, S.W., Kumar, A., Hnin, W.Y., Yu, D.Q., Jong, M.C., Kripesh, V., Pinjala, D. and Kwong, D.L., "Study of 15µm pitch solder microbumps for 3D IC integration," in *2009 Electronic Components and Technology Conference,* Vol. 59, May 2009, pp. 6-10.

[6] Lee, J.S., Byun, K.Y., Chung, Q.H., Suh, M.S., Kim, S.C. and Kim, Y.H., "Chip to Chip bonding using micro-*Cu* bumps with *Sn* capping layers," in *2009 European Microelectronics and Packaging Conference*, Jun. 2009, pp. 1-5.

[7] Solid State Technology, https://electroiq.com/2002/06/bga-csp-and-flip-chip/.

[8] Tu, K. N. (2007) *Solder Joint Technology*. Springer, New York.

[9] Huntington H. B. and Grone A. R., "Current-induced marker motion in gold wires," *J. Phys. Chem. Solids*, vol. 20, pp. 76-87, 1961.

[10] Hare, E. *Intermetallics in solder joints*, SEM Lab Inc Snohomish, 2013.

[11] Kelly, S. G., *Mechanical vibrations: theory and applications*. Cengage learning, 2012.

[12] Grishin, A. and Sutton, M., “xPSD: an external solver to compute linear responses to random base excitations (psd) in structures using ansys with the large mass method,” 2002.

[13] Ho, P. S. and Huntington, H. B., “Electromigration and Void Observation in Silver,” *J. Phys. Chem. Solids,* vol. 27, pp. 1319-1329, 1966.

[14] Khenner, M., Averbuch, A., Israeli, M. and Nathan, M., “Numerical Simulation of Grain-Boundary Grooving by Level Set Method," *J. Comp. Phys.*, vol. 170, pp. 764-784, 2001.

[15] Ogawa, E. T., Bierwag, A. J., Lee, K. D., Matsuhashi, H. and Justinson, P. R., ``Direct Observation of a Critical Length Effect in Dual-Damascene *Cu*/Oxide Interconnects," *Appl. Phys. Lett.*, vol. 78 (18), pp. 2652-2645, 2001.

[16] Clement, J. J. and Thompson, C. V., ``Modeling Electromigration-Induced Stress Evolution in Confined Metal Lines," *J. Appl. Phys.*, vol. 78 (2), pp. 900-904, 1995.

[17] Oates, A. S., and Lin, M. H., “Void Nucleation and Growth Contributions to the Critical Current Density for Failure in *Cu* Vias," in *2009 IEEE International Reliability Physics Symposium*, Vol. 47, July 2009, pp. 452-456.

[18] Schwartz, G. C. and Srikrishnan, K. V. (2006), *Handbook of Semiconductor Interconnection Technoogy,* Taylor and Francis Group, New York.

[19] Fisher, J. C., “Calculation of Diffusion Penetration Curves for Surface and Grain Boundary Diffusion," *J. Appl. Phys.*, vol. 22 (1), pp. 74-77, 1951.

[20] Basit, M. M., Motalab, M., Suhling, J. C., Hai, Z., Evans, J. L., Bozack, M. J. and Lall, P., “Thermal cycling reliability of aged PBGA assemblies - comparison of weibull failure data and finite element model predictions,” in *2015 Electronic Components and Technology Conference*, Vol. 65, May 2015, pp. 106-117.

[21] Alam, M. S., Hassan, KM. R., Suhling, J. C. and Lall, P. “Investigation of the Effects of High Temperature Aging on the Mechanical Behavior of Lead Free Solders,” in *2018 International Technical Conference and Exhibition on*

Packaging and Integration of Electronic and Photonic Microsystems, Aug. 2018, pp. 8396:1-9.

[22] Rzepka, S., Korhonen, M. A., Weber, E. R., and Li, C. Y., ``Three-Dimensional Finite Element Simulation of Electro and Stress Migration Effects in Interconnect Lines," *Proc. Mater. Research Soc. Symp.*, vol. 473, pp. 329-335, 1997.

[23] Ye, H., Basaran, C., and Hopkins, D. C., ``Numerical Simulation of Stress Evolution during Electromigration in IC Interconnect Lines," *IEEE Trans. Compon. Pack. Technol.*, vol. 26 (3), pp. 673-681, 2003.

[24] Lloyd, J. R., Clemens, J., and Snede, R., "Copper Metallization Reliability," *Microelectron. Reliab.*, vol. 39, pp. 1595-1602, 1999.

[25] Arnaud, L., Berger, T., and Reimbold, G., "Evidence of Grain-Boundary versus Interface Diffusion in Electromigration Experiments in Copper Damascene Interconnects," *J. Appl. Phys.*, vol. 93 (1), pp. 192-204, 2003.

[26] Harris, J. E., "Nucleation of Creep Cavities in Magnesium," *Trans. Met. AIME*, vol. 233, pp. 1509-1516, 1965.

[27] Besser, P. R., Madden, M. C., and Flinn, P. A., "In Situ Scanning Electron Microscopy Observation of the Dynamic Behavior of Electromigration Voids in Passivated Aluminum Lines," *J. Appl. Phys.*, vol. 72 (8), pp. 3792-3797, 1992.

[28] Lin, Y. H., Tsai, C. M., Hu, Y. C., Lin, Y. L. and Kao, C. R., "Electromigration-Induced Failure in Flip-Chip Solder Joints," *J Electron Mater.*, vol. 34, pp. 27-33, 2005.

[29] Suzuki, A. and Mishin, Y. "Atomic mechanisms of grain boundary diffusion: Low versus high temperatures," *J. Mater. Sci.,* vol. 40, pp. 3155-3161, 2005.

[30] Medvedev, A. S., "Aging of tin-lead solders and joints soldered by them," *Metallovedenie i Obrabotka Metallov,* vol. 7, pp. 16-23, 1956.

[31] Lampe, B. T., "Room temperature aging properties of some solder alloys," *Weld J*, vol. 55, pp. 330-340, 1976.

[32] Yoon, J. W., Lee, C. B. and Jung, S. B. "Growth of an intermetallic compound layer with *Sn*-3.5 *Ag*-5*Bi* on *Cu* and *Ni-P/Cu* during aging treatment," *J Electron. Mater.,* vol. 32, pp. 1195-1202, 2003.

[33] Alam, M. S., Hassan, KM. R., Suhling, J. C. and Lall, P. "Investigation of the Effects of High Temperature Aging on the Mechanical Behavior of Lead Free Solders," in *2018 International Technical Conference and Exhibition on Packaging and Integration of Electronic and Photonic Microsystems*, Aug. 2018, pp. 8396:1-9.

[34] Lall, P., Islam, M. N., Singh, N., Suhling, J. C. and Darveaux, R. "Model for BGA and CSP Reliability in Automotive Underhood Applications," in *2014 IEEE Transactions on Components and Packaging Technologies*, Vol. 27, Sep. 2014, pp. 585-593.

[35] Lin, Y. H., Tsai, C. M., Hu, Y. C., Lin, Y. L. and Kao, C. R., "Electromigration-Induced Failure in Flip-Chip Solder Joints," *J Electron Mater.*, vol. 34, pp. 27-33, 2005.

[36] Suzuki, A. and Mishin, Y. "Atomic mechanisms of grain boundary diffusion: Low versus high temperatures," *J. Mater. Sci.,* vol. 40, pp. 3155-3161, 2005.

[37] Medvedev, A. S., "Aging of tin-lead solders and joints soldered by them," *Metallovedenie i Obrabotka Metallov,* vol. 7, pp. 16-23, 1956.

[38] Choi, S., Bieler, T. R., Lucas, J. P. and Subramanian, K. N. "Characterization of the growth of intermetallic interfacial layers of *Sn-Ag* and *Sn-Pb* eutectic 248 solders and their composite solders on *Cu* substrate during isothermal long- term aging," *J Electron. Mater.*, vol. 28, pp. 1209-1215, 1999.

[39] Xu, L., Pang, J. H. L. , Prakash, K. H. and Low, T. H., "Isothermal and thermal cycling aging on imc growth rate in lead-free and lead-based solder interface," in *2005 IEEE Transactions on Components and Packaging Technologies*, Vol. 28, Sep. 2005, pp. 408-414.

[40] Zhang, J., Hai, Z., Thirugnanasambandam, S., Evans, J.L., Bozack, M.J., Zhang, Y. and Suhling, J.C., 2013. "Thermal aging effects on the thermal cycling reliability of lead-free fine pitch packages", *IEEE transactions on components, packaging and manufacturing technology*, 3(8), pp.1348-1357.

[41] Lee, T. K., Ma, H., Liu, K. C. and Xue, J. "Impact of isothermal aging on long term reliability of fine-pitch ball grid array packages with *Sn-Ag-Cu* solder interconnects: Surface finish effects," *J Electron. Mater.*, vol. 39, pp. 2564-2573, 2010.

[42] Chilton, A. C., Whitmore, M. A. and Hampshire, W. B., "Fatigue Failure in a Model SMD Joint," *Soldering and Surface Mount Technology*, vol. 1, pp. 21-24, 1989.

[43] Li, M., Lee, K. Y., Olsen, D. R., Chen, W. T., Tan, B. T. C. and Mhaisalkar, S., "Microstructure, joint strength and failure mechanisms of *SnPb* and *Pb*-free solders in BGA packages," in *2002 IEEE Transactions on Electronics Packaging Manufacturing*, Vol. 25, Jul. 2002, pp. 185-192.

[44] Basaran, C. and Lin, M., "Damage mechanics of electromigration induced failure," *Mech Mater.,* vol. 40, pp. 66-79, 2008.

[45] Liu, Y., Zhang, Y. and Liang, L. "Prediction of electromigration induced voids and time to failure for solder joint of a wafer level chip scale package," in *2010 IEEE Transactions on Components and Packaging Technologies*, Vol. 33, Sep. 2010, pp. 544-552.

[46] Chang, Y. W., Cheng, Y., Helfen, L., Xu, F., Tian, T., Scheel, M., Michiel, M. D., Chen, C., Tu, K. N. and Baumbach, T., "Electromigration mechanism of failure in flip-chip solder joints based on discrete void formation," *Sci. Rep.,* vol. 7, pp. 17950, 2017.

[47] Yang, P.C., Kuo, C.C. and Chen, C., "The effect of pre-aging on the electromigration of flip-chip *SnAg* solder joints". *JOM*, vol. 60(6), pp.77-80, 2008.

[48] Ma, H., Suhling, J. C., Lall, P. and Bozack, M. J., "Reliability of the aging lead free solder joint," in *2006 Electronic Components and Technology Conference*, Vol. 56, May 2006, pp. 849-864.

[49] Che, F. X., Zhu, W. H., Poh, E. S., Zhang, X. W., and Zhang, X. R., "The study of mechanical properties of *Sn–Ag–Cu* lead-free solders with different *Ag* contents and Ni doping under different strain rates and temperatures," J ALLOY COMPD, vol. 507(1), pp. 215-224, 2010.

[50] Yang, P. and Chen, Z. X., "Experimental approach and evaluation on dynamic reliability of PBGA assembly," in *2009 IEEE Transactions on Electron Devices*, Vol. 56(10), Oct. 2009, pp. 2243–2249.

[51] https://www.sharcnet.ca/Software/Ansys/17.0/enus/help/ans_mat/amp8sq21ddm.html.

[52] Zhang, Y., “Electromigration failure prediction and reliability evaluation of solder bumps for FCBGA package,” *Engineering Transactions*, vol. 63(2), pp. 215-232, 2015.

[53] Liu, Y., Zhang, Y., and Liang, L., “Prediction of electromigration induced voids and time to failure for solder joint of a wafer level chip scale package,” in *2010 IEEE Transactions on Components and Packaging Technologies*, Vol. 33(3), Sep. 2010, pp. 544–552.

[54] https://www.sharcnet.ca/Software/Ansys/17.0/enus/help/ans_mat/amp8sq21dldm.html.

[55] Lin, Y.H., Tsai, C.M., Hu, Y.C., Lin, Y.L. and Kao, C.R., “Electromigration-induced failure in flip-chip solder joints,” *J. Electron. Mater.,* vol. 34, pp. 27-33, 2005.

[56] Antonova, E.E. and Looman, D.C., “Finite Elements for Electromigration Analysis,” In *2017 IEEE 67th Electronic Components and Technology Conference,* Vol. 67, May. 2017, pp. 862-871.

[57] Chilton, A. C., Whitmore, M. A. and Hampshire, W. B., "Fatigue Failure in a Model SMD Joint," *Soldering and Surface Mount Technology*, vol. 1, pp. 21-24, 1989.

[58] https://www.sharcnet.ca/Software/Ansys/17.0/en-us/help/ans_mat/migr.html

[59] Motalab, M., Cai, Z., Suhling, J. C., Zhang, J., Evans, J. L., Bozack, M. J. and Lall, P. “Improved Predictions of Lead Free Solder Joint Reliability that Include Aging Effects,” in *2012 Electronic Components and Technology Conference*, Vol. 62, May 2012, pp. 513-531.

[60] Che, F. X., Zhu, W. H., Poh, E. S., Zhang, X. W., and Zhang, X. R., “The study of mechanical properties of *Sn–Ag–Cu* lead-free solders with different Ag contents and Ni doping under different strain rates and temperatures,” J ALLOY COMPD, vol. 507(1), pp. 215-224, 2010.

[61] Lall, P., Zhang, D., Yadav, V., and Locker, D. “High strain rate constitutive behavior of SAC105 and SAC305 leadfree solder during operation at high temperature,” *Microelectron Reliab.,* vol. 62, pp. 4-17, 2016.

[62] Zhang, Y., “Electromigration failure prediction and reliability evaluation of solder bumps for FCBGA package,” *Engineering Transactions*, vol. 63(2), pp. 215-232, 2015.

[63] Liu, Y., Zhang, Y., and Liang, L., “Prediction of electromigration induced voids and time to failure for solder joint of a wafer level chip scale package,” in *2010 IEEE Transactions on Components and Packaging Technologies*, Vol. 33(3), Sep. 2010, pp. 544–552.

[64] Wang, S., Liang, L., and Liu, Y., “Solder joint reliability under electromigration and thermal-mechanical load,” in *2006 Electronic Components and Technology Conference*, Vol. 56, May 2006, pp 1074-1083.

[65] Chao, B., Chae, S. H., Zhang, X., Lu, K. H., Im, J. and Ho, P. S., “Investigation of diffusion and electromigration parameters for *Cu–Sn* intermetallic compounds in Pb-free solders using simulated annealing,” *Acta Mater.,* vol. 55, pp. 2805-2814, 2007.

[66] Dandu, P., Fan, X. J., and Liu, Y., (2010). “Some remarks on finite element modeling of electromigration in solder joints,” in *2010 Electronic Components and Technology Conference*, Vol. 60, May 2010, pp 396-402.

[67] Che, F.X., Zhu, W.H., Poh, E.S.W., Zhang, X.W. and Zhang, X.R. “The study of mechanical properties of *Sn–Ag–Cu* lead-free solders with different Ag contents and Ni doping under different strain rates and temperatures,” *J ALLOY COMPD*, vol. 507, pp. 215-224, 2010.

[68] Mehrer, H. (2007) *Diffusion in Solids*. Springer, New York.

[69] Ma, H., Suhling, J. C., Lall, P. and Bozack, M. J., “Reliability of the aging lead free solder joint,” in *2006 Electronic Components and Technology Conference*, Vol. 56, May 2006, pp. 849-864.

[70] Suh, D., Kim, D.W., Liu, P., Kim, H., Weninger, J.A., Kumar, C.M., Prasad, A., Grimsley, B.W. and Tejada, H.B., “Effects of Ag content on fracture resistance of *Sn-Ag-Cu* lead-free solders under high-strain rate conditions”, *Materials Science and Engineering: A*, vol. 460, pp. 595-603, 2007.

[71] Song, J.M., Lin, J.J., Huang, C.F. and Chuang, H.Y., “Crystallization, morphology and distribution of Ag_3Sn in *Sn-Ag-Cu* alloys and their influence

on vibration properties", *Materials Science and Engineering: A*, vol. 466, pp. 9-17, 2007.

[72] Kim, K.S., Huh, S.H. and Suganuma, K., "Effects of intermetallic compounds on properties of *Sn-Ag-Cu* lead-free soldered joints", *J ALLOY COMPD*, vol. 352, pp. 226-236, 2003.

[73] Zeng, K. and Tu, K.N., "Six cases of reliability study of Pb-free solder joints in electronic packaging technology", *Materials Science and Engineering: R: Reports*, vol. 38, pp. 55-105, 2002.

[74] Cheng, Y.K., Tsai, C.H., Teng, C.C. and Kang, S.M.S. (2002). *Electrothermal Analysis of VLSI Systems*. Springer. New York.

[75] Choudhury, S.F. and Ladani, L., 2015. Effect of intermetallic compounds on the thermomechanical fatigue life of three-dimensional integrated circuit package microsolder bumps: finite element analysis and study. *Journal of Electronic Packaging*, *137*(4), p.041003.

[76] Chen, X., Liang, L. and Liu, Y., (2008). "Electromigration simulation with consideration of the atomic concentration gradient". in *2008 International Conference on Electronic Packaging Technology & High Density Packaging,* July 2008, pp. 1-7.

[77] Wang, S., Liang, L. and Liu, Y., "Solder joint reliability under electromigration and thermal-mechanical load," in *2006 Electronic Components and Technology Conference*, Vol. 56, May 2006, pp 1074-1083.

[78] Kim, K.S., Huh, S.H. and Suganuma, K., "Effects of intermetallic compounds on properties of *Sn-Ag-Cu* lead-free soldered joints", *J ALLOY COMPD*, vol. 352, pp. 226-236, 2003.

[79] An, T., Fang, C., Qin, F., Li, H., Tang, T., and Chen, P. "Failure study of *Sn*37*Pb* PBGA solder joints using temperature cycling, random vibration and combined temperature cycling and random vibration tests," *Microelectron Reliab*., vol. 91, pp. 213-226, 2018.

Appendix

A.1 Variation of Modal Shape and Modal Frequency with Isothermal Aging Conditions

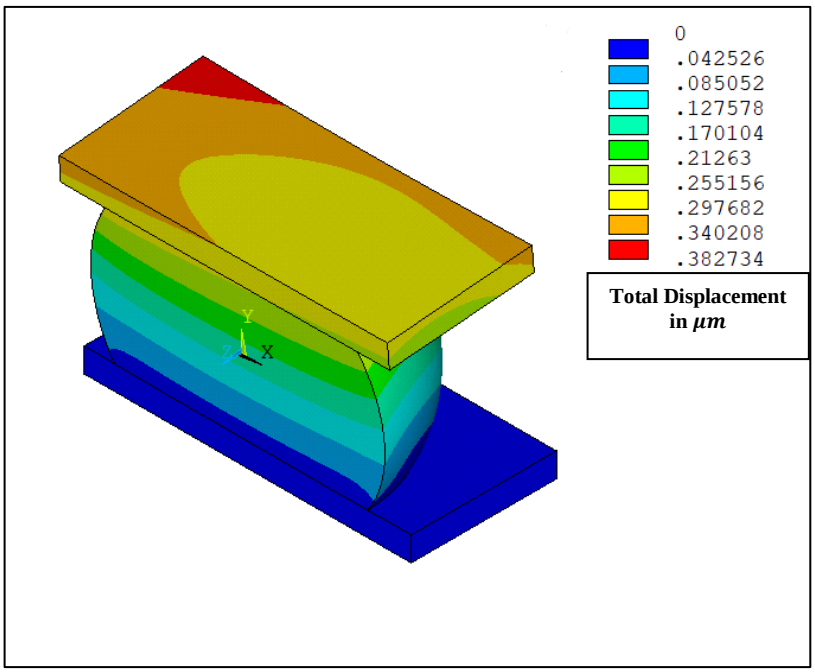

(a)

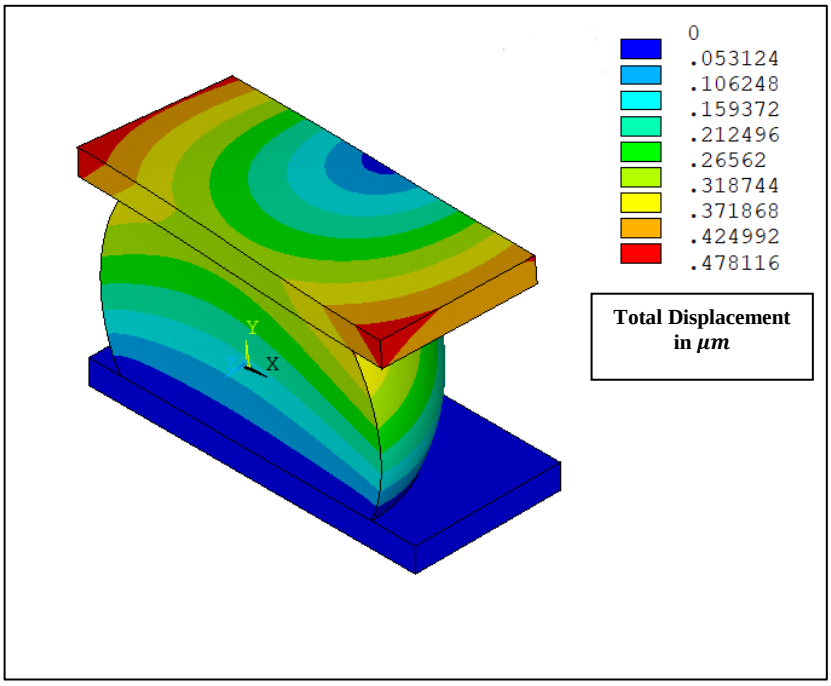

(b)

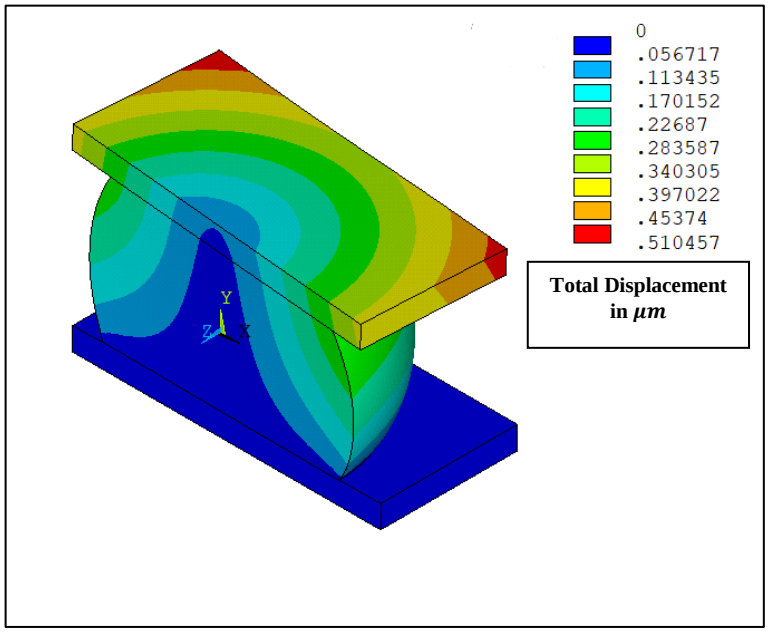
0
.056717
.113435
.170152
.22687
.283587
.340305
.397022
.45374
.510457
Total Displacement in μm
Y
Z
X

(c)

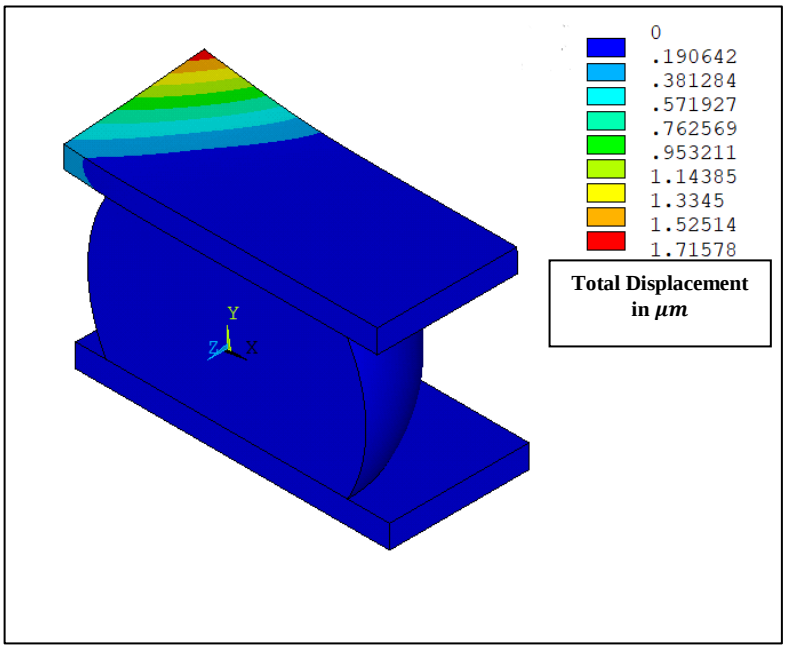
0
.190642
.381284
.571927
.762569
.953211
1.14385
1.3345
1.52514
1.71578
Total Displacement in μm
Y
Z
X

(d)

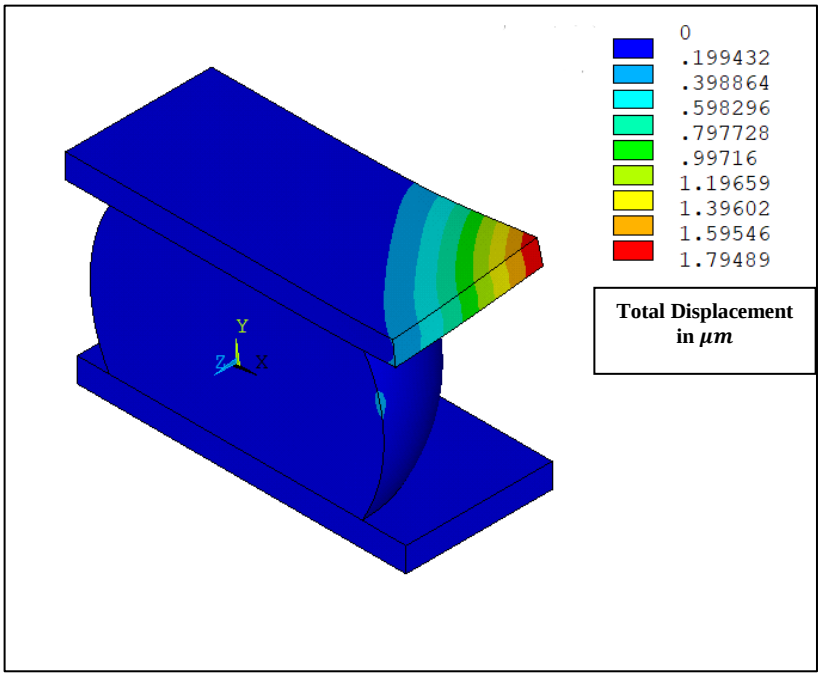

(e)

Figure A.1: Modal shapes for SAC305 solder joint under base constraint with natural frequencies of (a) 18.7543 Hz, (b) 24.0477 Hz, (c) 25.7506 Hz, (d) 36.3911 Hz and (e) 42.1848 Hz in μm after 1 day aging condition

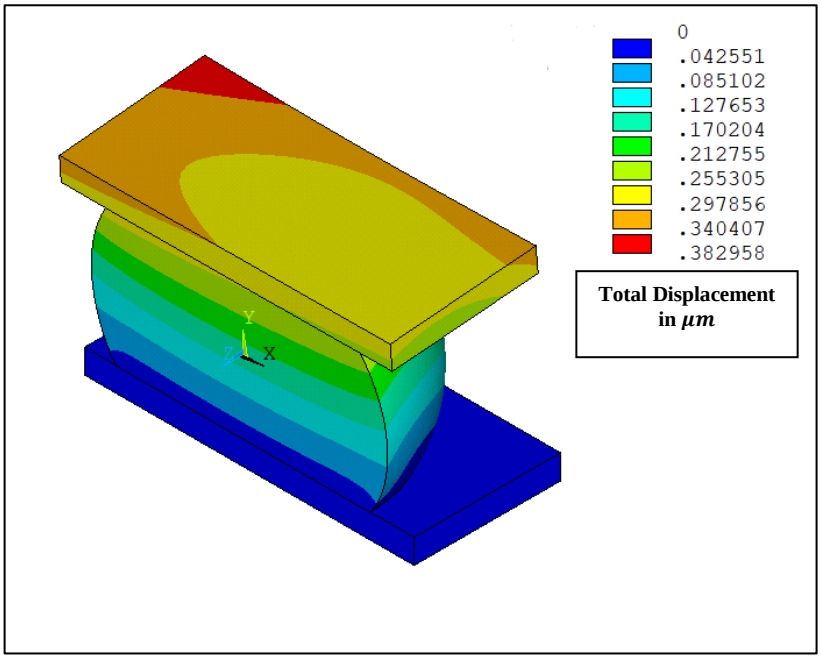

(a)

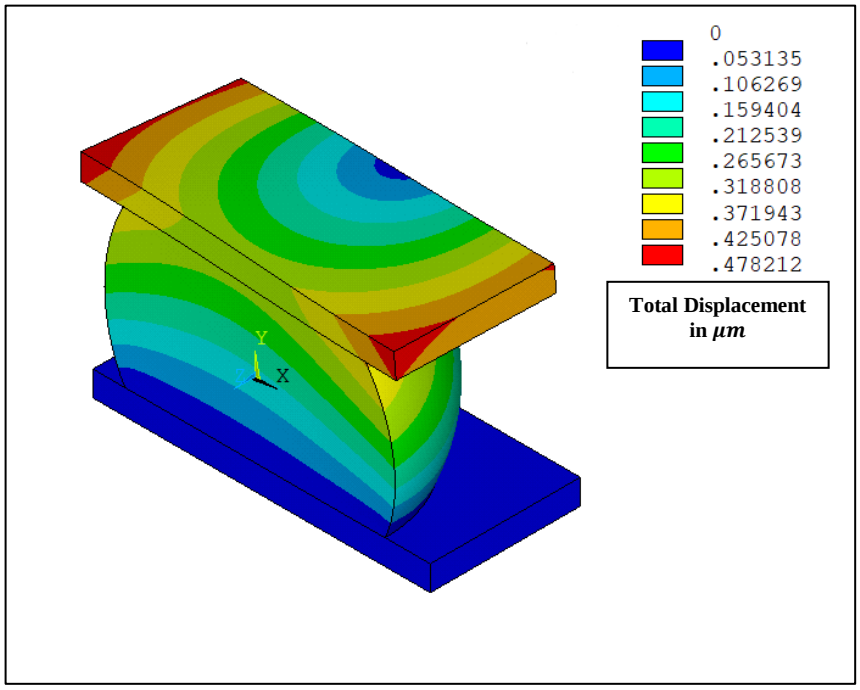
0
.053135
.106269
.159404
.212539
.265673
.318808
.371943
.425078
.478212
Total Displacement in μm
Y
X

(b)

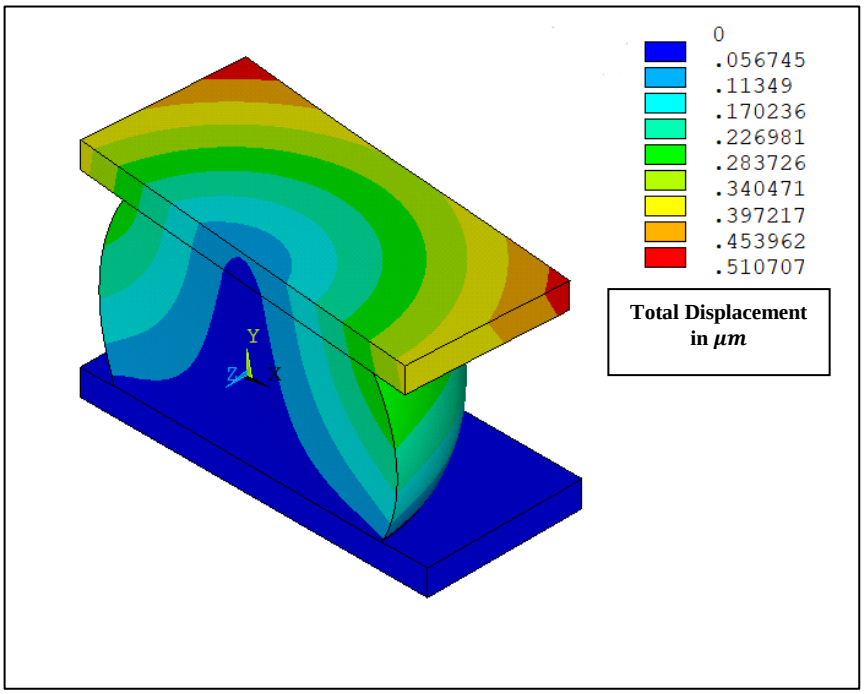
0
.056745
.11349
.170236
.226981
.283726
.340471
.397217
.453962
.510707
Total Displacement in μm
Y
Z
X

(c)

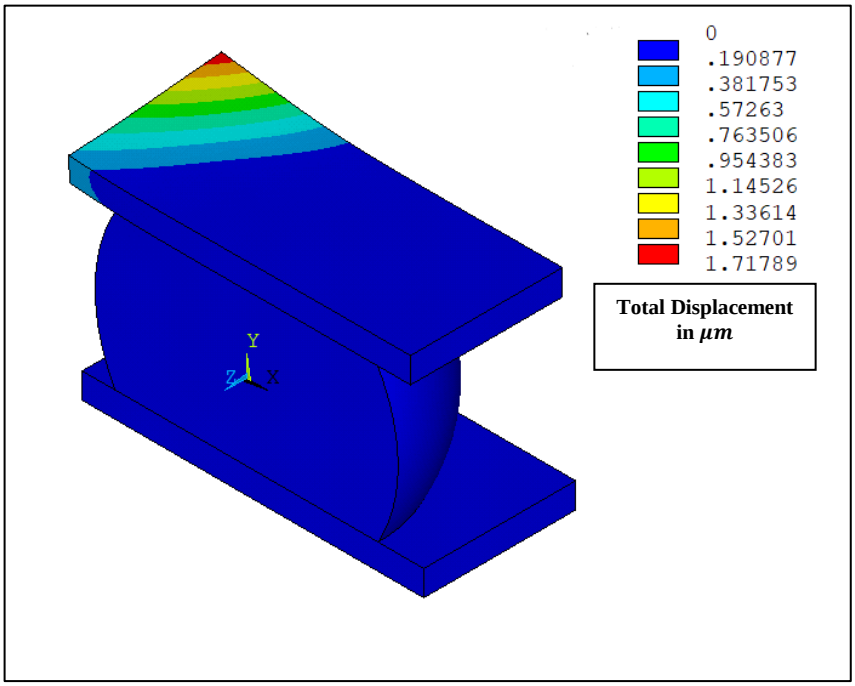

(d)

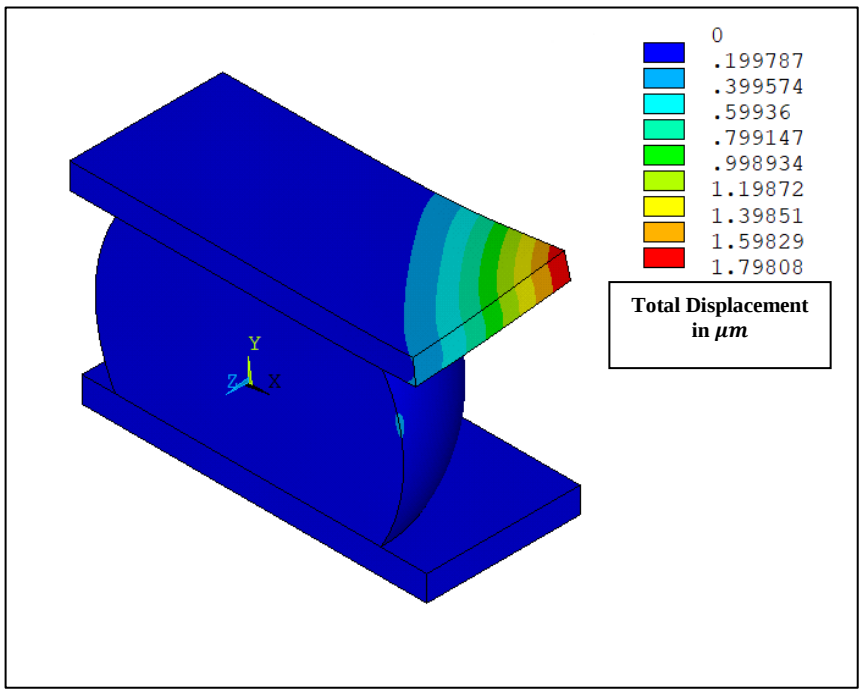

(e)

Figure A.2: Modal shapes for SAC305 solder joint under base constraint with natural frequencies of (a) 16.1592 Hz, (b) 20.7669 Hz, (c) 22.206 Hz, (d) 33.7088 Hz and (e) 38.7619 Hz in μm after 5 day aging condition

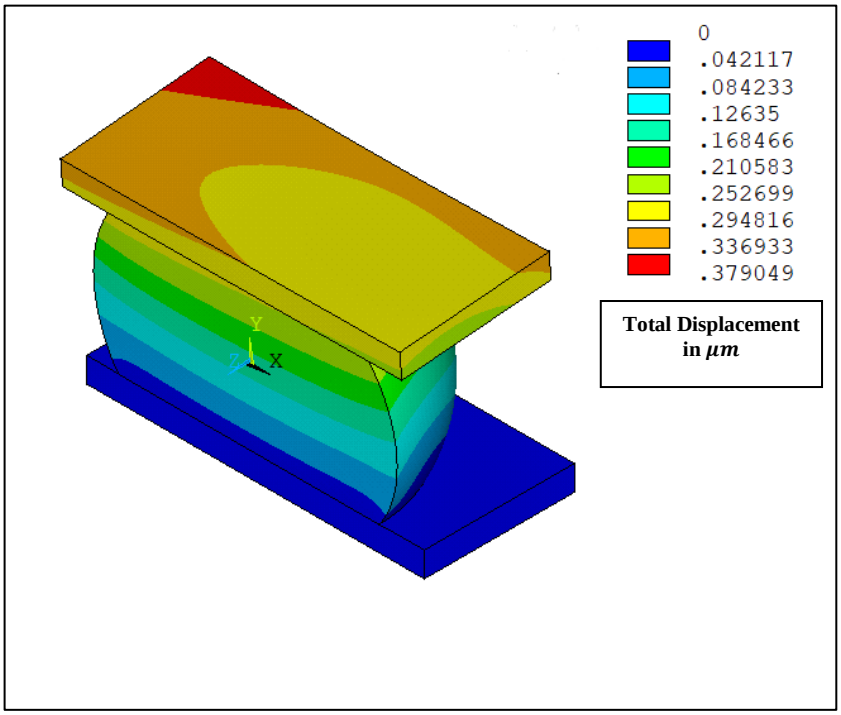
0
.042117
.084233
.12635
.168466
.210583
.252699
.294816
.336933
.379049
Total Displacement in μm
Y
X

(a)

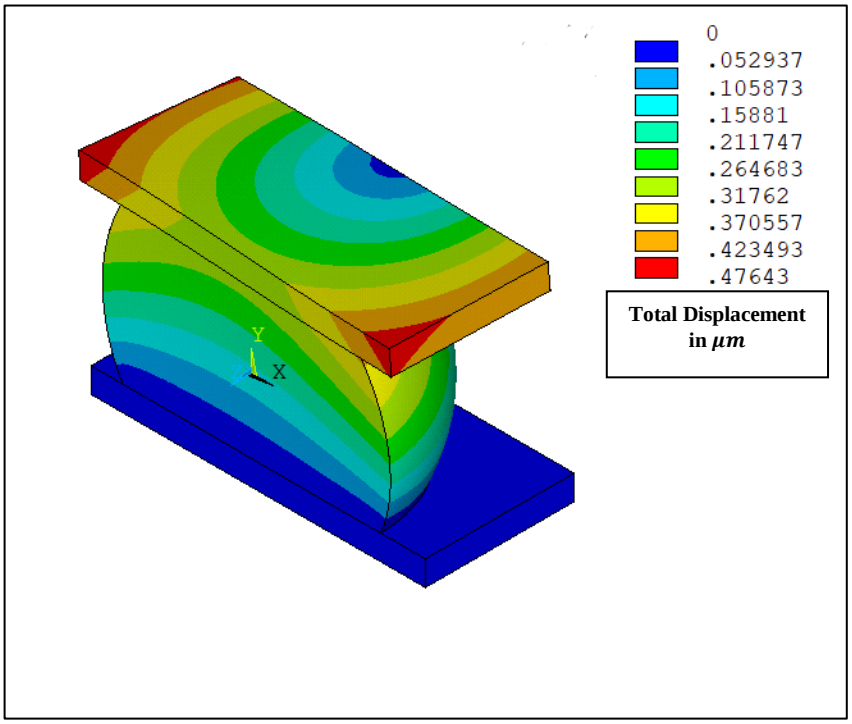
0
.052937
.105873
.15881
.211747
.264683
.31762
.370557
.423493
.47643
Total Displacement in μm
Y
X

(b)

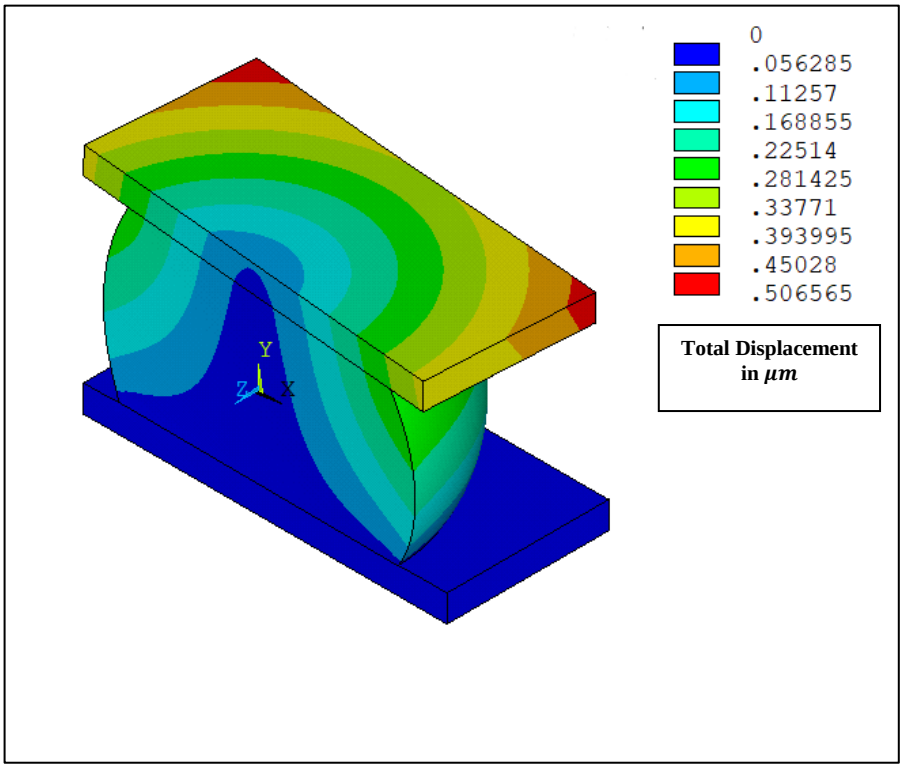
0
.056285
.11257
.168855
.22514
.281425
.33771
.393995
.45028
.506565
Total Displacement in μm
Y
Z
X

(c)

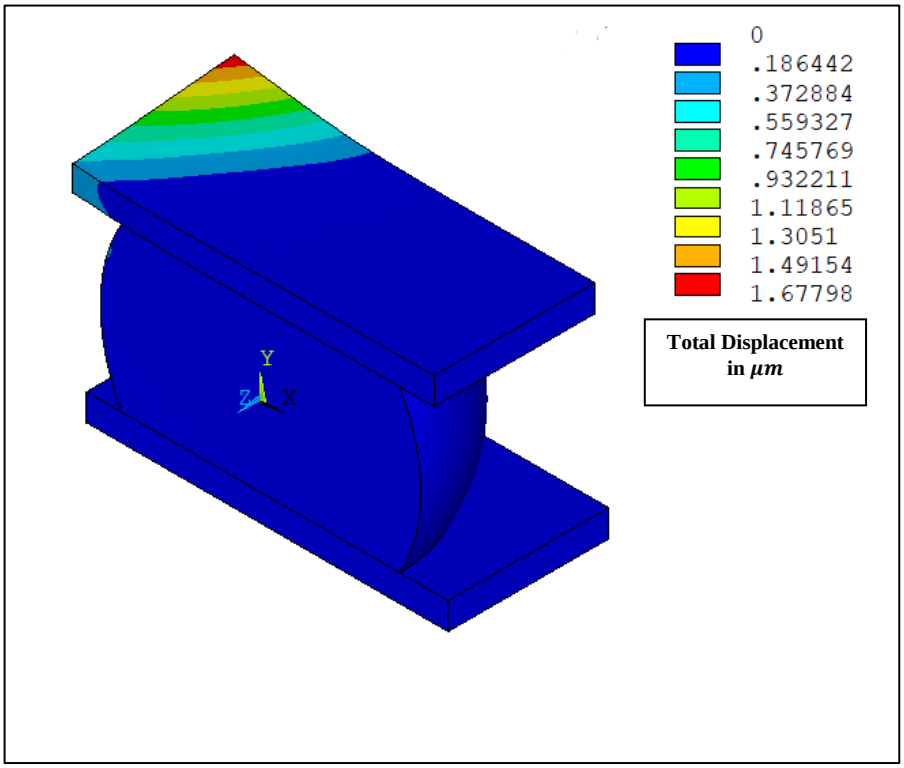
0
.186442
.372884
.559327
.745769
.932211
1.11865
1.3051
1.49154
1.67798
Total Displacement in μm
Y
Z
X

(d)

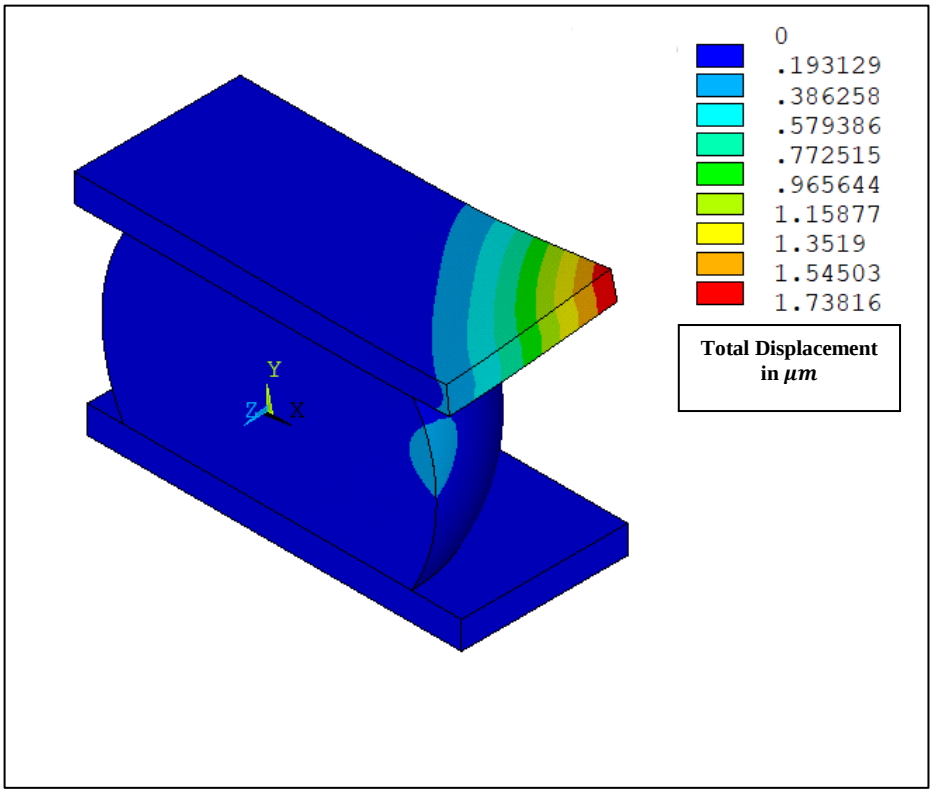

(e)

Figure A.3: Modal shapes for SAC305 solder joint under base constraint with natural frequencies of (a) 15.2697 Hz, (b) 19.5812 Hz, (c) 20.9273 Hz, (d) 32.6216 Hz and (e) 37.3655 Hz in μm after 20 day aging condition

A.2 Grid Independence Test

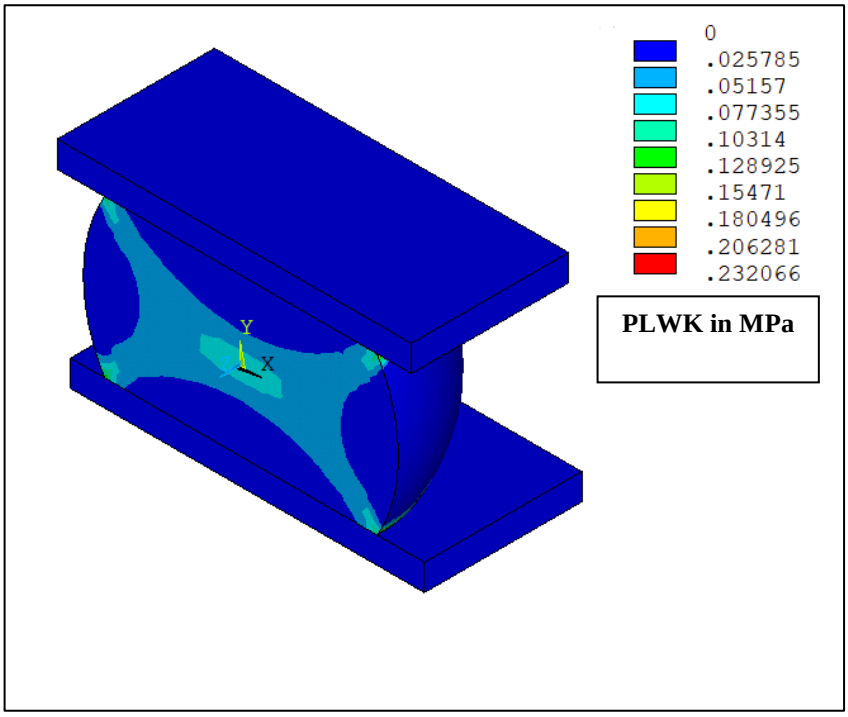

(a)

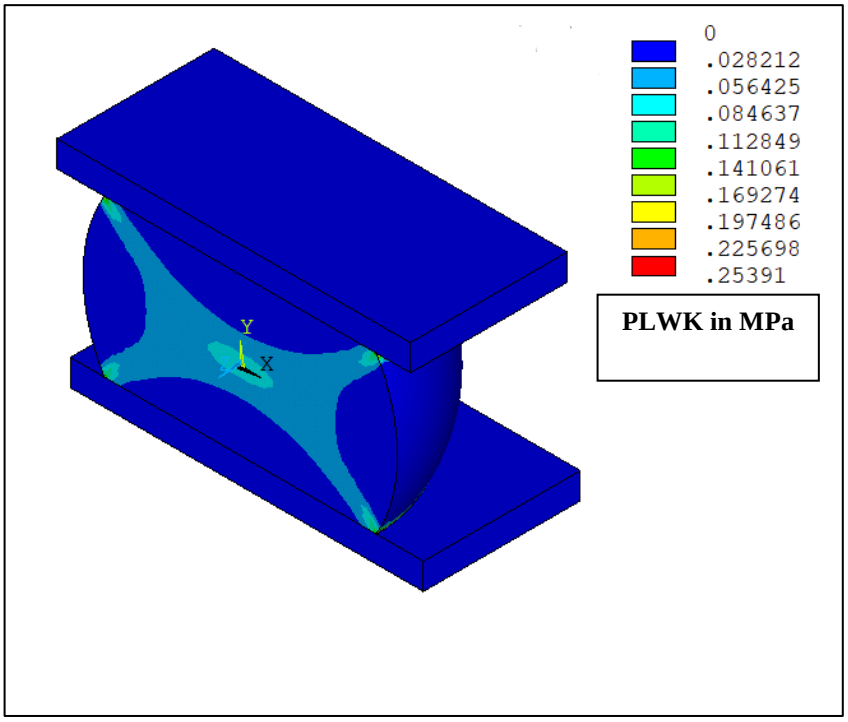

(b)

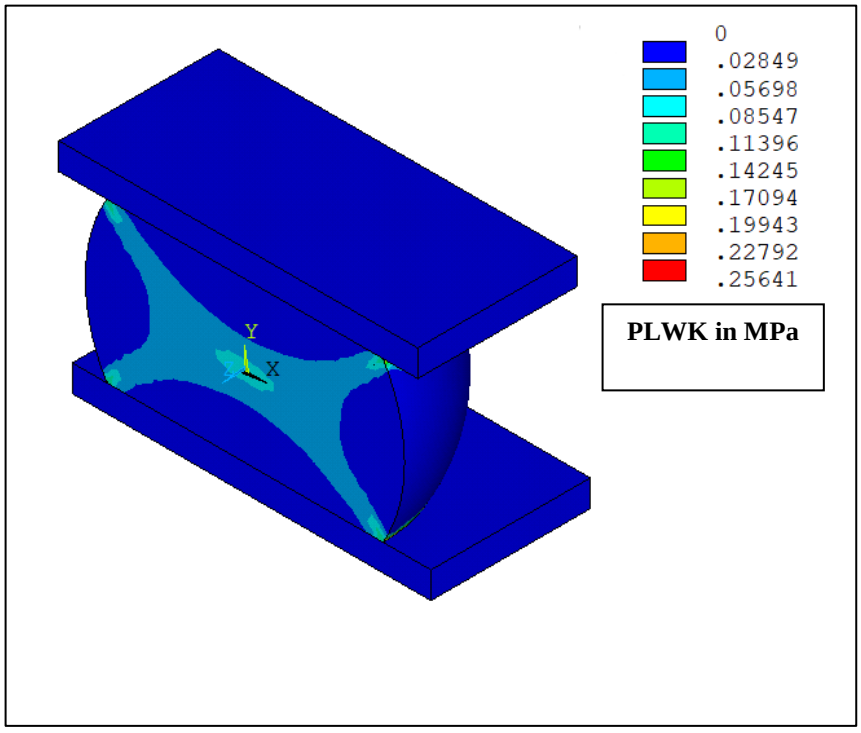

(c)

Figure A.4: Variation of PLWK with element number for a flip-chip SAC305 solder joint for current stressing of 100 hr at applied current of 0.01A at a temperature of 100°C for unaged condition for an element number of (a) 17271 (b) 29599 (c) 55068

A.3 Comparison of Diffusion Parameters

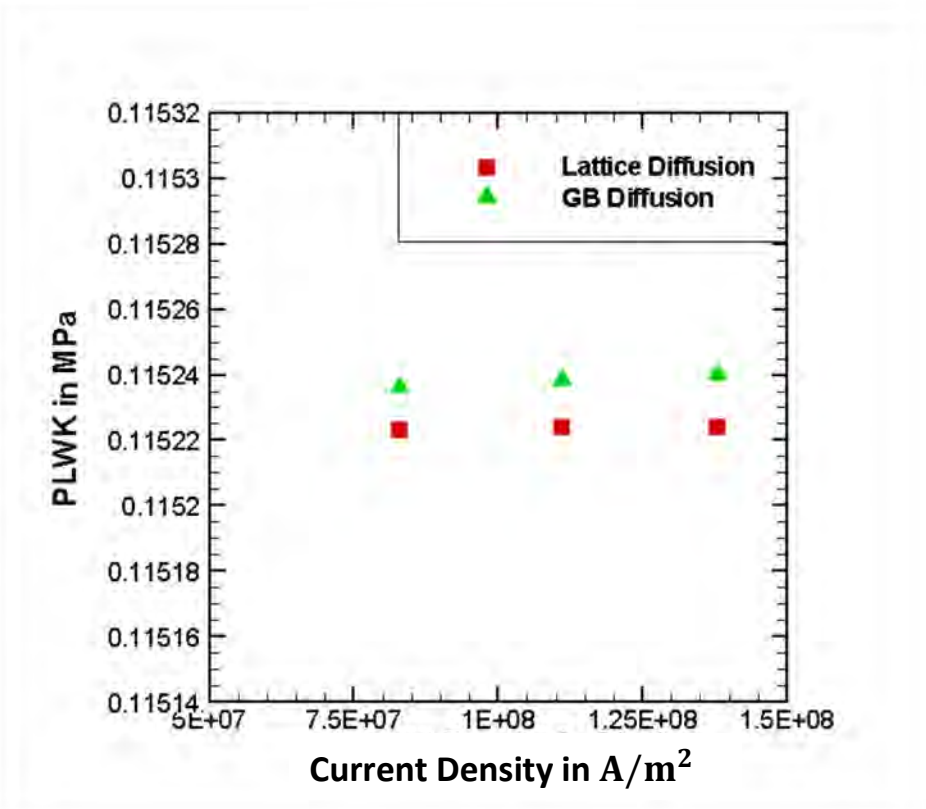

Figure A.5: Variation of PLWK with considering lattice diffusion and grain boundary diffusion for SAC105 solder joint